Gas Permeation Properties, Physical Aging, and Its Mitigation in High Free Volume Glassy Polymers

Gas Permeation Properties, Physical Aging and its Mitigation in High Free Volume Glassy Polymers

Ze-Xian Low[a], Peter M. Budd[b,*], Neil B. McKeown[c,*], and Darrell A. Patterson[a,d]

[a] Centre for Advanced Separations Engineering and Department of Chemical Engineering, University of Bath, Claverton Down, Bath BA2 7AY, UK

[b] School of Chemistry, The University of Manchester, Manchester M13 9PL, UK

[c] EastCHEM School of Chemistry, University of Edinburgh, David Brewster Road, Edinburgh EH9 3FJ, UK

[d] Darrell Patterson sadly passed away on 19th February 2017. This contribution is dedicated to his memory

Abstract

Hundreds of polymers have been evaluated as membrane materials for gas separations, but fewer than ten have made it into current commercial applications, mainly due to the effects of physical aging and plasticization. Efforts to overcome these two problems are a significant focus in gas separation membrane research, in conjunction with improving membrane separation performance to surpass the Robeson upper bounds of selectivity versus permeability for commercially important gas pairs. While there has been extensive research, ranging from manipulating the chemistry of existing polymers (e.g., thermally rearranged or crosslinked polyimides) to synthesizing new polymers such as polymers of intrinsic microporosity (PIMs), there have been three major oversights that this review addresses: (1) The need to compare the approaches to achieving the best performance, in order to identify their effectiveness in improving gas transport properties and in mitigating aging, (2) a

common standardized aging protocol that allows rapid determination of the success (or not) of these approaches, and (3) standard techniques that can be used to characterize aging and plasticization across all studies to enable them to be robustly and equally compared. In this review, we also provide our perspectives on a few key aspects of research related to high free volume polymer membranes: (1) The importance of Robeson plots for membrane aging studies, (2) eliminating thermal history, (3) measurement and reporting of gas permeability and aging rate, (4) aging and storing conditions, and (5) promising approaches to mitigate aging.

Table of Content

1. Introduction

It is now over 35 years since the first installation of an industrial gas separation membrane system. The continuous growth of membrane-based gas separation has generated sales of around 1 billion dollars.[1] The separation of nitrogen from air and the separation of CO_2 from natural gas represent some 60% of the membrane gas separation market, while other large applications include the separation of C2−C4 olefins from nitrogen in petrochemical plants, of hydrogen from light hydrocarbons in refineries and of hydrogen from nitrogen/argon mixtures in ammonia plants. Other emerging applications at their early stage include the separation of CO_2/H_2 mixtures, CO_2/N_2 separation for carbon capture, oxygen or nitrogen enrichment from air and olefin/paraffin separations.[1,2]

Membrane technology has the advantages of small footprint, ease of operation and lower cost compared to other separation technologies, such as distillation. Hundreds of polymers have been evaluated for gas separations, but fewer than 10 membrane materials have made it to current commercial applications and this has not changed for decades (**Figure 1**).[1] This is mainly due to two phenomena: plasticization and physical aging.

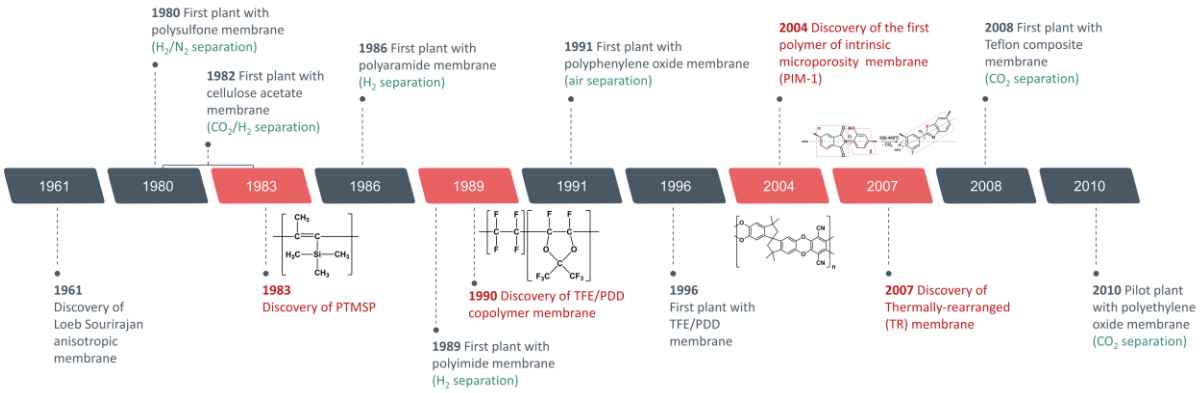

Figure 1. Milestones in the development of high free volume membrane gas separation materials (**PTMSP**,[3] TFE/PDD,[4] **PIM-1**,[5] and TR-membrane[6]) and industrial applications of membrane gas separation systems.[7-9] (**PTMSP**= poly(1-trimethylsilyl-1-propyne, TFE/PDD= tetrafluoroethylene/perfluoro-2,2-dimethyl-1,3-dioxole, PIM= polymer of intrinsic microporosity, and TR= thermally-rearranged).

Plasticization refers to the molecular chain reorganization of a polymer driven by high sorption of a condensable gas (such as CO_2), resulting in lower selectivity and increased product loss at the permeate side.[10,11] Physical aging in general involves the reversible change in a property of the polymer as a function of storage time under no influence from any other external conditions and without permanent modification of the structure, chemically or physically.[12] More specifically, physical aging in the non-equilibrium glassy state of a polymer involves a reversible polymer chain rearrangement driven towards an ever unachievable equilibrium state of polymer chain packing, and is sometimes referred to as the densification of the polymer. This relaxation of non-equilibrium chain conformations leads to the collapse of the “pores” or free volume elements (FVEs) within the polymer film.[13]

Physical aging occurs in all glassy polymers. However, for glassy polymers with high free volume, such as certain polyacetylenes, physical aging occurs much more rapidly and continues to take place for many years. In addition to low selectivities for one gas over another, aging of poly(1-trimethylsilyl-1-propyne) (**PTMSP**), a polyacetylene that was discovered over 30 years ago, is a reason why it has not found commercial use as a gas separation membrane. Yet, **PTMSP** remains one of the most permeable of all polymers to gases ever discovered, with almost one-third of the polymer being unoccupied space (Note: the most permeable polymer ever

recorded to date is indan-based polyacetylene[14]).[3] Other notable high free volume polymers are shown in **Figure 2**.

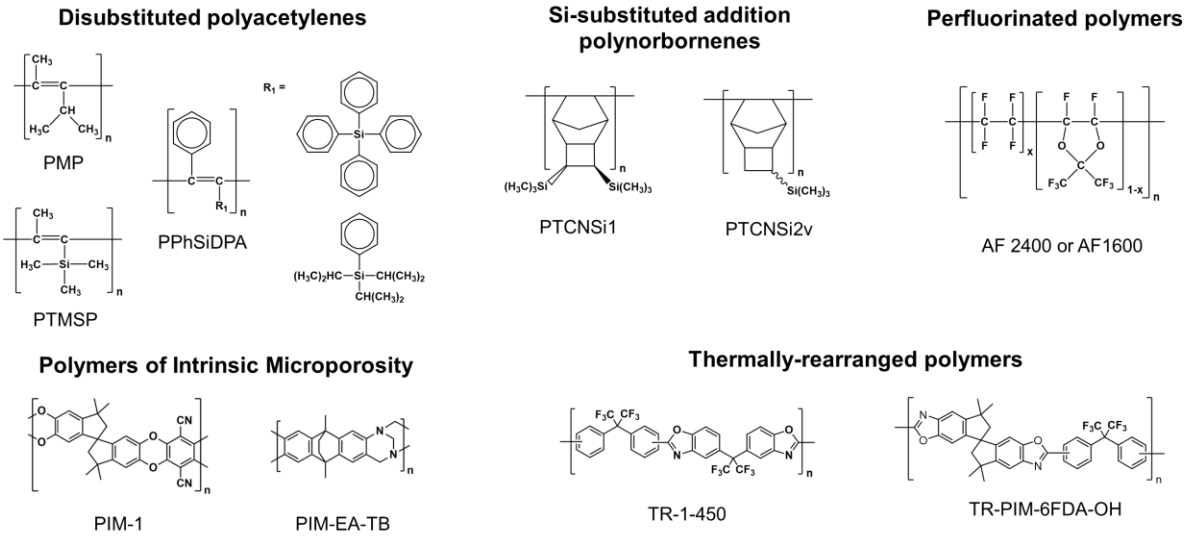

Figure 2. Examples of high free volume glassy polymers used for gas separation membranes.[15]

Over a decade ago, a new class of polymers, known as polymers of intrinsic microporosity (PIMs), was invented by Budd and McKeown.[5] PIMs have unique rigid and contorted macromolecular backbone structures which induce poor molecular packing, leading to interconnected, irregularly-shaped FVEs behaving like micropores (i.e. pores of diameter < 2 nm according to IUPAC).[16,17] Thus, the term *intrinsic microporosity* was coined for such polymers as "a continuous network of interconnected intermolecular voids, which forms as a direct consequence of the shape and rigidity of the component macromolecules."[18] Unlike conventional microporous materials, PIMs are *solution-processable*.[5] The extraordinary gas separation performance of PIMs contributed to the redefinition of Robeson's upper bounds[19] in 2008[20] and 2015.[21] The new 2015 upper bounds for the O_2/N_2, H_2/N_2 and H_2/CH_4 gas pairs were significantly shifted from the 2008 upper bounds,

demonstrating the substantial impact of highly rigid, molecular sieving PIMs and PIM-polyimides (PIM-PIs) derived from triptycene components.[21]

However, like **PTMSP**, PIMs suffer from physical aging.[22] Therefore, significant research is focused on mitigating physical aging of such high free volume polymers (sometime referred to as superglassy polymers). This review summarises studies related to physical aging, for which the timescale of the aging studies can vary from several weeks to a couple of years. However, the difficulty lies in the different protocols used to introduce aging, to measure aging and to measure the gas transport properties of the membranes. In this review, efforts have been made to compare the literature fairly, and to do so the gas separation results were reinterpreted in terms of selectivity and permeability as a function of time and in the form of double logarithmic Robeson plots for different gases. This review aims to identify effective approaches in mitigating physical aging and to identify standardized methods of aging and gas permeation measurement techniques, as well as procedures to erase aging history.

The review is divided into seven sections covering: Physical aging in glassy polymers (Section 2), preparation of PIM powders and films (Section 3), methods to measure the size and size distribution of free volume elements (Section 4), laboratory practices to study aging and to measure gas permeability (Section 5), approaches to prevent aging (Section 6), and concluding remarks (Section 7).

2. Physical aging in glassy polymers

Physical aging is a ubiquitous phenomenon in glassy materials, whereby change in a property is observed as a function of storage time under no influence from any other

external conditions.[12,23,24] The phenomenon originates from the fact that they are generally out-of-equilibrium[23] and involves a wide range of properties, including both bulk properties, such as specific volume, enthalpy, mechanical and dielectric response, as well as properties at the molecular level, such as the free volume distribution. It is important to note that physical aging only involves reversible changes in properties, with no permanent modification of the structure.[12] This important feature of physical aging is distinct from other factors that may influence the properties over time, including chemical aging, degradation, absorption or contamination.[24]

In order to understand physical aging, consider what happens when an amorphous polymer is cooled from above to below its glass transition temperature (T_g). Below the T_g, the polymer exhibits excess enthalpy or free volume with respect to its equilibrium state.[16] The non-equilibrium state of glassy polymers below the T_g can be schematically represented as a plot of enthalpy (or volume) as a function of temperature (**Figure 3**). As long as the polymer is kept at a temperature $T_a < T_g$, the thermodynamically stable state (as represented by the broken line) is slowly but indefinitely recovered during the course of physical aging towards an ever unachievable equilibrium state.[23] The lowering of cooperative molecular mobility with decreasing temperature can be regarded as the main reason for the inability of the glassy polymer to follow the line of the equilibrium liquid.[25]

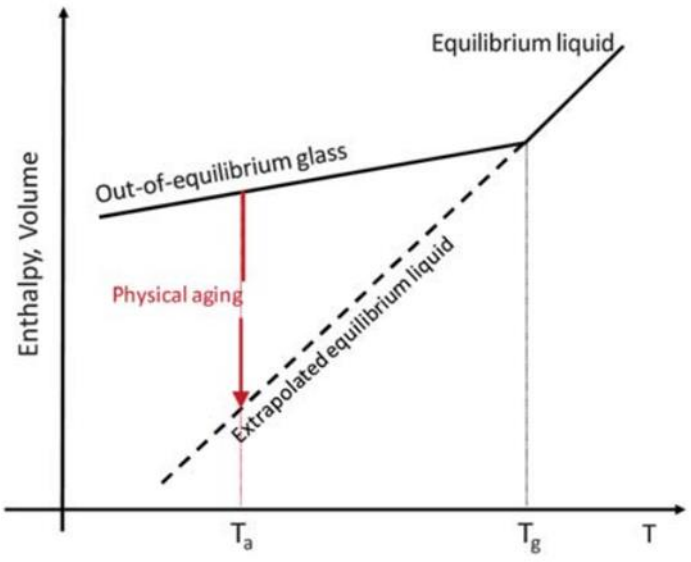

Figure 3. Schematic representation of volume or enthalpy of glassy materials as a function of temperature. Reproduced with permission from Ref. [23]. Copyright 2018 The Royal Society of Chemistry.

Physical aging in polyacetylenes and PIMs differs from conventional glassy polymers, as no T_g is observed below their decomposition temperatures. Unlike conventional polymers that can change their conformation in the rubbery state or in solution, PIMs do not have any single bonds in the backbone about which rotation can take place and are therefore unable to undergo large-scale conformational change without breaking bonds, which explains why it does not have a T_g below its decomposition temperature. Because of this restriction on long-range segmental motion, PIM films prepared by solution casting, followed by thermally-induced phase separation, are always 'more' out-of-equilibrium than conventional glassy polymers, and therefore exhibit higher free volume. However, after film formation, because of the much higher free volume in PIMs, they tend to age more rapidly than conventional glassy polymers.[26] It was also previously discovered that aging rate correlates strongly to the T_g of the polymer[27] and that T_g increases with physical aging.[28]

Although physical aging occurs without any external influence, its rate is found to be dependent on several factors, such as temperature,[29-32] gas environment,[33-35] and polymer structure.[33,36] More importantly, it was observed that physical aging occurs more rapidly in a thin polymer film (i.e. rate of aging in a film is inversely proportional to its thickness), as evident in both conventional polymers (polyimide,[33,36-38] polysulfone,[32,33,36-40] and PPO[32,33,36,38]) and high free volume polymers (**PTMSP**,[27,41] **Teflon AF**,[27,42,43] **Hyflon AD**[27,42,43] and **PIM-1**[27,44,45]). The accelerated aging of thin films is attributed to the enhanced mobility near the surface,[24,40] or the diffusion of free volume to the surface of the film,[36] that allows the polymer to reach a lower free volume state more quickly than bulk samples. Also, thin films of **AF2400** show similar aging rates in thicknesses ranging from 50 nm to 800 nm,[27] suggesting that there is a maximum mobility of free volume that can be achieved near the surface.

3. Preparation of PIM polymer and film

3.1. Summary of PIM synthesis

The synthesis of PIMs is the subject of a recent review[46] so the subject is only briefly summarised here.

The preparation of the first generation of PIMs was based on a double aromatic nucleophilic substitution (S_NAr) reaction, specifically the benzodioxin-forming reaction between a spirocyclic biscatechol and a tetrahalo monomer. Generally, S_NAr reactions are known to proceed especially readily if the halide-containing monomer is activated by an electron-withdrawing group (e.g. –CN, F, etc.).[47]

Several variations in reaction conditions for PIM synthesis have been described in the literature.[5,48-56] Most variations were investigated to enable the production of linear **PIM-1** with high molecular weight (M_w) and narrow molecular weight

distribution for gas separation. The original method (also referred to as the “low temperature method”), co-developed by McKeown and Budd at the University of Manchester, involves mixing the two monomers (3,3,3',3'-tetramethyl-1,1-spirobisindane-5,5 ',6,6 '-tetrol (TTSBI) and 1,4-dicyanotetrafluorobenzene (DCTB)) in equimolar quantities in a solution of anhydrous dimethylformamide (DMF) with twofold excess of fine powdered dry potassium carbonate (K_2CO_3) at 50–60 °C for 24–72 h.[5,48] An alternative “high temperature” method, developed by Michael Guiver’s group at the Canadian NRC laboratories (now Tianjin University, China), involves high speed stirring of the mixture in dimethyl acetamide (DMAc) at 155 °C for 8 minutes, with the addition of toluene to enable the continuation of stirring.[49] Both methods produce **PIM-1** with sufficiently high average molecular mass for film casting. Nowadays, variations of the high temperature method are often used, e.g. heating at 160 °C for 40 min.[50] Furthermore, the used of dimethyl sulfoxide (DMSO), to replace the toxic solvents DMF and DMAc, was also reported.[51] By varying the synthesis conditions (temperature between 60 to 120 °C and reaction time between 2 to 7 hours), **PIM-1** with similar M_w and polydispersity index (PDI) values as those of the previous recipes can be produced in DMSO.[51]

The synthesis of **PIM-1** by mechanochemistry was recently demonstrated by Zhang et al.[52] The monomers of **PIM-1** in the presence of K_2CO_3 were ground in a mortar with a pestle, or by ball milling, to produce **PIM-1** with higher average molar mass of 485 000 g mol^{-1}, and lower polydispersity of 1.4, than the **PIM-1** counterpart from solution synthesis. This was ascribed to the physical effect of mechanical action that breaks down the particles to smaller sizes and exposes fresh active sites, maintaining reaction and overcoming premature chain-termination suffered in the wet synthesis of **PIM-1**. It was observed in the same work that the initial polymer product

would rapidly precipitate out from the reaction mixture during the synthesis of **PIM-1** in DMF at 60 °C.[52]

Other notable synthesis strategies for **PIM-1** are based on trimethylsilyl (TMS)-derived bischatechol[53,54] and a fluoride-mediated polymerization method.[55] The use of fluoride as catalyst enables mild reaction conditions, neutral condensate byproducts and eliminates the use of basic neutralizer.[56]

DMF is reported to be the ideal solvent for maximized reaction rate and M_w at a given temperature, while the use of DMAc will lead to slower reaction rate than DMF.[57] The reaction rate was sensitive to the quality and molar ratio of K_2CO_3, and generally powder is preferred to granular K_2CO_3. An optimum temperature is needed for controlling polydispersity and cross-linking.[57] Additionally, the purity of the monomers is crucial in maintaining the molar ratio between the two monomers. The monomers are usually purified before use. The concentration of the monomers is equally important, as at high concentration insoluble crosslinked materials are produced,[57] whereas at lower concentrations a large number of cyclic oligomers of modest molecular mass are produced.[54,58] Before being re-dissolved to form a solution for making films, PIM products are also purified, typically by precipitation in methanol.

PIMs can be designed without spirocenters so long as highly rigid fused structural components that introduce kinks into the polymer backbones are used (e.g. triptycene for **TPIM-1**,[59] **TPIM-2**,[59] **PIM-TRIP-TB**[60] and ethanoanthracene for **PIM-EA-TB**[61]).

In addition to the dibenzodioxane-forming reaction, formation of imide has been used to form PIMs termed PIM-PIs. Even though the imide link is not composed of fused

ring units, by selecting suitable diamine aromatic monomers, rotation about the C–N single bond can be sufficiently restricted to inhibit conformational rearrangement, yielding significant intrinsic microporosity.[62]

More recently, a class of PIM has been developed utilizing a new form of polymerization based on some very old chemistry, Tröger's base (TB) formation. Julius Tröger[63] reported in 1887 that the reaction of *p*-toluidine with dimethoxymethane in acidic solution gave an unexpected product, later shown to be a V-shaped, bridged bicyclic diamine fused with two aromatic rings.[64] The extension of this chemistry to diamine monomers has enabled a range of TB-PIMs to be prepared by step-growth polymerization.[60,61,65-67]

3.2. Preparation of thick PIM films and PIM hollow fibers

Preparation of a thick PIM film for gas permeability measurements is generally similar to any other polymer film preparation, but differs in practice between research groups. The original procedure to prepare the first **PIM-1** membrane by solution casting was as follows: **PIM-1** solution was prepared by dissolving **PIM-1** powder in tetrahydrofuran (THF). The polymer solution was poured into a flat-bottomed glass Petri dish and the solvent was allowed to evaporate under a steady flow of nitrogen over a period of about 4 days, and further dried in a vacuum oven at 70 °C for 18 h.[48] Since then, an additional step of soaking the film in methanol overnight at room temperature was followed, to remove the trapped solvent or impurities, before drying in a vacuum oven. Most of the recent PIM film preparation techniques involve filtration through glass wool[61,68] or a 0.45 μm polypropylene filter[21,69] to remove undissolved high M_w or crosslinked polymer, with some variations to solvents (chloroform or DMAc), temperature (RT to 80 °C during film formation; RT to 120 °C

during evaporation of methanol), and evaporation time (1 to 4 days during film formation; 1 to 5 days during evaporation of methanol).[21,61,68,69] Examples of the preparation technique for PIM films from key research groups can be found here: Ingo Pinnau's research group (KAUST, Saudi Arabia),[21] Michael Guiver's research group (previously at the Canadian NRC laboratories, Canada),[69] Peter Budd's research group (University of Manchester, U.K.),[70] and Neil McKeown's research group (University of Edinburgh, U.K.).[61]

Very recently, **PIM-1** hollow fiber membranes have also been successfully produced at Georgia Institute of Technology.[71] Lively et al. utilized an immiscible liquid protective layer that reduces the evaporation of the volatile solvent (THF) to fabricate defect-free, integrally skinned, asymmetric **PIM-1** hollow fiber membranes.[71] The spinning apparatus with triple orifice spinneret is typically used in dual-layer spinning, but for the spinning of **PIM-1** hollow fiber the secondary polymer dope was replaced with an inviscid non-solvent fluid (**Figure 4**). **PIM-1** hollow fiber membranes exhibited higher gas selectivities than those in previous work on dense films,[72-74] which has been observed for other glassy polymers, and has been ascribed to partial polymer chain alignment along the spinning axis due to the high shear environment of the dope solution within the spinneret.[75,76]

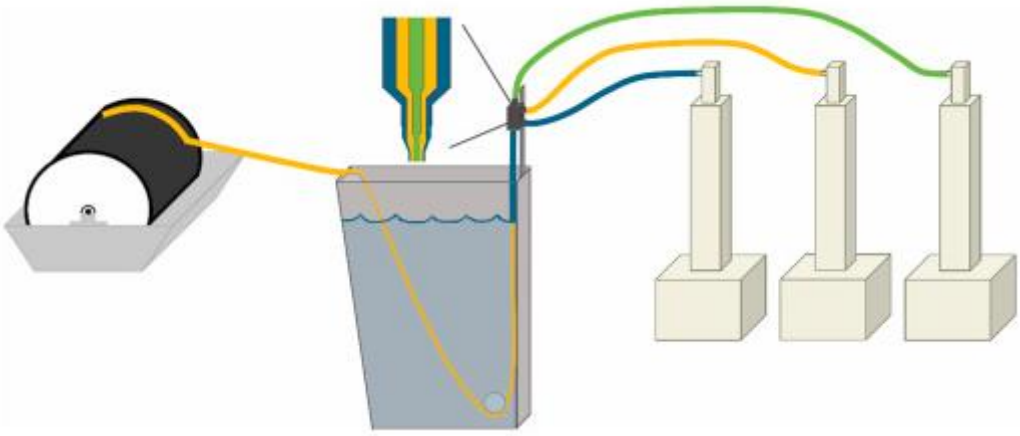

Figure 4. Schematic of a spinning apparatus and triple orifice spinneret to produce PIM-1 hollow fiber membranes. Green = bore fluid, yellow = polymer dope solution, and blue = sheath layer. Reproduced with permission from Ref. [71]. Copyright 2018 Elsevier.

4. Measurement of size and size distribution of free volume elements

The free volume in a polymer sample is the space not occupied by polymer molecules.[77] Various methods are used to characterize the size and size distribution of FVEs of high free volume glassy polymers, including Positron Annihilation Lifetime Spectroscopy (PALS), Inverse Gas Chromatography (IGC), cryogenic physisorption (N_2 sorption), ^{129}Xe NMR spectroscopy, molecular modelling and scattering methods (e.g. small angle x-ray scattering (SAXS) and x-ray diffraction (XRD)). More details about each of these techniques are given below.

The total quantity of free volume in a polymer sample, commonly expressed as fractional free volume (FFV), is related to the specific volume and specific van der Waals volume of the polymer as follows:

$$FFV = \frac{V - 1.3V_w}{V}$$

where V is the specific volume of the polymer (i.e., the reciprocal of density) and V_w is the specific van der Waals volume, calculated by the group contribution method described by Van Krevelen.[78]

4.1. Positron Annihilation Lifetime Spectroscopy (PALS)

The PALS technique is based on the measurement of the lifetimes of positrons in a material. A positron can either exist as a free positron (e^+) or as positronium (Ps), a metastable hydrogen-like bound state of an electron (e^-) and positron (e^+) which can exist in two spin states. The triplet state (*o*-Ps; with lifetime of 142 ns in vacuum) is assumed to interact with the electrons from the walls of the FVEs, which leads to a reduction of the *o*-Ps lifetimes to ~1.5–4.0 ns. Different lifetimes can be measured. The two shortest lifetimes are τ_1 (~0.2 ns) and τ_2 (~0.3–0.5 ns) and are due to the annihilation of singlet state Ps (*p*-Ps) and the free positrons (e^+), respectively. The long-lived lifetime(s) τ_i (*i*= 3 or 4) are due to *o*-Ps localized in FVEs and depend on the size of the FVEs; the larger the FVEs, the longer the lifetimes. Thus, it can be used to characterize the free volume. The collected data, lifetimes (τ_i) and corresponding intensities (I_i) can be processed using computer programs such as PATFIT (for finite-term analysis), CONTIN (for continuous analysis), or maximum entropy lifetime method (MELT; continuous analysis).[79] **Figure 5** shows an example of positron annihilation lifetime (PAL) spectra and size distributions of FVEs in **PTMSP** and **PIM-1**.[22] The lifetimes can be related to the mean size of FVE in the materials according to the Tao-Eldrup formula.[80,81]

$$\tau_i = \left\{\lambda_0^T + 2\left[1 - \frac{R_i}{R_i + \Delta R} + \frac{1}{2\pi}\sin\left(\frac{2\pi R_i}{R_i + \Delta R}\right)\right]\right\}^{-1}$$

where $\tau_i = \tau_3$ or τ_4 are the positronium lifetimes (ns) and R_i = R_3 or R_4 (Å) are the radii of FVE, respectively; λ_0^{T} is the intrinsic *o*-Ps annihilation rate (0.7×10^9 s^{-1}); and ΔR (the adjustable parameter) = 1.66 Å.

For high free volume materials, measurements of PAL spectra have to be performed in an inert atmosphere to eliminate the contribution of additional o-PS decay due to the reaction with sorbed oxygen.[82]

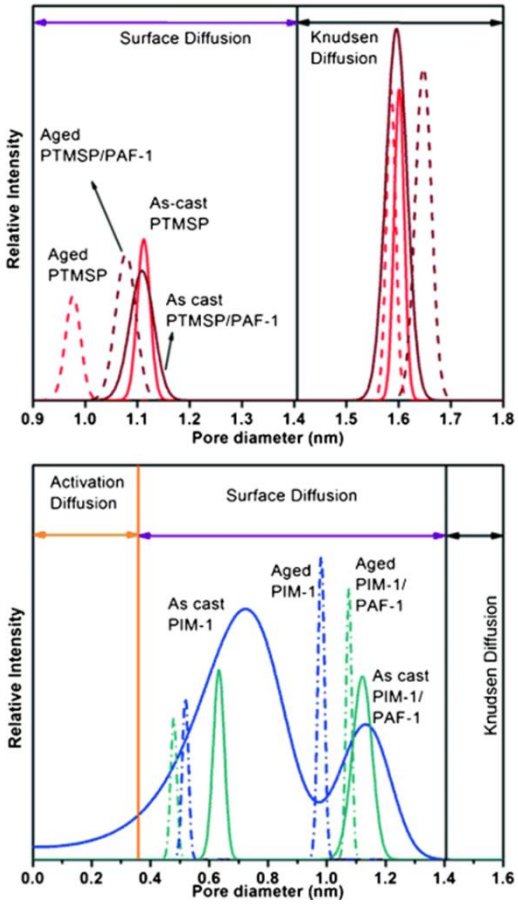

Figure 5. Size distributions of free volume elements in **PTMSP**, **PTMSP**/PAF-1, **PIM-1** and **PIM-1**/PAF-1 based on PALS. Reproduced with permission from Ref. [22]. Copyright 2018 John Wiley and Sons.

PALS has been used to characterize the free volume in many high free volume polymers, including **PTMSP**, **PIM-1** and TR-polymers (TR= thermally rearranged). **Table 1** shows the radii of FVEs (Å) of common high free volume polymers, as estimated by PALS and other techniques (discussed below). It should be noted that PALS often gives a strongly bimodal distribution of the size of the FVEs which is not

evident in molecular modelling studies or pore size distribution from the analysis of nitrogen adsorption data using appropriate parameters.

Table 1. Radii of free volume elements (Å) of high free volume polymers as estimated by different methods.[a]

Polymer	PALS		IGC	N_2 sorption	MD (molecular dynamics)	^{129}Xe NMR
	R_3	R_4				
Disubstituted polyacetylenes						
PTMSP	3.41 [82]	6.81 [82]	-	6.5-14 [83]	2-10 [84]	7.8 [85]
PPrSiDPA	3.83 [82]	6.38 [82]	-	-	1-7 [84]	-
PPhSiDPA	2.87 [82]	3.78 [82]	-	-	2-8 [84]	-
PVTMS	3.2 [82]	4.35 [82]	5.3 [86]	-		-
Si-substituted addition polynorbornene						
PTCNSi2g	4.2 [15]	7.3 [15]	-	7.0 [15]	-	-
Perfluorinated polymers						
AF 2400	2.68 [82]	5.9–6.4 [87]	6.4 [86]	-	1-13 [84]	8.0 [85]
AF 1600	2.5 [84]	4.89 [82]	5.8 [86]	-	2-9 [84]	6.7 [85]
Hyflon AD60X	4.78 [88]	-	-	-	3.87 [88]	6.0 [85]
Hyflon AD80X	5.22 [88]	-	5.3 [88]	-	4.53 [88]	6.12 [85]
PIM						
PIM-1	3.0 [74]	5.2 [74]	6.0 [74]	6-8 [74]	1-6 [89]	10-11 [90]
Thermally rearranged polymer						
TR-1-450	3.7 [6]	-	-	~5 [6]	-	-

[a]data evaluation assuming spherical holes. Only polymers with free volume measured by more than one method are compared. Abbreviation: PTMSP, poly(1-trimethylsilyl-1-propyne); PPrSiDPA, poly(1-phenyl-2-[p-triisopropylsilylphenyl]acetylene); PPhSiDPA, poly(1-phenyl-2-[p-triphenylsilylphenyl]acetylene); PVTMS, poly(vinyltrimethyl silane); PTCNSi2g, poly(3,3-bis-[trimethylsilyl] tricyclononene-7); AF2400, copolymer of 87 mol.% 2,2-bis(trifluoromethyl)-4,5-difluoro-1,3-dioxole and of 13 mol.% tetrafluoroethylene; AF1600, copolymer of 65 mol.% 2,2-bis(trifluoromethyl)-4,5-difluoro-1,3-dioxole and of 35 mol.% tetrafluoroethylene; Hyflon AD60X, copolymer of 60 mol.% 2,2,4-trifluoro-5-trifluoromethoxy-1,3-dioxide (TTD) and 40 mol.% tetrafluoroethylene (TFE); Hyflon AD80X, copolymer of 80 mol.% 2,2,4-trifluoro-5-trifluoromethoxy-1,3-dioxide (TTD) and 20 mol.% tetrafluoroethylene.

4.2. Inverse Gas Chromatography (IGC)

IGC is used for the investigation of polymer properties through interaction of the polymer with volatile probes (low M_w compounds). It is based on the measurement of the retention times of probes introduced into the carrier gas flow (mobile phase) into a column that contains the polymer film under investigation as the stationary phase. More detailed introduction and background of IGC used for polymer studies are reported in Yampolskii's perspective paper.[91]

IGC is used as one of the probe methods for the estimation of the size of FVEs in polymers.[92] The interaction or the vapor sorption (enthalpy of sorption, ΔH_s) can be regarded (in terms of the Hess cycle) as a sequence of two stages: (1) a transition from vapor to condensed phase of the solute in the condition of infinite dilution (enthalpy of condensation of the solute, ΔH_c)[93] and (2) mixing with the polymer matrix (ΔH_m), as shown in the equation below.[91]

$$\Delta H_s = \Delta H_c + \Delta H_m$$

The interactions between the solute molecule and the polymer are reflected in the latter term, as the enthalpy of condensation (ΔH_c) is a characteristic of the phase transition of a pure solute, which is independent of the polymer (stationary phase). In glassy polymers below their T_g, it can be observed that the partial molar enthalpy of mixing (ΔH_m) increases in magnitude with increasing solute critical volume (V_c) until a maximum value, before decreasing again (**Figure 6**). This can be interpreted as follows: For smaller solutes the bulk sorption involves the loading of the FVEs in the polymer by the sorbed molecules. When the size of the solute increases beyond a critical value, accommodation in FVEs is restricted and dissolution takes place in the denser matrix.[94] The correlation of the minimum of the dependence of ΔH_m on V_c, where the prevailing FVE-filling mechanism of sorption is encumbered, can be correlated to the average size of FVEs of the polymer. This has been shown to be in agreement with data from the PALS method.[92] A problem with IGC (and any analysis using adsorption probes) is that the polymer structure is not fixed and can swell during analysis, thereby implying a greater proportion of larger pore sizes than would be encountered during gas permeability measurements.

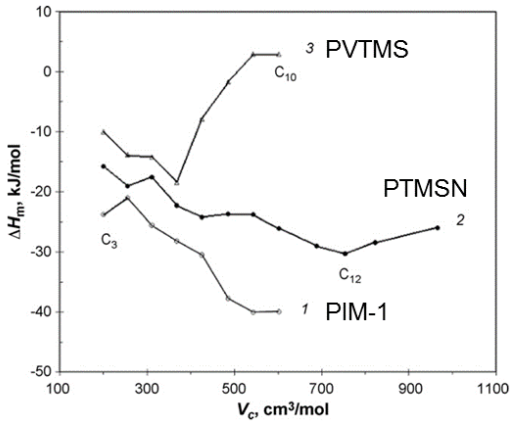

Figure 6. Partial molar enthalpies of mixing vs critical volume of sorbates based on IGC results. Reproduced with permission from Ref. [74]. Copyright 2018 Elsevier.

Abbreviation: PVTMS, poly(vinyltrimethyl silane); PTMSN, poly(trimethylsilyl norbornene).

4.3. Physisorption

Physisorption (physical adsorption) with adsorbates like N_2, CO_2, Ar, He, CH_4, benzene and nonane[95] is one of the best established techniques to measure the characteristics of solids, such as surface area, pore size and pore size distribution. N_2 adsorption at 77 K (under cryogenic conditions) is most widely used. In the case of polymers with high free volume, the use of gas sorption techniques has provided some insights into the size of the FVEs. The nitrogen adsorption isotherm of polymers with high free volume can be analyzed by the Horvath-Kawazoe (HK) method using a slit-pore model, or by non-local density functional theory (NLDFT), to obtain a pore size distribution (example shown in **Figure 7**). These methods have been applied for various polymers, such as PIMs[15,74,96,97], TR membranes[6], **PTMSP**[83] and PIM-PIs[98]. The PSD obtained for PIMs using NLDFT has been questioned due to the apparent absence of pores in the range 0.9–1.1 nm in diameter, which appears to be an artifact of the parameters typically applied during the analysis and is very different from the smoother distribution obtained from HK analysis or from chain packing simulations.[99] Another problem when N_2 is used as probe molecule at 77 K, is that the uptake of N_2 does not reach a plateau and a large hysteresis is usually observed, suggesting swelling of the polymer matrix during measurement. Moreover, often no significant gas uptake is observed at very low pressure, but above a certain pressure, a strong uptake is observed.[100] This is because N_2 molecules are unable to probe pores smaller than 3.6 Å.[101] It was generally accepted that N_2 adsorption is not satisfactory for probing the

microporosity, especially in the range of ultramicropores (pore widths < 0.7 nm).[102] The less common approach is to use CO_2 as probe molecule (at 273 K) to determine the pore size of microporous polymers.[100,103-105] CO_2 adsorption has been used since 1964, especially on conventional microporous solids such as activated carbons[106-108] and carbon molecular sieves.[109,110] CO_2 adsorption at 273 K enables the diffusion of CO_2 molecules into narrower pores than cannot be probed by N_2 at 77 K.[111,112] The CO_2 adsorption/desorption isotherms can be analyzed by NLDFT or GCMC (grand-canonical Monte Carlo) methods (**Figure 7**).[108,113] The models assume carbon materials with slit pores, which is not ideal but provides a reasonable estimate of the microporosity.[100]

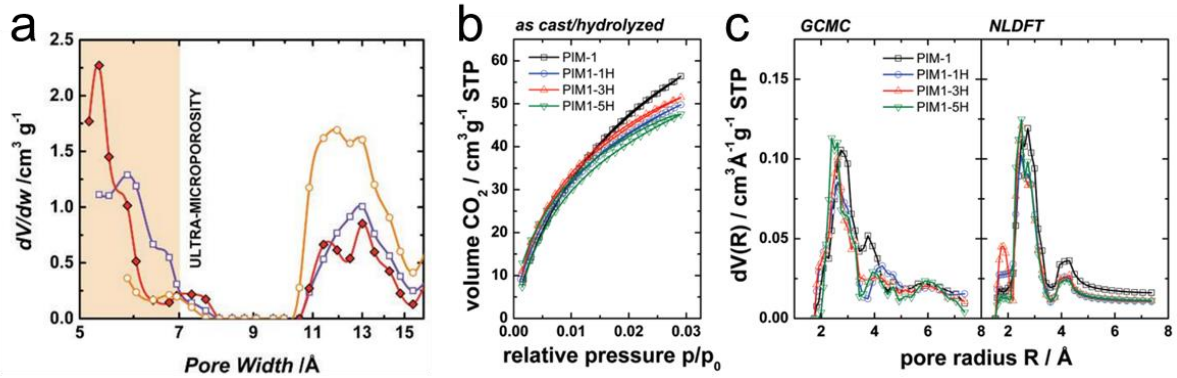

Figure 7. Examples of (a) N_2 sorption based NLDFT-analyzed pore-size distributions of **PTMSP** (yellow), **PIM-1** (purple), and **KAUST-PI-1** (red). Reproduced with permission from Ref. [98]. Copyright 2018 American Chemical Society. (b) CO_2 sorption isotherms of **PIM-1** and hydrolyzed **PIM-1** and (c) corresponding pore-size distributions obtained by GCMC and NLDFT methods. Reproduced with permission from Ref. [100]. Copyright 2018 American Chemical Society.

4.4. ^{129}Xe NMR spectroscopy

The use of ^{129}Xe NMR spectroscopy is based on the chemical shift of ^{129}Xe nuclei that is sensitive to the local environment of the material or the size of the microcavity hosting it. Therefore, the size of the FVE can be determined; the larger the FVE, the smaller the chemical shift of ^{129}Xe relative to the gas phase. The chemical shift of ^{129}Xe atoms sorbed into a nanoporous medium in the absence of paramagnetic particles that form local electrostatic fields can be presented according to Fraissard and Ito as:[114]

$$\delta_{\sum} = \delta_o + \delta_g + \delta_{Xe/Xe} \times \rho$$

where $\delta_{\sum}$ is a sum of the reference value (δ_o), the chemical shift related to the collisions with the wall (δ_g), and the product of the chemical shift related to collisions of Xe molecules in gas phase ($\delta_{Xe/Xe}$) and density of the gas phase (ρ).[79]

By extrapolating the $\delta_{\sum}$ value to zero pressure of Xe gas, the difference $\delta = \delta_{\sum} + \delta_o$ characterizes only the collisions with the walls of the microcavity, which is represented by an empirical relationship based on the data for various zeolites [114]:

$$\delta = 499.1/(2.054 + \lambda)$$

where λ (Å) is the mean free path of a Xe atom in a microcavity. λ can be related to the diameter of either a spherical hole (D_{sp} (Å); where $\lambda = 1/2(D_{sp} - 4.4)$) or a cylindrical hole (D_c (Å); where $\lambda = D_c - 4.4$). The values of 2.054 and 4.4 are the radius of a Xe atom[79] and atomic diameter of Xe according to Breck,[115] respectively.

This method has been used in studies of the size of microcavities in zeolites[114] and polymers having widely varying chemical structure and properties.[116,117] ^{129}Xe NMR has been applied to **PIM-1** and a PIM copolymer incorporating ethanoanthracene units, and results are compared to data from PALS, N_2 sorption and Xe sorption.[90]

4.5. Molecular modeling

Molecular modeling techniques have been widely used in the past to obtain a deeper insight into the structure and the transport behavior of nonporous amorphous polymer membranes.[84] When applied to glassy polymers with high free volume, a molecular modeling approach also permits a more detailed insight into free volume distributions. Both force field-based molecular mechanics and molecular dynamic (MD) methods have been applied to predict the permeation properties of small gases, to calculate N_2-sorption isotherms and to determine free volume distributions of high free volume polymers of interest such as **PTMSP**[84] and PIMs. [9]

MD simulation appeared to be the most efficient method for simulation of the free volume in amorphous polymers. In MD simulation of an amorphous polymer, the free volume is defined using a cuboid of certain size filled with polymer chains.[92] The cuboid will usually contain 2000 to 10000 atoms in the polymer chain to produce reliable results.[118] All the atoms in the polymer chains are represented by spheres of defined diameters and masses, with interactions of covalently bonded atoms and non-covalent intermolecular interactions described. Both 'United Atoms' and 'All-atom Strategy' can be used, where the former strategy benefits from lower computation time but produces less reliable results. The sum of all atom-atom interactions is known as the force field and should reproduce the equilibrium structure, thermodynamics and dynamic properties of the polymer.[92,119]

Different approaches have been used in MD simulations in order to produce reliable results within reasonable computation time. For example, an efficient box-filling procedure can be used in which a propagating virtual chain that reaches and starts

to ‘penetrate’ a face of the cuboid will introduce a similar propagating chain on the opposite face, until the cuboid is filled to a pre-set density of the polymer. A more realistic packing often requires an additional stage of the process, i.e., a relaxation stage. An example of a procedure to accelerate relaxation is to introduce plasticizer such as methanol into the cuboid, which is later removed upon polymer relaxation.[120,121]

4.6. Scattering methods

Scattering methods, such as small angle x-ray scattering (SAXS) and wide angle x-ray scattering (WAXS) or x-ray diffraction (XRD), are among the most commonly used techniques in the analysis of porous materials, although they are less straightforward to use and interpret for amorphous polymers.[122] However, these techniques have been proven useful for estimating the “pore size” of PIMs down to 0.5 Å.[101,123-127] It is thought that these *d*-spacings (calculated from Bragg’s law) can be related to either interchain or intersegmental distances, which define the pore dimensions in PIMs.[128,129] Features in WAXS patterns from amorphous polymers are typically limited to one or two amorphous halos, while in PIMs they typically include several broad peaks (**Figure 8**).[100,127]

One advantage of scattering methods is the ability to analyze the pore dimensions with respect to parameters such as temperature and pressure. For instance, in the work of Weber *et al.*,[100] the FVE size of carboxylated PIM was increased by breaking the inter- and intramolecular hydrogen bonds at elevated temperature (**Figure 8a**). The sensitivity of scattering patterns to time, temperature, film thermal history and

film thickness is also shown qualitatively to be consistent with physical aging of PIM (**Figure 8b,c**).[127,129]

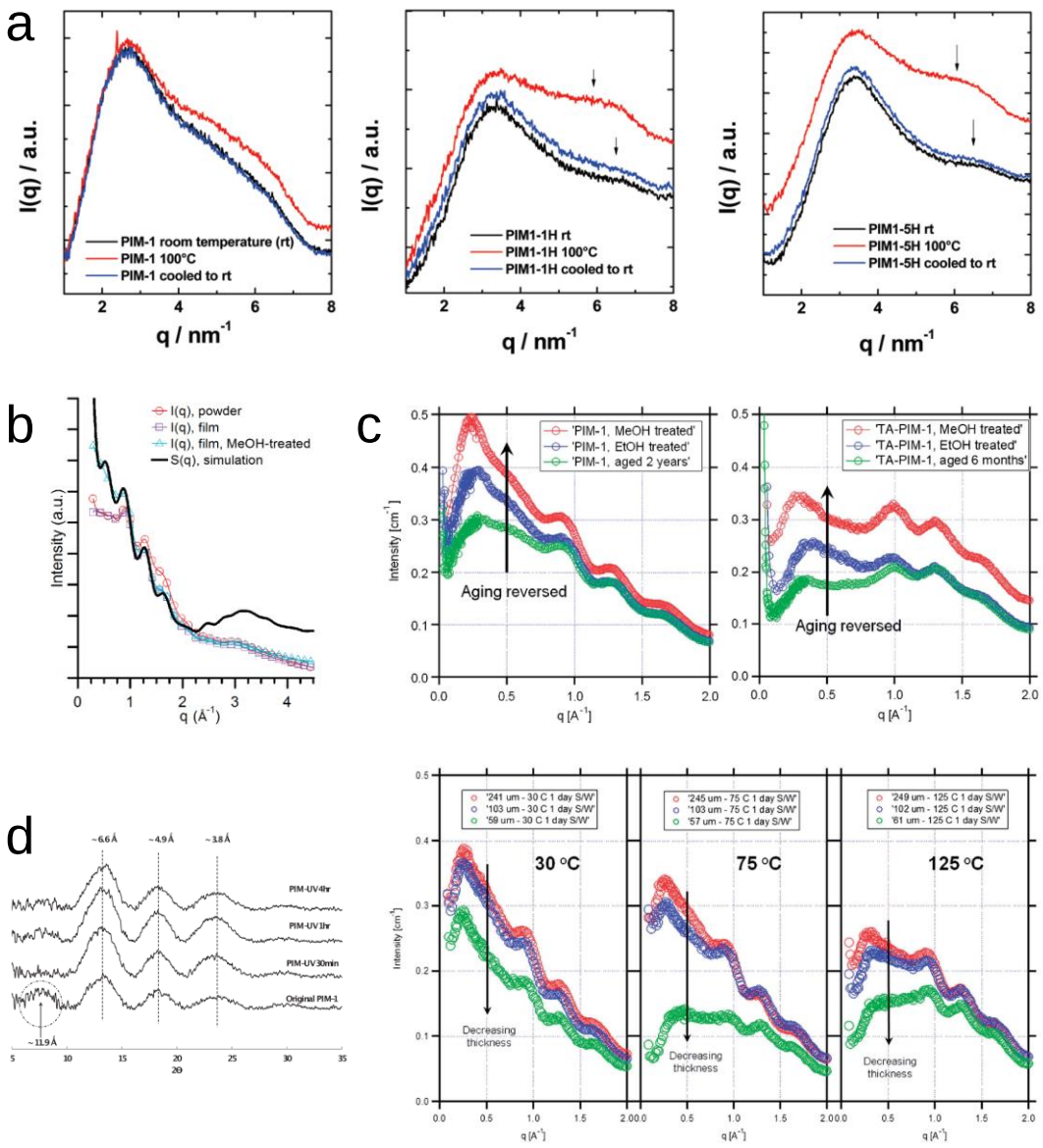

Figure 8. (a) SAXS patterns of **PIM-1** (left), 1-h hydrolysed **PIM-1** (**PIM1-1H**), and 5-h hydrolysed **PIM-1** (**PIM1-5H**), before and after heating to 100 °C. Reproduced with permission from Ref. [100]. Copyright 2017 American Chemical Society; (b) simulated and experimental WAXS intensity of **PIM-1** samples in powder and film form. Reproduced with permission from Ref. [129]. Copyright 2017 American Chemical Society; (c) Combined SAXS/WAXS patterns of **PIM-1** with different sample histories.

Reproduced from Ref. [127] with permission from The Royal Society of Chemistry; (d) XRD analyses of **PIM-1** and UV-irradiated **PIM-1**. Reproduced from Ref. [130].

4.7. Summary

A summary of the methods for determining size and size distribution of free volume elements of PIMs is tabulated as Table 2.

Table 2. Methods for determining size and size distribution of free volume elements of PIMs

Method	Probe	Size[a] (Å)	Information	Ref
Positron annihilation lifetime spectroscopy	o-Ps	1.06	Size, size distribution, concentration, temperature-dependence, pressure-dependence, and mechanical deformation of the FVE	[79,92]
Inverse gas chromatography	Organic vapours (e.g., n-alkanes)	> 5	Temperature-average mean size of the FVE	[79,92]
Physisorption	Most common: N_2 and CO_2	> 4.5	Size, size distribution of the FVE	[95,102]
^{129}Xe NMR	^{129}Xe	3.2 – 4.6	Size and temperature-dependence of the FVE	[79,92]
Molecular modeling	-	-	In addition to information provided by probe methods, molecular modeling provides visualization of the free volume, analysis of connectivity of FVE, construction of FVE size distribution and dynamic studies of the FVE.	[84,118,121]
Scattering	x-ray	0.5	Size, temperature-dependence and pressure-dependence of the FVE	[101,123-127]

[a]*Size refers to the smallest cavity size that can be probed.*

5. Laboratory practices for measuring gas permeability and aging

5.1. Gas permeability measurement

Measurement of the gas permeability of a glassy polymer is often performed by one of the following three methods: (1) Constant-pressure variable-volume method, (2)

constant-volume variable-pressure method (also known as the time-lag method), and (3) mixed gas method (**Figure 9**). The constant-pressure variable-volume method is most suitable for the study of polymeric films with high gas fluxes, such as **PTMSP** and PIMs, due to the limited sensitivity of the bubble flowmeter. The constant-volume variable pressure method uses a pressure transducer to monitor the pressure increase of collected permeate gas in a closed volume and is suitable for all types of films. The mixed gas method follows principles similar to pure-gas permeability measurements but requires a detector (e.g. gas chromatography) to separate and measure the individual gas concentrations in the permeate stream. The same instrument can also be used for pure-gas studies. Common practice for aging studies involves measurements performed in both pure gas and binary gas mode to take account of the interaction or competing effect between different gas molecules. The mixed gas method is recommended for its high sensitivity and capability to perform both pure and binary gas measurements. The constant-pressure variable-volume method is least recommended, due to its limited sensitivity.

Gas permeability measurement is usually performed after methanol soaking in order to reset the aging of the membrane. The removal of methanol is sometimes performed on the gas permeation apparatus under vacuum on the permeate stream at room temperature. This ensures that the gas permeation of the film is constantly monitored, such that the reading can be obtained at the beginning of the aging of the film. Other practices include heating the methanol-soaked film at elevated temperature under vacuum to first remove all the methanol in the film before measuring the gas permeation of the film.

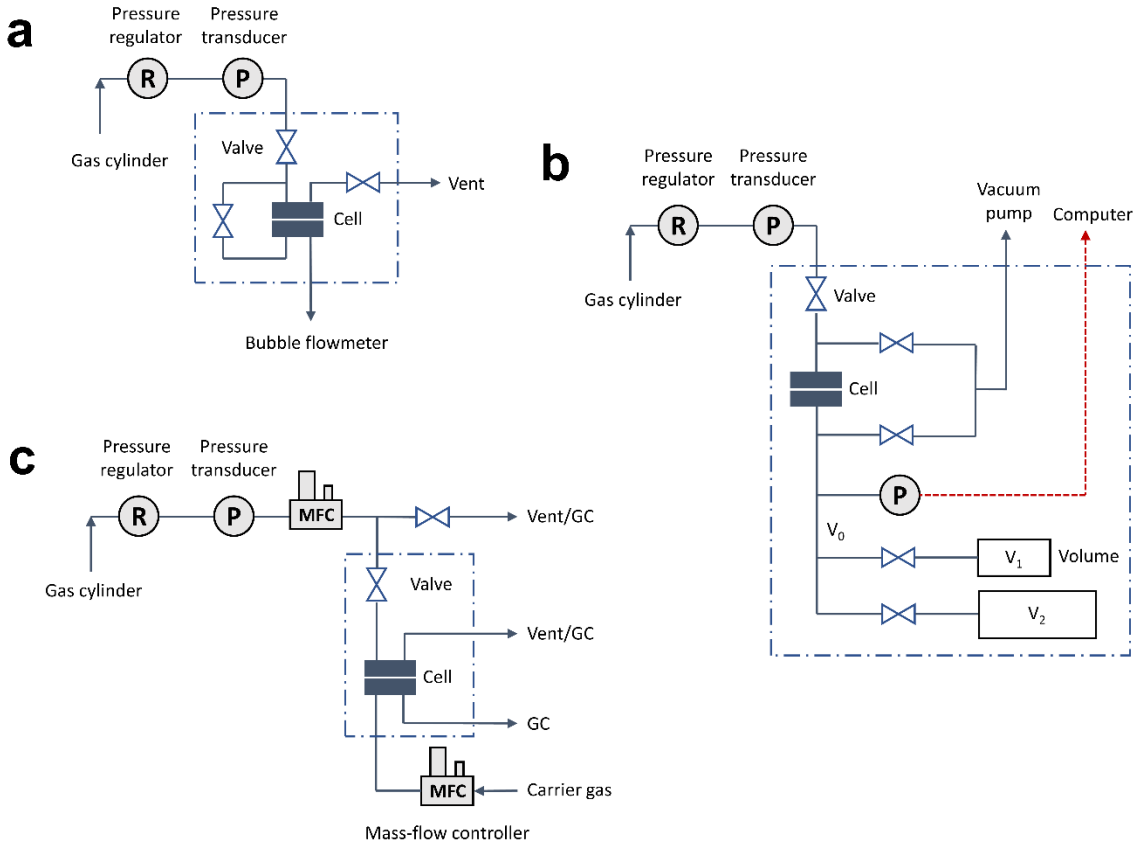

Figure 9. Schematic of (a) constant-pressure variable-volume apparatus, (b) constant-volume variable-pressure apparatus and (c) mixed-gas permeability apparatus for gas permeability measurement. The parts within the dashed box are in a temperature-regulated chamber. Adapted from Ref. [131].

Studies of membrane aging have been performed using various methods. The most commonly used method is to age the glassy membrane in air for a fixed period of time. It has been found that the aging rate is highly dependent on the thickness of the film.[45,132-136] For example, Paul's group performed a systematic study of the physical aging of polysulfone and Matrimid® membranes of various thicknesses, from ~20 to ~500 nm, in a dry environment, measuring their gas permeabilities. It was previously observed that thin glassy polymer films, less than 1 μm in thickness, exhibit dramatically faster physical aging relative to bulk behavior (i.e. thick film).[132-

[134] When the membrane thickness was further reduced to ~20 nm, the permeability of these films reduced to ~30–50% of their initial value after 1000 h, significantly more than the 10% decrease reported for bulk films at similar aging times.[135] Likewise, more rapid aging was also observed for thin **PIM-1** film.[45] A study on **PIM-1** films with thickness of less than 1 μm reveals that aging is nearly complete after three months.[136] Such studies are important in predicting the long-term permeation properties of gas separation membranes. Commercially useful membranes are generally asymmetric or thin film composite membranes with very thin separation layers, so future research will need to focus on thin films, rather than the relatively thick membranes that have been the subject of most of the aging studies reported to date. In very thin films, rapid aging may be a positive advantage, leading to stable membranes with favorable properties in a relatively short time. At similar thickness of film, polymers with high free volume (such as **PTMSP** and PIMs) undergo a much more rapid physical aging when compared to the traditional glassy polymers.

Gas permeation in glassy polymers usually follows the solution diffusion model,[137] or the dual-sorption–dual-mobility model,[138] and aging effects are generally reversible within reasonable time periods.[139] In certain cases, the membrane is swollen by highly soluble penetrants such as CO_2. CO_2 tends to plasticize glassy polymers, a process in which the polymer chain segmental mobility is increased by the sorption of the plasticizing penetrants, thus increasing the permeability and reducing the separating efficiency of the membrane.[140-142] Plasticization is not immediately reversible and the effect is sometimes referred to as “conditioning” (the polymer does not return to its initial state after the removal of the plasticizing molecules).[143] Hence, aging studies of polymers is sometimes carried out without introducing CO_2 to the systems.[26,144] However, there is some evidence that aging of a polymer film may

occur more rapidly in the presence of CO_2 (e.g., amine-modified **PIM-1**[70] and 6FDA-based polyimide[145]). Over a long exposure time at low pressure, the aging effect will eventually dominate over the plasticization effect.[45] Understanding the effect of plasticization (and its effect on membrane aging) is important in industrial membrane applications.[139] **Table 3** shows various examples of methods of aging and plasticization for glassy polymer membranes.

Table 3. Examples of methods of performing and measuring aging for conventional and high free volume glassy polymer membranes.

Membrane	Aging environment	Temperature (°C)	Pressure	Duration	Ref
Conventional glassy polymers					
Polysulfone	Dry air	35	atm	Up to ~83 days	[144]
Matrimid® 5218					[144]
6FDA-6FpDA	air	RT			[26]
6FDA-DAM					[26]
6FDA-6FpDA:-DABA 2:1					[26]
6FDA-DAM:-DABA 2:1					[26]
High free volume glassy polymers					
PIM-1	air	RT	plastic bag in a dark place	370 days	[146]
PIM-1	air	RT	Polyethylene bag	118 and 293 days	[136]
PTMSP, PMP, PIM-1	air	RT	atm	240 days, 365 days, and 400 days	[22,101,147]
PIM, PIM-PI	Sealed plastic bag	RT	atm	100, 150, 200, 273, 470, 660, 720, 780, 870, 1380 days	[59]
PIM-1	air	RT, 30, 75, 125	vacuum	1 and 13 days	[127]
UV-rearranged PIM-1	H_2, O_2, N_2, CH_4	35	3.5 atm	100 days	[148]
PTMSP	Air	RT	atm	~9–17 days	[132]
PIM-EA-TB	Air	RT	atm	100, 470 days	[60]
TPIM	Air	120	vacuum	14 days	[96]

PIM-TMN-Trip	Air	RT or 120	atm	14, 39, 365 days	[149]

5.2. Methods of rejuvenation

The gas separation performance of traditional glassy polymers, such as polysulfone (PSf) and polyimide (PI), can be recovered by heating the sample to temperatures above the glass transition temperature (T_g), followed by rapid quenching to room temperature. However, this is not practical for high free volume polymers such as **PTMSP** and PIMs, due to very high or undetectable T_g. To recover the gas transport properties of high free volume polymers, the films are soaked in a non-solvent such as methanol.[59,62,74,136,146,150,151] Such a step also frees up pores previously occupied by the trapped solvent(s) used for film preparation. After methanol soaking, the film may be heated under vacuum to remove the methanol. **Table 4** summarizes a list of the common methods for recovering the gas transport properties of conventional glassy polymers and high free volume polymers.

Table 4. Methods of recovery of gas transport properties.

Membrane	**Method**	**Ref**
Conventional glassy polymers		
PPO	Annealed at 15 °C above T_g in N_2, rapidly quenched to room temperature	[139]
Matrimid® 5218		
PSf		
PEI		
High free volume glassy polymers		
PIM-1	Immersed in ethanol and heated in vacuum oven	[127]
	Heated overnight in high vacuum at 120 °C	[90]

	Reprecipitated	[90]
	Treated in Xe at 100 °C and 3 bar	[90]
PIM-1, TZPIM	Boiled in water (with HCl, pH = 4 – 5), washed in water, and subsequently soaked in methanol and dried in a vacuum oven at 120 °C for 24 h	[69]
PTMSP, PIM-1	Immersed in methanol and heated in vacuum oven (120 °C for 24 h under vacuum)	[59,74,136,146,150]
PIM-EA-TB	Immersed in methanol or ethanol and aging in air or under vacuum in time-lag apparatus	[151]

5.3. Summary

In studies of aging in conventional and next generation glassy polymeric membranes (including PIM membranes), a variety of protocols have been used. PIM films were mostly aged at room temperature and atmospheric pressure, while limited studies were performed at elevated temperature and at pressures other than atmospheric. There is no standardized aging protocol to allow the determination and reasonable comparison of the effectiveness of each approach. While it is undeniable that physical aging would occur regardless of the environment in which the membrane is housed, the aging protocol could be done more effectively or more closely to the conditions of the actual gas separation process where the aging occurs (at high pressure, at high temperature, in thin films and/or in a gas mixture). This is particularly important for high free volume polymers such as PIMs, where aging in thick films under room temperature conditions continues to take place for many years. A more rapid aging protocol would be beneficial in screening suitable approaches when designing such membranes for gas separation.

6. Approaches to prevent and/or minimize aging

Various approaches have been taken to improve the aging resistance of high free volume polymers, including polymer backbone design, post-synthetic modification, crosslinking, heat treatment, blending of nanomaterials, and combinations of the above methods. The approaches generally target the rigidity of the polymer chain, the interchain spacing and interchain interactions to reduce aging effects, as indicated by changes in permeability over time. **Figure 10** is an illustration of the approaches to solving the aging problem. Gas transport properties are included at the end of the section, in **Table 5**, for the important membranes (focusing on PIMs and PIM-PI membranes) discussed below.

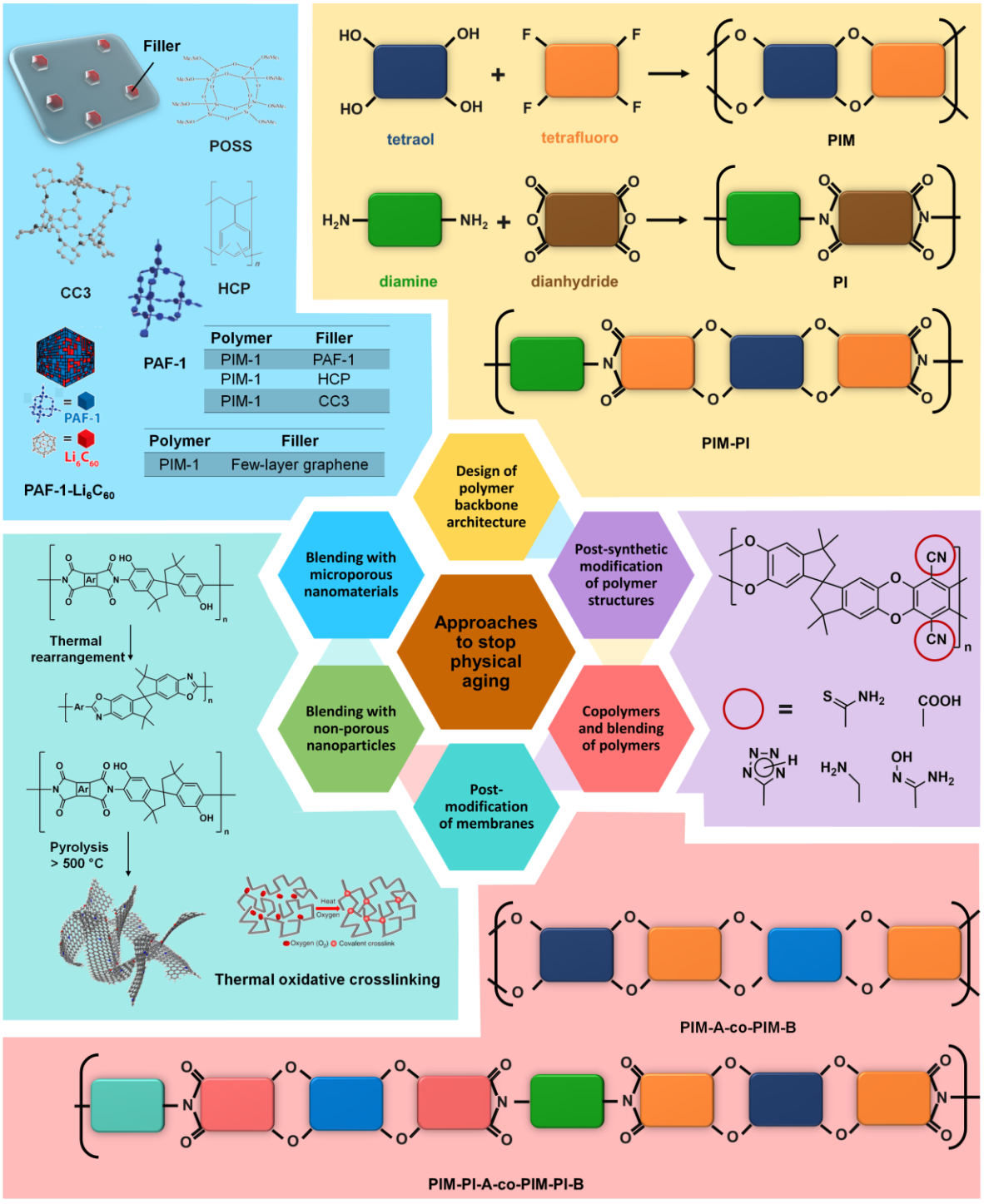

Figure 10. Methods to stop physical aging. Some images were adapted with permission from Ref. [147]. Copyright 2017 American Chemical Society; Ref. [152]. Copyright 2017 Elsevier; Ref. [153]. Copyright 2017 Nature Publishing Group, Ref. [154]. Copyright 2018 American Chemical Society; Ref. [155]. Copyright 2018 John Wiley & Sons.

6.1. Design of polymer backbone architecture

6.1.1. PIMs

Ever since the discovery of the promising properties of **PIM-1** and **PIM-7** for gas separation, there has been continuing effort to create PIMs or PIM-like polymers, with improvements not only to gas permeability and selectivity, but also to aging resistance of the membrane.[5] Early approaches led to the synthesis of **PIMs-1–6**,[5] **PIMs-7–10**[156] and **Cardo-PIMs 1** and **2** (**Figure 11**).[156] One approach to achieving even higher performance enhancement is by designing polymers with greater shape persistence, as suggested by Freeman's theoretical analysis of the position of the Robeson upper bounds.[157]

Following this approach, McKeown and coworkers replaced the relatively flexible spirobisindane (SBI) component of archetypal **PIM-1** with the more rigid spirobifluorene unit (**PIM-SBF**), achieving gas permeability-selectivity combinations above the 2008 Robeson upper bounds for most gas pairs.[158] However, **PIM-SBF** still inherited the flexibility arising from the spiro-centers and dioxane linking groups used to assemble these PIMs.[89] Thus, a fundamental structural redesign of PIMs was necessary to achieve high free volume polymers with significant increases in rigidity and resulting performance.[61] The same group a year later prepared a new highly shape-persistent PIM based on Tröger's base (TB) and ethanoanthracene (EA), both inflexible and rigid compared to their counterparts (dioxane and SBI).[61] The result, **PIM-EA-TB** (**Figure 11**), exhibited excellent gas separation performance, well above the 2008 Robeson upper bounds for most gas pairs, due to its enhanced diffusivity selectivity of smaller gas molecules (He = 2.69, H_2 = 2.89, and O_2 = 3.46 Å) over those with larger diameters (CO_2 = 3.3, N_2 = 3.64, and CH_4 = 3.87 Å). The enhanced performance relative to the upper bound is remarkable for gas pairs with

H_2 (**Figure 12**). Interestingly, the more rigid **PIM-EA-TB** showed signs of faster aging, where O_2 permeability dropped by more than 50% after 3 days, but with commensurate increase in O_2/N_2 selectivity.[61] The results indicate that a more rigid polymer chain does not always translate into more restricted polymer chain movement on the larger scale associated with physical aging. Other factors, such as interchain rigidity (arising from interchain interactions) and interchain spacing (result of polymer chain packing) are equally important.[159]

Noticing the less restrictive polymer chain mobility of **PIM-EA-TB** (evident from the rapid loss in O_2 permeability) and conceivably less than the ideal gas selectivity of the EA unit, due to the turnstile-like rotary thermal motion of the methyl substituents at the bridgehead of the EA unit, which facilitate the transport of larger gas molecules through smaller FVEs, McKeown's group replaced the EA unit with triptycene, commonly used to generate free volume and intrinsic microporosity,[160,161] yielding **PIM-Trip-TB** (**Figure 11**).[60] The use of triptycene was anticipated to maintain inter-chain distances, and improve the gas selectivity of **PIM-EA-TB**. The ideal selectivities for **PIM-Trip-TB** were significantly higher than its counterpart, **PIM-EA-TB**, for some gas pairs (O_2/N_2, CO_2/CH_4 and CO_2/N_2), whilst being similar for other gases (H_2/N_2, H_2/CO_2 and H_2/CH_4). In this work, **PIM-Trip-TB** and **PIM-EA-TB** were aged for 100 days and 470 days, respectively, to compare the long-term gas separation performance of the two PIMs. Both membranes showed enhanced performance after aging, especially for O_2/N_2 and H_2/N_2 gas pairs (where the position on the corresponding Robeson plot moves away from the upper bounds after aging, **Figure 12**). Interestingly, **PIM-EA-TB** showed a slower aging rate than **PIM-Trip-TB**, as indicated by the similar drop in gas permeability but at a much later time (470 days).[60]

Anomalously, the position of **PIM-EA-TB** on the O_2/N_2 Robeson plot after 470 days aging did not deviate much from the original work (after 3 days aging, **Figure 12**).[61] This could be explained by rapid aging in the first week after film conditioning with a non-solvent like methanol. This time-dependent rapid gas permeation loss in the first two weeks was also independently investigated for other PIMs by Pinnau and coworkers.[162] It was proposed that the permeability for a PIM is most appropriately reported at an "aging knee" when the non-equilibrium free volume trapped by casting and solvent exchange steps relaxes, i.e. quasi-steady-state. At such a state, the change in the transport properties is small on the experimental time-scale.[162] This would allow a better comparison of transport properties and also of resistance to aging.

The McKeown group also confirmed the additional interchain distance created by the propeller-like structure of the triptycene, using an extended benzotriptycene monomer, **PIM-BTrip-TB** (**Figure 11**).[67] **PIM-BTrip-TB** showed similar BET surface area to that of **PIM-Trip-TB** (870 to 899 $m^2\ g^{-1}$) but with lower CO_2 adsorption (3.0 mmol g^{-1} at 1 bar/273 K as compared to 4.0 mmol g^{-1} reported for **PIM-Trip-TB**[60]). **PIM-BTrip-TB** also demonstrated enhanced permeability for all gases as compared to **PIM-Trip-TB**, due to the anticipated higher free volume created by the extended triptycene unit. Physical aging of **PIM-BTrip-TB** for 166 days led to a decrease of gas permeability (e.g. P_{O_2} falls from 3290 to 1170 Barrer) with an increase in gas selectivity, yielding data points significantly above the 2008 upper bound (**Figure 12**).[67]

Cardo-polymers based on TB polymerization were prepared.[65] Six different polymers were studied and only one (**TB-Ad-Me**) possessed intrinsic microporosity, with an apparent BET surface area of 615 $m^2\ g^{-1}$ (**Figure 11**). Overall, the gas permeabilities

for **TB-AD-Me** were lower than for other PIMs discussed above, reflecting the lower BET surface area. After aging for six months, gas permeabilities decreased with proportional increase in the selectivities, but were consistently lower than the 2008 upper bound.[65]

Hexaphenylbenzene (HPB), which is a rigid propeller-like shaped structural unit, was also used to prepare PIMs, yielding **PIM-HPB-1** and **PIM-HPB-2**.[163] However, only **PIM-HPB-2** was able to form robust, optically clear self-standing films.[163] Different substituents (CH_3, Br, and CN) were also designed onto the HPB unit of **PIM-HPB-2**. **PIM-HPB-2** with CH_3 substituents showing a higher BET surface area of 560 m^2 g^{-1}, while **PIM-HPB-2** with Br and CN substituents showed reduced BET surface areas of 410 and 440 m^2 g^{-1}, respectively. The CO_2 permeability of the **PIM-HPB-2** is affected by the substitution and decreases as follows: **PIM-HPB-2** > **PIM-CH_3-HPB** > **PIM-CN-HPB** > **PIM-Br-HPB**. However, both aged and fresh PIM-HPBs exhibited gas permeability-selectivity data points well below the 2008 upper bound.[164]

Pinnau and co-workers [96] synthesized two triptycene-based ladder polymers, **TPIM-1** and **TPIM-2**, which contain triptycene moieties substituted with either branched isopropyl or linear propyl chains at the 9,10-bridgeheads (**Figure 11**). The two polymers have unprecedented gas permeability/selectivity combinations, significantly transcending the upper bounds for H_2/N_2 O_2/N_2, and H_2/CH_4 separations. **TPIM-1** and **TPIM-2** were aged for 780 and 720 days, respectively. After aging, both **TPIM-1** and **TPIM-2** showed significant improvement to gas transport performance; i.e. the gain in selectivity is substantially higher than the loss in gas permeability, especially for the H_2/N_2 pair (**Figure 12**). This is because of the much faster decrease in N_2 permeability than H_2 permeability over time (~98% vs 74% decline since day 1) attributable to preferential contraction of larger FVEs over the smaller ones.[96]

Furthermore, **TPIM-1** gained ~60% more O_2/N_2 selectivity than **TPIM-2**, despite both losing ~95% of O_2 permeability. These observations indicate that physical aging in TPIMs considerably affected a narrow range of ultra-microporosity between 3.46 Å and 3.64 Å, due to its distinctive chain architecture and conformation of ribbon-like two-dimensional geometry of TPIM chains.[59] On another note, the drop in gas permeability in both new PIMs were among the highest in all PIMs thus far. The authors hypothesized that the chain structural design and conformation are also part of the cause in physical aging; that is, the unique ribbon-like two-dimensional geometry of TPIM chains may be more susceptible to more efficient packing than the more contorted and three-dimensional configurations of PIMs such as **PIM-EA-TB** and **PIM-1**. The aged **TPIM-1** showed the highest gas transport performance ever reported so far (especially in H_2/N_2 and O_2/N_2 separation, **Figure 12**).[96]

Very recently, building on the previous reports on high performance PIM membranes based on triptycene, two-dimensional ribbon-shaped, ultrapermeable polymers, **PIM-TMN-Trip** and **PIM-TMN-SBI,** were prepared (**Figure 11**).[149] The TMN substituents generate high BET surface area and FVE of 1050 $m^2\ g^{-1}$ and 31.4%, respectively, in **PIM-TMN-Trip**. The gas permeability of **PIM-TMN-Trip** is consistent with other triptycene-based PIMs used to define the 2015 upper bound.[21] **PIM-TMN-SBI** on the other hand, exhibits performance that resembles spirobisindane-based PIMs (2008 upper bound), but with enhanced gas permeability due to the TMN substituents. The enhanced performance of **PIM-TMN-Trip** is attributed to the greater 2D aspect ratio provided by the TMN substituents. The gas permeability of **PIM-TMN-Trip** decreases on aging, with commensurate increases in gas selectivity, especially for O_2/N_2, as shown by **PIM-TMN-Trip** with different film histories (**Figure 12**). Furthermore, the thermal stability of **PIM-TMN-Trip** was also demonstrated from mixed gas

permeation tests at 100 °C and 200 °C. The importance of the 2D chain structures were confirmed by preparing **PIM-TMN-Trip-TB** within which the TMN-triptycene units are linked together using Tröger's base to give a 3D structure. It was demonstrated that ultrapermeability is achieved with 2D **PIM-TMN-Trip**, but not with 3D **PIM-TMN-Trip-TB**.[149]

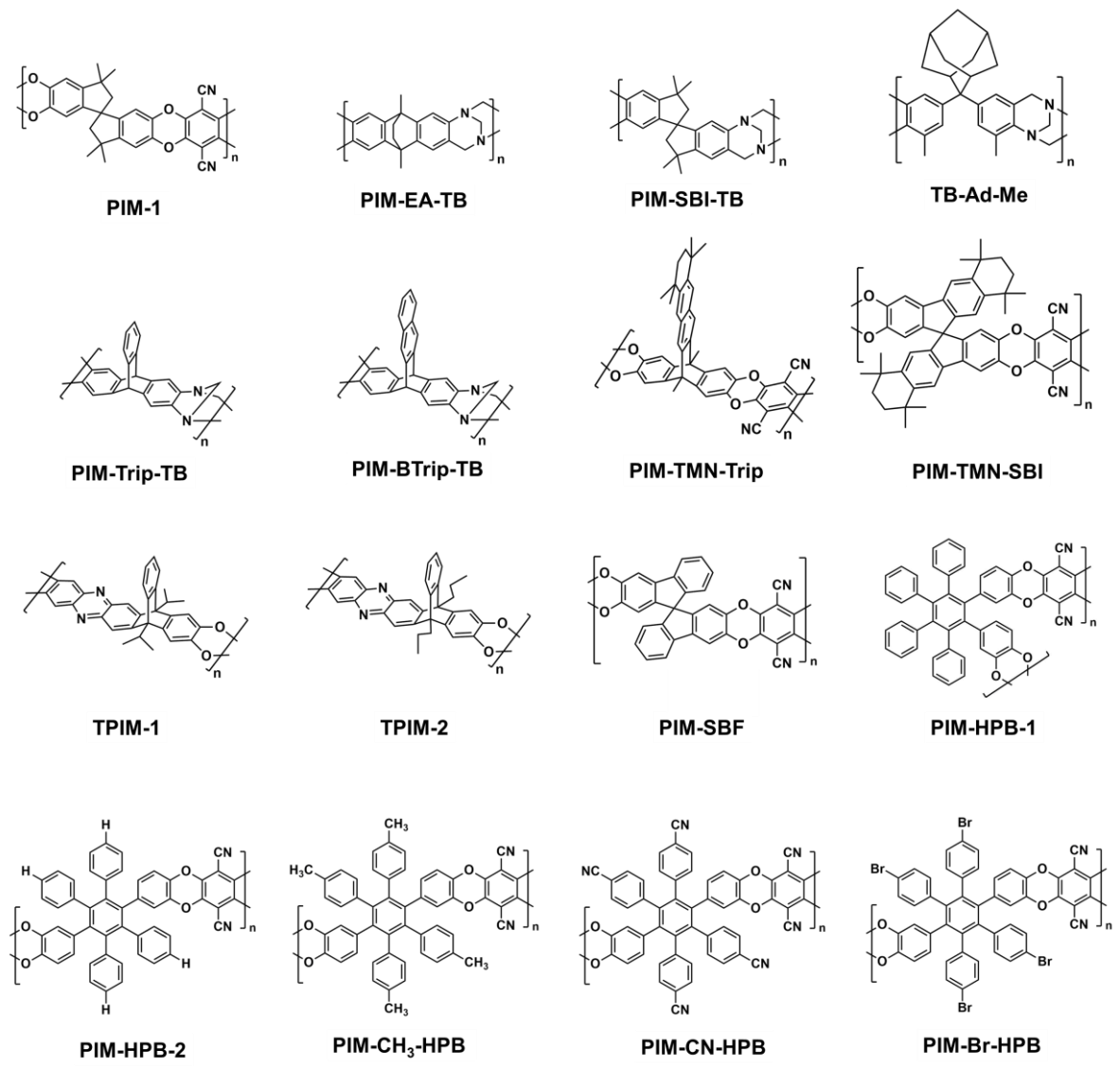

Figure 11. Chemical structures of PIMs.

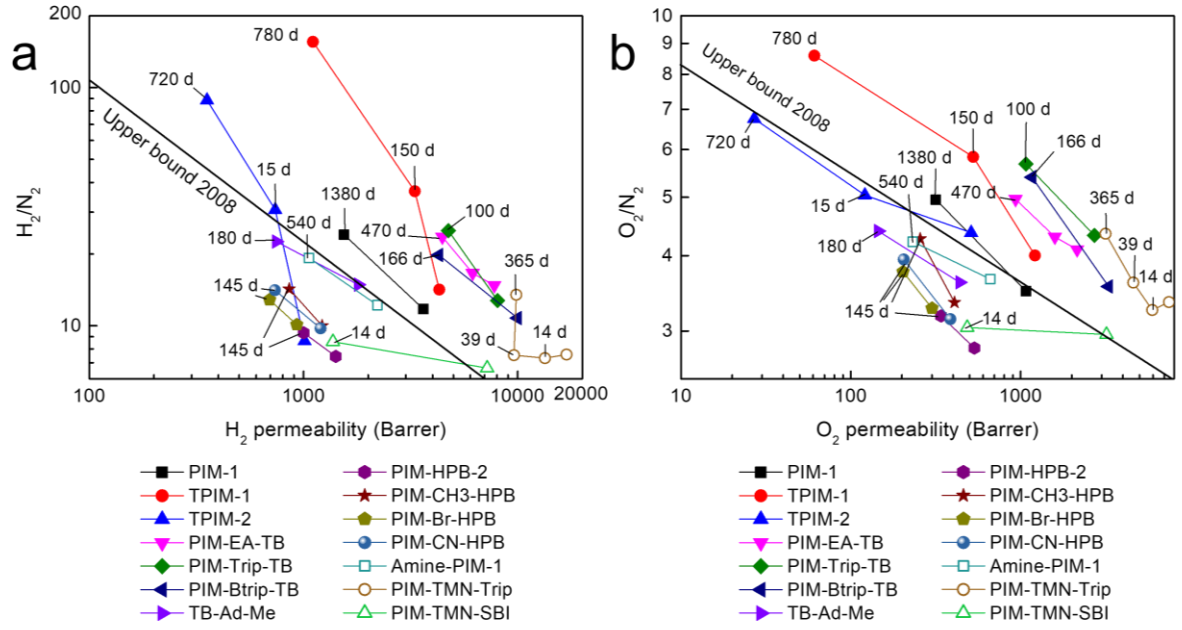

Figure 12. Double logarithmic Robeson plots of selectivity versus the permeability of the fastest gas, for the gas pairs (a) H_2/N_2 and (b) O_2/N_2, showing the effects of aging of PIMs.

6.1.2. PIM-PIs

Following the success of PIMs, a different class of polymer based on the concept of intrinsic microporosity was introduced based on the well-established synthesis of polyimides but with monomers that create microporosity and restrict rotation about the imide linkage, yielding polyimides of intrinsic microporosity (PIM-PIs).[165] PIM-PIs are designed by either tailoring the dianhydride component[162,166-168] or the diamine component,[165,169-172] ultimately to improve gas transport performances.

Spirobisindane (SBI). PIM-PIs (**PIM-PI-1–8**) that are structurally akin to **PIM-1** (i.e. the presence of spirobisindane (SBI) and dibenzodioxane moieties) were systematically prepared and studied by Ghanem *et al.* (**Figure 13**).[165,169] A molecular modeling study has suggested that the dibenzodioxin units of **PIM-1** and these PIM-PIs (**PIM-PI-1–8**) are relatively flexible.[89] Thus, PIM-PIs (**PIM-PI-9–11**)[170] that lack

this structural unit were also prepared by McKeown and co-workers, to increase the backbone rigidity. The resulting PIM-PIs (**PIM-PI-9–11**) did not show significant differences from **PIM-PI-1–8**. However, it was shown that methyl groups adjacent to the imide linkage severely restrict the rotation about the C–N bond (in **PIM-PI-9** and **PIM-PI-10**), giving higher permeability than that without methyl groups (**PIM-PI-11**).[170] Subsequent work from the same group showed that replacing the SBI component in **PIM-PI-10** with EA significantly improved gas separation performances.[167] Compared to **PIM-PI-10**, the new **PIM-PI-EA** (**PIM-PI-12**) showed enhanced permeability for smaller molecules such as H_2 and CO_2 and much lower permeability for larger molecules such as CH_4, demonstrating the superior molecular sieving of the rigid EA unit as a component for inducing high gas selectivity. Furthermore, the aged **PIM-PI-EA** (after 273 days) showed remarkable gas pair permeability-selectivity, well above the upper bounds, especially for the O_2/N_2 gas pair (O_2/N_2 of 5 and $P_{O2} > 600$ Barrer; **Figure 14**). Such an aging route is desirable as the gain in gas selectivity far outweighs the loss in gas permeability (% permeability drop of H_2, O_2 and N_2; 32.4%, 52.2% and 64.5%, respectively, after 273 days).[167]

Pinnau and coworkers[172] designed SBI-based diamine monomers containing hydroxyl groups, from which two types of hydroxyl-functionalized PIM-PIs were prepared (**PIM-6FDA-OH** and **PIM-PDMA-OH**). The presence of hydroxyl containing spirocenters enabled the polyimide to be soluble in most common organic solvents, such as THF, acetone and ethyl acetate, compared to traditional polyimides that are only soluble in strongly polar aprotic solvents (i.e. DMF, DMSO and N-methyl-2-pyrrolidone (NMP)). The films have much lower gas permeability and higher gas selectivity (especially CO_2/CH_4) compared to **PIM-1** but remain more permeable than

conventional OH-containing polyimides. The improved CO_2/CH_4 selectivity is the result of the enhanced affinity of the polymers to CO_2 molecules by the polar OH groups. Both films also showed fairly stable separation of CO_2/CH_4 in a binary gas test (>20 at 20 bar), indicating significant enhancement in resistance to plasticization.[172]

Spirobifluorene (SBF). Pinnau and coworkers [173] studied a series of SBF-based PIM-PIs (**6FDA-SBF**, **PMDA-SBF**, and **SPDA-SBF**) and their corresponding brominated counterparts (**6FDA-BSBF**, **PMDA-BSBF**, and **SPDA-BSBF**; **Figure 13**). The successful use of bulky SBF to create intrinsic microporosity was previously demonstrated,[124,158] while bromine substitution was known to improve the gas transport properties of polyimides.[174] The resulting films showed comparable results to other previously reported PIM-PIs, but remained below the Robeson 2008 upper bound (**Figure 14**). Nevertheless, it was verified that bromination of SBF leads to the formation of films with a higher BET surface area and gas permeability, coupled with a slight drop in gas pair selectivity.[173] Pinnau and coworkers[168] also investigated the pairing of a SBF unit and 3,3'-dimethylnaphthidine (DMN). DMN-based PIM-PIs were previously reported to exhibit excellent gas transport properties, especially for aged **PIM-PI-EA** (**PIM-PI-12**).[167] The new PIM-PI (**SBFDA-DMN**) showed a BET surface area of 686 $m^2\ g^{-1}$, that dropped to 608 $m^2\ g^{-1}$ after aging for 200 days. Before aging, gas transport performance was well below the Robeson 2008 upper bound, especially for O_2/N_2 (**Figure 14**). The 200 day aging of **SBFDA-DMN** improved the gas transport performance to a region above the upper bound, attributed to the shrinkage of pores larger than 10 Å, which increases the number of ultramicropores (<7 Å).[168] PIM-PI-EA remains the most successful DMN-based PIM-PI.

Tröger's base (TB). Tröger's base, a rigid V-shaped bridged bicyclic linking group, has been incorporated into a PIM to produce a highly permeable polymer membrane (**PIM-EA-TB**) with gas transport properties above the 2008 Robeson upper bound.[61] It provides a highly rigid site of contortion for suppressing the formation of coplanar molecular patterns and thus inhibits efficient interchain packing.[61] Following the success of TB as a moiety for PIMs, TB units were incorporated into polyimides to provide rigid PIs with intrinsic microporosity. Guiver, Lee and coworkers reported the synthesis and gas permeability of **PI-TB-1** and **PI-TB-2 (Figure 13**).[175] These polymers exhibited larger interchain distance than common polyimides derived from 6FDA and BTDA and have higher overall gas transport performances, indicating the effectiveness of TB in creating microporosity.[175] Subsequent synthesis of a series of PIM-PIs based on TB units (**PI-TB-3–5**,[176] **TBDA1–2,**[177] and **TBDA1–2-SBI-PI**[178]; **Figure 13**) confirmed the enhancement in gas transport performance.

An aging study of TB-based PIM-PIs was performed by McKeown and coworkers.[166] Four different PIM-PIs with TBs were prepared with four different dianhydrides (two from conventional polyimides (PDMA and 6FDA); and two with spirocenters (SBIDA, and SBFDA)). Unlike **TBDA1-SBI-PI** and **TBDA2-SBI-PI**, the SBIDA studied in this work does not possess benzodioxin units (resembling that of **PIM-PI-9–11** and not **PIM-PI-1–8**). Also, the novel TB-based PIM-PIs have a second methyl substituent adjacent to the two amino groups on the TB monomer (**Figure 13**). The four new TB-based PIs showed good solubility, excellent thermal stability and high BET surface areas (584–739 m^2 g^{-1}). Both PIM-PIs with spirocenters (**TBDA-SBIDA**, **TBDA-SBFDA**) showed gas separation performances near the 2008 Robeson upper bound, while PIM-PIs (**4MTBDA-PMDA**) prepared with a simple pyromellitic anhydride (PMDA) exceeded the upper bound for O_2/N_2, H_2/N_2 and H_2/CH_4 (**Figure 14**).

Furthermore, **4MTBDA-PMDA** aged along the upper bound, maintaining its gas transport competitiveness after 330 days.[166] Comparing the results from the work of Guiver *et al*.,[175,176] Jin *et al*.[177,178] and McKeown and coworkers,[166] the location, number and presence of methyl substituent in the diamine are key to producing ineffective packing of polymer chains that gives excellent gas transport properties.

Triptycene (Trip). Swager *et al*. prepared a series of soluble, thermally stable triptycene-based PIs (**Figure 13**).[179] TPI1 (named as **6FDA-DATRI** in [180] or **6FDA-DAT1** in [171]) and **TPI2** (**6FDA-DAT2**[171]) have been studied for their gas transport properties.[171,180] In the work of Cho and Park,[180] **6FDA-DATRI** exhibited gas transport performances below the 2008 Robeson upper bound for all gases (the upper bounds in Figure 4 of Ref. [180] are not from 2008). Remarkably, **6FDA-DATRI** showed excellent tolerance to CO_2 plasticization compared to other 6FDA-based PIs. This might be due to the pseudo-physical crosslinking by interlocking and π–π interactions in triptycene moieties.[180] In separate work, Pinnau and coworkers,[171] reported that the permeability and selectivity of **6FDA-DAT1** (which is the same chemical structure as **6FDA-DATRI**) could be modified using different polymerization protocols, film formation, post-treatment and permeation test conditions, optimized to lower permeability and increase selectivity. On the other hand, **6FDA-DAT2**, prepared using the same protocol as **6FDA-DAT1**, had higher permeability coupled with lower selectivity in comparison, due to less efficient packing caused by the additional benzene ring on the triptycene moiety. The gas transport performance of both **6FDA-DAT1** and **6FDA-DAT2** still fall below the upper bound, and deviate away from the upper bound after aging (**Figure 14**).[171]

High performing PIM-PIs based on triptycene were realized by integrating a three-dimensional 9,10-diisopropyltriptycene contortion center into a rigid fused-ring

dianhydride. Initially, two PIM-PIs were reported, **KAUST-PI-1** and **KAUST-PI-2**.[98] The triptycene moiety had a greater intramolecular rigidity (as demonstrated by the narrower energy wells in the dihedral angle distributions) and clear three-dimensional character from the design of the diamine that maintained inefficient packing leading to ultramicroporosity. Both **KAUST-PI-1** and **KAUST-PI-2** had higher BET surface areas (750 and 740 m^2 g^{-1}, respectively) than previously reported for a polyimide, and the most outstanding gas transport performance for a PIM-PI, well above the 2008 Robeson upper bounds for all gases (**Figure 14**). In particular, **KAUST-PI-1** showed the highest potential, as its gas separation performance far exceeded the 2008 Robeson upper bound. **KAUST-PI-2** also showed remarkable performance, but the enhancement from the triptycene moiety was less due to the more flexible backbone contributed by 3,3',5,5'-tetramethylbenzidine (TMBZ).[98] Having a more flexible backbone also resulted in more typical aging in **KAUST-PI-2** (870 days), with changes to gas transport properties parallel to the 2008 upper bound. The aged **KAUST-PI-1** (150 days) showed impressive selectivities, especially for H_2/N_2 and O_2/N_2 (**Figure 14**).[59]

Aging and plasticization studies were also performed for **KAUST-PI-5** (**TPDA-6FpDA**) and compared to **KAUST-PI-1**.[159] **KAUST-PI-5** has a high torsional freedom 6FpDA diamine, giving a lower BET surface area (500 m^2 g^{-1}) and lower initial gas permeabilities. Compared to **KAUST-PI-5**, **KAUST-PI-1** was more affected by plasticization, whereby its ultramicroporosity (around 3–4 Å) was more sensitive to CO_2-induced dilations, leading to increasing CO_2 and CH_4 permeability and a drastic decrease in CO_2/CH_4 selectivity with increasing CO_2 partial pressure. Furthermore, **KAUST-PI-5** possessed 6FpDA with bulky CF_3 groups, which increased interchain spacing, but was offset by the intrinsic flexibility of 6FpDA which promotes denser

chain packing, backbone coplanarization and consequently higher interchain interactions, as shown by the red-shift in its fluorescence excitation spectra and lower BET surface area than **KAUST-PI-1**.[159] It was recognized that interchain interaction plays a significant role in resisting plasticization.[59] Aging studies show that **KAUST-PI-5** loses its gas permeability and gains gas selectivity in return, in parallel with the Robeson upper bound, while **KAUST-PI-1**, as discussed earlier, has significantly improved performance, especially after aging.[159]

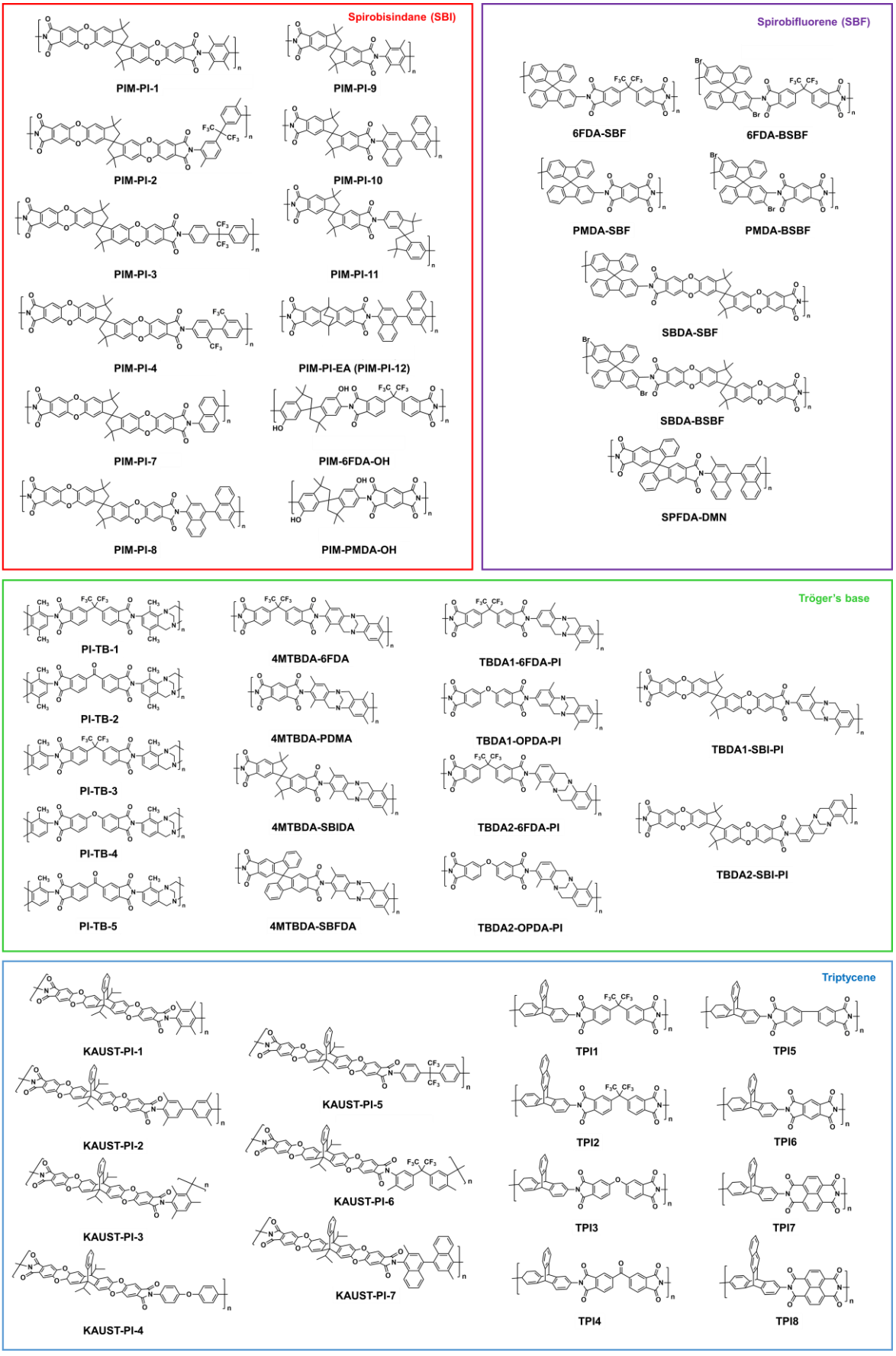

Figure 13. Chemical structures of PIM-PIs.

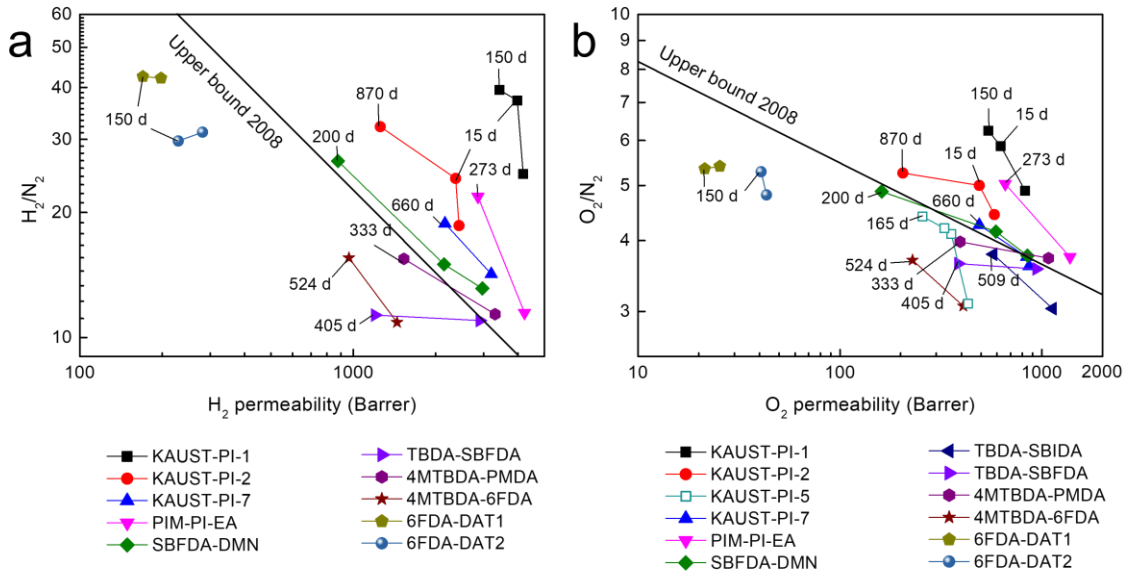

Figure 14. Robeson plots of PIM-PIs for (a) H_2/N_2 and (b) O_2/N_2.

6.2. Modification of polymer structures

6.2.1. PIMs

Various chemical post-modifications of **PIM-1** have been studied, including the conversion of the nitrile groups in **PIM-1** to carboxylic acid,[100,181] tetrazole,[69] thioamide,[182] amidoxime,[183] and amine (**Figure 15**).[70] Only one study involved the effect of post-modification on aging.[70] Mason *et al*.[70] studied the effect of reducing the nitrile groups in **PIM-1** to primary amines using borane complexes. Adsorption results indicated that **amine-PIM-1** had significantly higher CO_2 uptake than **PIM-1,** while gas permeation experiments showed that **amine-PIM-1** had higher H_2 permeability than CO_2, an evidence for the size-sieving ability of the polymer, also observed for the more rigid **PIM-EA-TB**[61] (Usually **PIM-1** has much higher CO_2 permeability owing to its high CO_2 solubility). The lower CO_2 permeability in **amine-PIM-1** can be explained by the very high affinity of **amine-PIM-1** for CO_2. Apparently, the stronger interaction reduces the CO_2 diffusion rate, outweighing the relative

increase in solubility, therefore producing an overall decline in CO_2 permeability. Ethanol treated **amine-PIM-1** showed a drop in gas permeability of ~65–75 % for O_2, N_2, CO_2, and CH_4; ~50% for He and H_2 after 18 months, but the gas permeabilities remained higher than an as cast **amine-PIM-1** without alcohol treatment. The aged membrane was methanol-treated to reverse the aging process and the gas permeability was even higher than before aging, with significant improvement in CO_2/N_2 and CO_2/CH_4 selectivities.[70] This was probably due to the higher effectiveness of the methanol compared to ethanol in restoring the permeability of PIMs.[74]

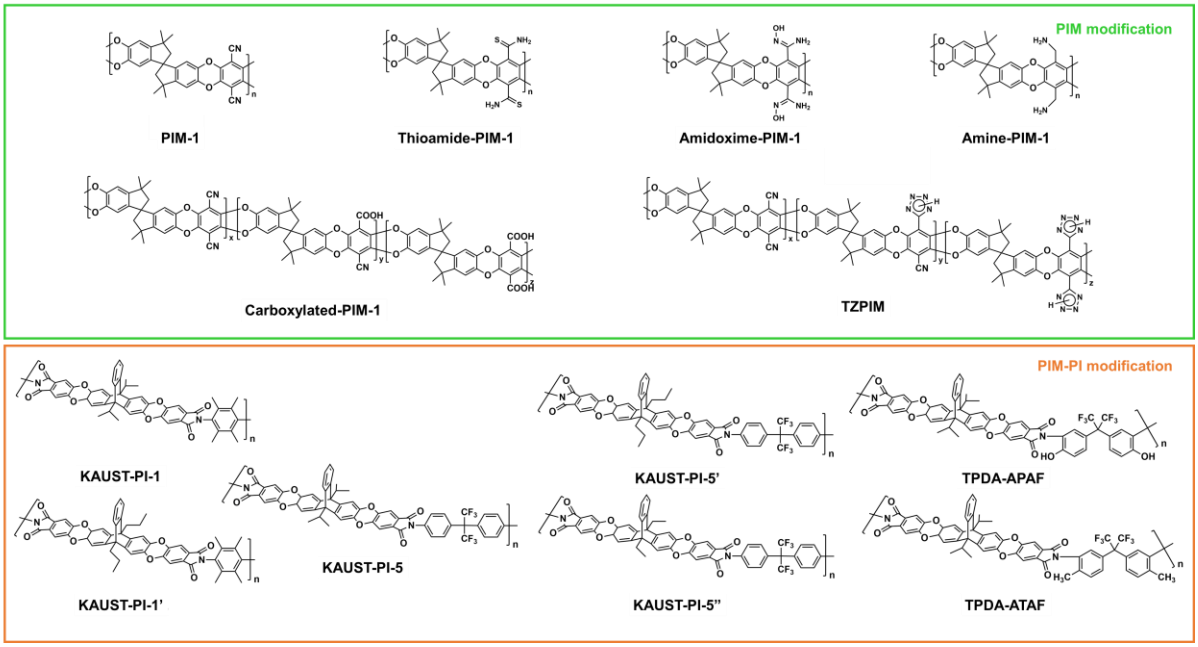

Figure 15. Side group variation in PIMs and PIM-PIs.

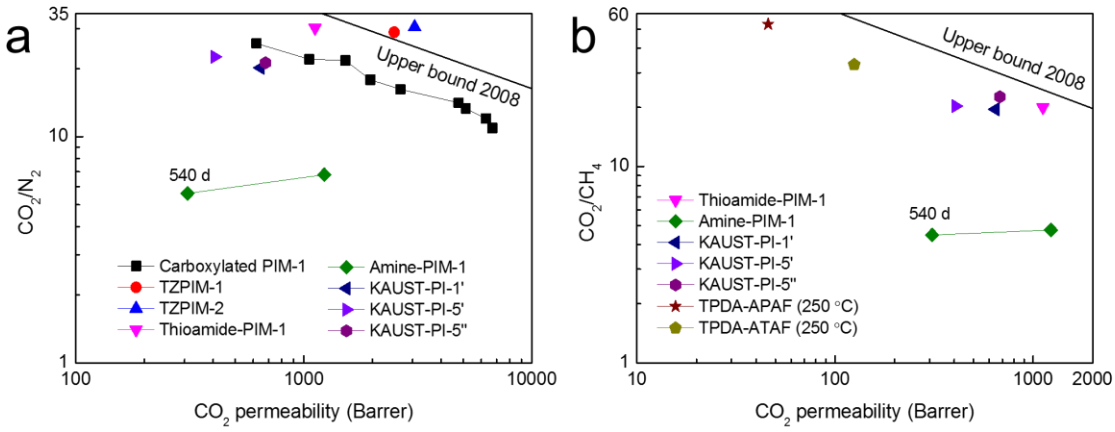

Figure 16. Double logarithm Robeson plots of PIMs and PIM-PIs with various side groups for (a) CO_2/N_2 and (b) CO_2/CH_4. Note: carboxylated **PIM-1** data (filled black squares) are based on different synthesis conditions (temperature and heat treatment duration) and are not results of aging.

6.2.2. PIM-PIs

Studies have shown the impact of the geometry, rigidity and three-dimensional character of the contortion site on the macromolecular rigidity, pore-size distributions and the resulting gas transport properties of the polymer film.[184] Pinnau and coworkers investigated the effect of the triptycene moiety on tuning the gas transport and mechanical properties of triptycene-based PIM-PI films.[162] Triptycene with various alkyl bridgehead substituents (R = i-C_3, n-C_3, and C_2) were used to prepare different types of PIM-PI film (**Figure 15**). Gas sorption results confirmed that the substitution of three-dimensional and shape-persistent bridged bicyclics into fully fused-ring backbones favored chain packing disruption and development of amorphous microporous macromolecular structures. Large declines in BET surface area were observed in these PIM-PIs when the branched isopropyl chain (i-C_3) was replaced with a linear alkyl chain (n-C_3 or C_2). i-C_3-substituted polymer generally

showed larger N_2 uptake at very low pressure, while the NLDFT-derived pore size distribution showed an obvious increase in the smaller FVEs and a slight increase in the larger ones, indicating that the short bulky branched substituent enhanced the gas transport. Consequently, the gas permeabilities are the largest when the bridgehead is a branched i-C_3, but the effectiveness of bridgehead substitution depends on the diamine. Selection of the alkyl bridgehead substituents needs to be balanced between intersegmental spacing and intrasegmental mobility; i.e. with short and bulky isopropyl substituents and rigid torsion-resistant diamines.[162]

Furthermore, hydroxyl-functionalization of **KAUST-PI-5** to improve plasticization resistance by increasing inter-chain rigidity was also investigated.[185] The hydroxyl-functionalized PI, **TPDA-APAF** was compared to the same PI with hydroxyl groups substituted with methyl groups (**Figure 15**). As expected, **TPDA-ATAF** (with CH_3 moieties) showed larger porosity than **TPDA-APAF** (with OH moieties) due to the bulkier CH_3 group and the lack of inter-chain hydrogen bonding. Both **TPDA-ATAF** and **TPDA-APAF** showed improved gas separation properties and resistance to plasticization after thermal annealing. Particularly, **TPDA-APAF** annealed at 250 °C, with a tighter packing, showed lower CO_2 permeability of 46 Barrer coupled with higher CO_2/CH_4 selectivity of 53 (**Figure 16**).[185]

6.3. Copolymers and blending of polymers

It is recognized that gas transport properties of polymeric membranes can be tuned by making copolymers, and there are many exemplary PIM-based copolymers.[186-189] By blending another polymer, a range of gas permeability-selectivity pairs along the upper bound can be achieved. Most work was either aimed at modifying the distribution of FVEs or is exploratory, without much emphasis given to solving

physical aging. However, blending with a slower aging polymer could be an effective method to slow aging in a membrane.

Guiver and coworkers[190] explored a different contorted center, 2,2',3,3'-tetrahydroxy-1,1'-dinaphthyl (THDN) monomer in **PIM-1** (which consists of TTSBI:TFTPN of 1:1) to realize a new copolymer **DNPIM** series. For instance, **DNPIM-33** has a molar ratio of THDN:TTSBI:TFTPN of 1:2:3, where 33 is the ratio of THDN to TFTPN. THDN monomer is fully aromatic and has a highly kinked unit which arises from the twisted bond between the two ring systems (**Figure 17**). Incorporation of this unit leads to a zig-zag structure in **DNPIM-33**, which is more contorted than the original **PIM-1** (a shorter distance between contorted centers) and therefore less efficiently packed. The unique structure gives rise to higher gas selectivity without sacrificing much of its gas permeability, settling just above the 2008 Robeson upper bound (P_{O_2}= 907 Barrer, O_2/N_2= 3.75).[190] Other similar copolymers were also synthesized by Guiver's group, including a series of **DNPIM**, **TOTPIM**, and **DNTOTPIM** (copolymers derived from the aforementioned three monomers and a tricyclic monomer, 2,3,7,8-tetrafluoro-5,5',10,10'-tetraoxide thianthrene (TFTOT)).[186] Furthermore, new **PIM-1**-based copolymers were also prepared from three different TFTOT monomers, to incorporate bulky, rigid groups into the copolymers, yielding **DSPIM1–3** with different ratios of TFTOT:TTSBI:TFTPN. The results are a wide range of gas transport performances along the 2008 O_2/N_2 upper bound (**Figure 18**).[191]

Tröger's base-based copolymers (with different ratios of THTB:TTSBI:TFTPN) were also prepared.[192] Increasing the fraction of TB monomer shifts the gas transport properties closer to the upper bound, in line with other **TB-PIMs**.[192] The arrow in **Figure 18** indicates the decreasing ratio of PIM-1 component in the copolymer.

Pinnau and coworkers designed several PIM-based copolymers of **TPE** (tetraphenylethylene) and **PIM-1**,[187] as well as copolymers of **PIM-6FDA-OH** and **6FDA-DABA (PIM-6FDA-OH-co-6FDA-DABA)**.[193] Interestingly, the latter copolymers with a SBIDA to DABA ratio of 80/20 showed a remarkable ~50% enhancement in the BET surface area from **PIM-6FDA-OH** (300 m^2 g^{-1} compared to 190 m^2 g^{-1}). The enhancement may be due to the additional hydrogen bonding between the COOH (from DABA) and OH group (from SBIDA), creating additional free volume. Increasing the ratio to 50:50 showed much lower porosity, potentially due to excessive hydrogen bonding. Also, the copolymers demonstrated very stable performances after one month aging.[193]

A similar approach is to blend PIM-based polymers with commercially available polymers such as **Matrimid® 5218** (polyimide),[188,194] **Ultem® 1010** (polyetherimide),[189] polyphenylenesulfone (PPSU)[195] and sulfonated polyphenylenesulfone (sPPSU).[195] As the loading of **PIM-1** increases, **PIM-1/Matrimid**, **PIM-1/Ultem** and **PIM/sPPSU** became more permeable to gas and less selective, with performance closer to the 2008 Robeson upper bound, contributed by the high performance of **PIM-1**.[188,189,194,195]

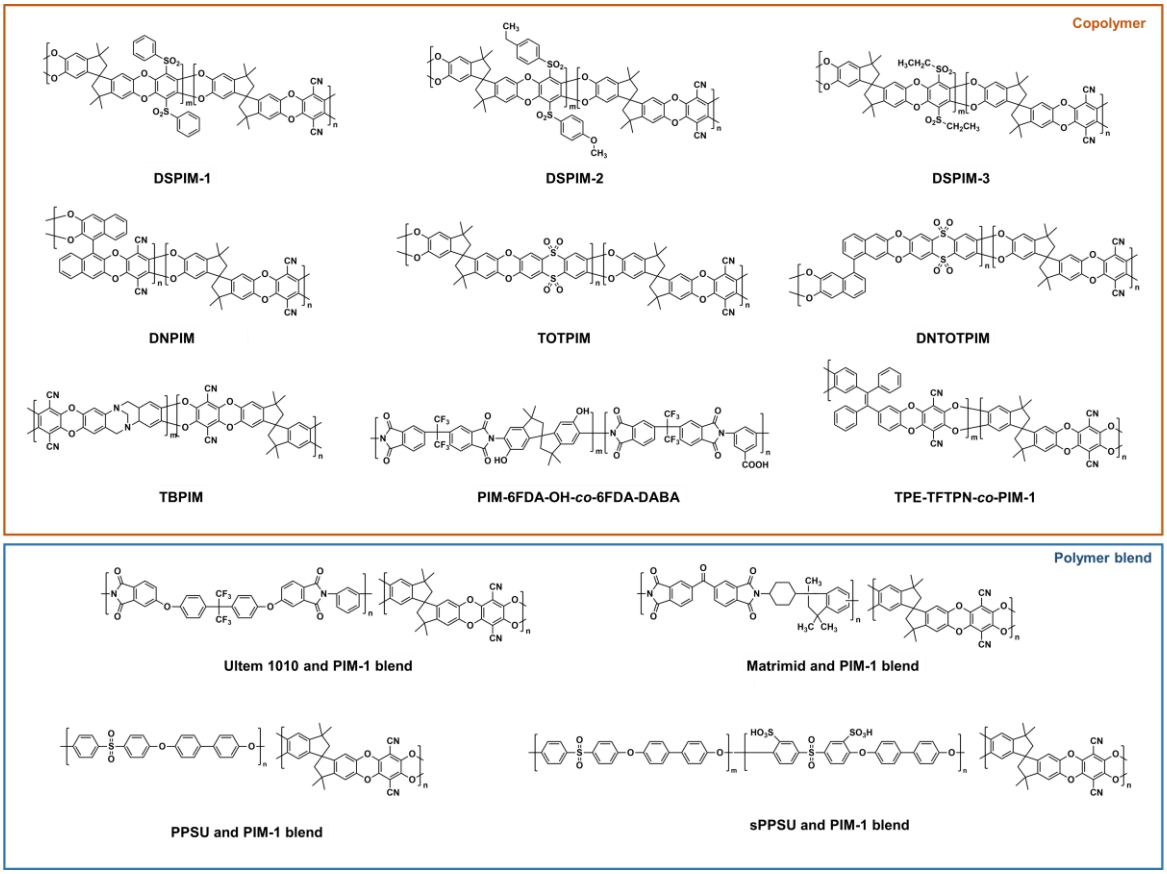

Figure 17. Chemical structures of PIM-based copolymers and polymer blends with **PIM-1**. General names are used for the copolymers (DSPIM, DNPIM, TOTPIM, DNTOTPIM and TBPIM series).

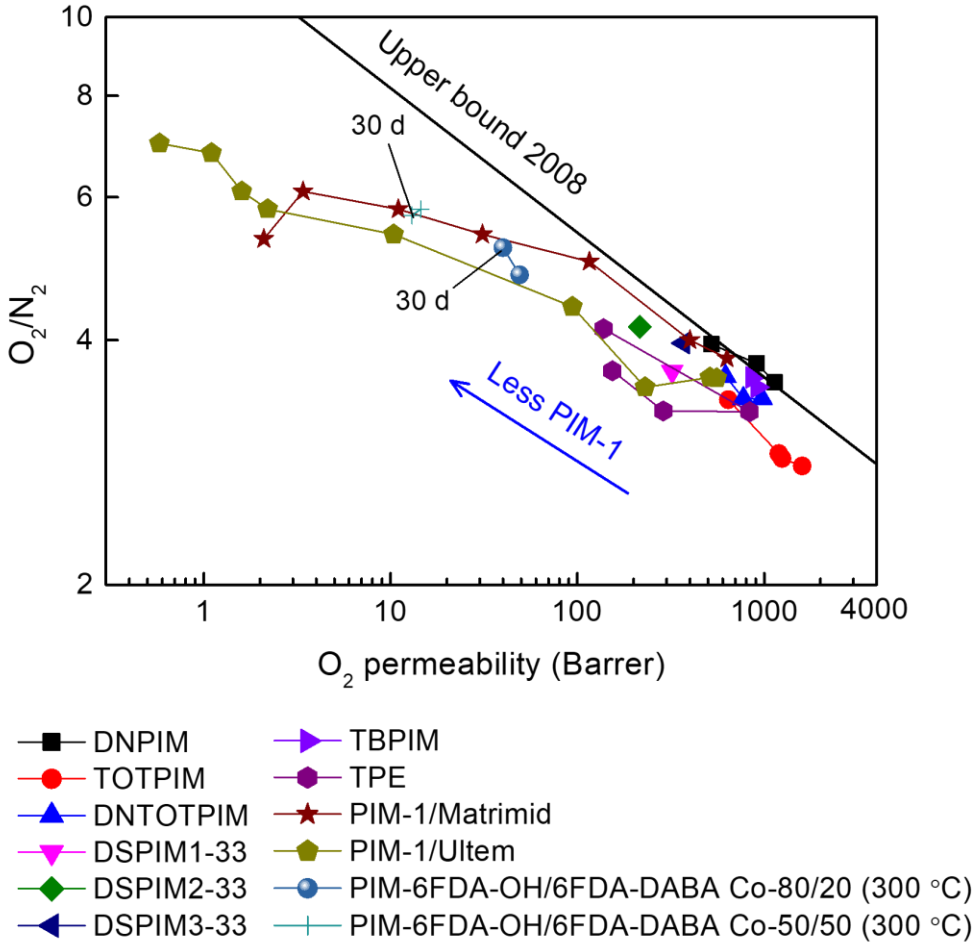

Figure 18. Robeson plot of PIM-based copolymers and polymer blends for O_2/N_2. Arrow shows decreasing ratio of **PIM-1** component leads to higher selectivity and lower O_2 permeability.

6.4. Post-modification of membranes

6.4.1. Thermal crosslinking

Thermal crosslinking of **PIM-1** was performed by Chung and coworkers[154] to improve the gas separation performance. **PIM-1** films were thermally treated in a vacuum furnace at 250–300 °C for 0.5–2 days. TGA results showed that thermally

crosslinked **PIM-1** exhibited improved thermal stability compared to pure **PIM-1**; the decomposition rate decreased with increasing thermal treatment time. Triazine structures were reported to be responsible for crosslinking, on the basis of FT-IR and XPS analyses. A drastic decrease of gas permeability without selectivity enhancement was observed when a **PIM-1** film was treated at 250 °C for 1 day, probably due to densification of the **PIM-1** membrane without any crosslinking. When the period was extended to 2 days, a further decrease in gas permeability was observed, with a significant enhancement in gas selectivity. When the temperature was raised to 300 °C, simultaneous increases in gas permeability and selectivity were observed for a heating period of 0.5–2 days. The thermally induced crosslinking of polymer chains and tightening of polymer chains were verified by PALS experiments, where free volume radius dropped from 3.69 to 3.23 Å. Also, FFV was increased when heat treatment time was increased from 1 day to 2 days. The representative film (**PIM-300–2.0d(TC)**) exhibited H_2 and CO_2 permeabilities of ~3900 and ~4000 Barrer, with H_2/N_2 and CO_2/CH_4 selectivity of 40.3 and 54.8, respectively. **PIM-300–2.0d(TC)** showed much lower N_2 and CH_4 permeability of 96 and 73 Barrer, respectively, compared to 337 and 472 Barrer of methanol-treated **PIM-1**, hinting that there are less large FVEs but comparable smaller FVEs in **PIM-300–2.0d(TC)**. This led to a performance surpassing the Robeson upper bound for all industrially important gas pairs. Also, resistance to physical aging is expected for such crosslinked PIMs. Aging of membranes for 10 days showed that the thermally crosslinked membrane tended to have better membrane performance stability, but a longer aging period is needed to confirm this (**Figure 19**).[154]

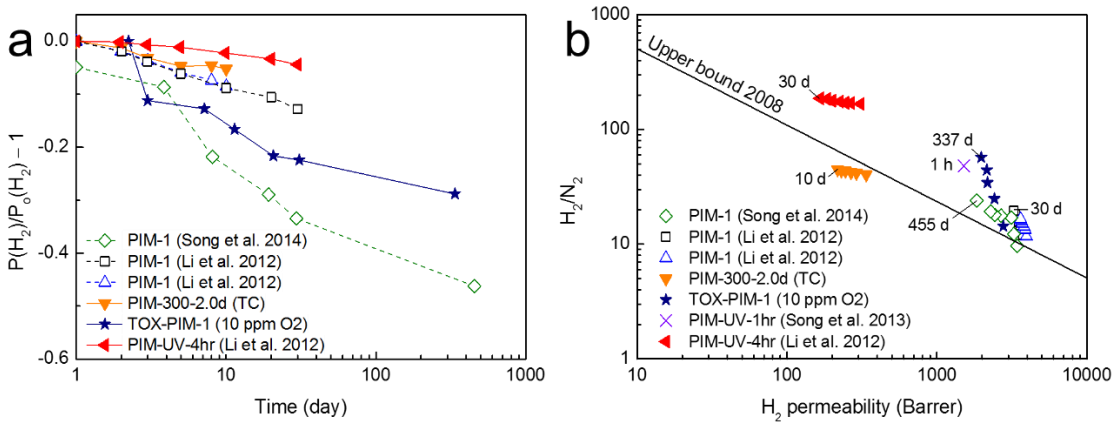

Figure 19. (a) Changes to relative H_2 permeability against time and (b) double logarithmic H_2/N_2 Robeson plot of UV and thermally crosslinked **PIM-1**.

Song *et al*. studied the effect on the gas transport performance of a **PIM-1** film of thermal oxidative crosslinking of the film by heat treatment in a controlled oxygen environment and at much higher temperature than had been considered previously.[153] Controlled thermal oxidative crosslinking at 385 °C in the presence of trace amounts of oxygen caused the crosslinked **PIM-1** (termed **TOX-PIM-1**) to be largely insoluble in solvents that readily dissolve the **PIM-1**. Mechanical testing revealed that the polymer film became stiff after slow crosslinking but remained mechanically robust. In contrast, **PIM-1** film annealed in air (20.9 vol.% O_2) or in trace oxygen for a prolonged period caused the film to become brittle. It was shown that a temperature window between 350 and 450 °C was crucial in controlling the degree of oxidative degradation, as degradation of **PIM-1** film was found to occur at 350 °C in air, which released CO_2 as the major gaseous product, and an optimal crosslinking temperature of 375–385 °C was found to induce crosslinking without excessive degradation or carbonization. After thermal-oxidative crosslinking, **TOX-PIM-1** film showed two orders of magnitude lower gas permeability for larger gas molecules (such as N_2 and CH_4), while the high gas permeabilities of smaller gas molecules (H_2,

CO_2 and O_2) were retained. The representative **TOX-PIM-1** showed significant increase in CO_2/CH_4 selectivity to 70, with comparable high CO_2 permeability of 1100 Barrer, surpassing the Robeson upper bound considerably. It was also demonstrated that the gas transport properties can be tuned by controlling the degree of crosslinking via temperature, heating time and oxygen concentration. Aging studies over a year showed that **TOX-PIM-1** generally aged at a similar rate as pure **PIM-1** film (i.e. rapid aging in the first month followed by slow aging) as indicated by the comparable decrease in CO_2 permeability (**Figure 20**).[153] However, comparing H_2 permeability and H_2/N_2 selectivity of **TOX-PIM-1** to pure **PIM-1** (by replotting the results obtained from this work[153] as shown in **Figure 20**), it is observed that the rate of drop of H_2 permeability in **TOX-PIM-1** is slower than pure **PIM-1**, yet the relative gain in H_2/N_2 selectivity of **TOX-PIM-1** is significantly higher than **PIM-1** (**Figure 20**). On the contrary, CO_2 permeability decreases more rapidly in **TOX-PIM-1** than pure **PIM-1**. Interestingly, the CO_2/N_2 selectivity of **TOX-PIM-1** decreases with aging time (**Figure 20**). This clearly indicates some sort of selective aging of larger FVEs over smaller FVEs. This could be explained by the more localized crosslinking at the vicinity of smaller FVEs caused by the preferential diffusion of O_2 under the controlled experiment (385 °C, 10 ppm O_2, 24 h). It is therefore worth studying the aging of such crosslinked PIM more closely using other microporosity analysis techniques, such as PALS, to better understand the aging mechanism.

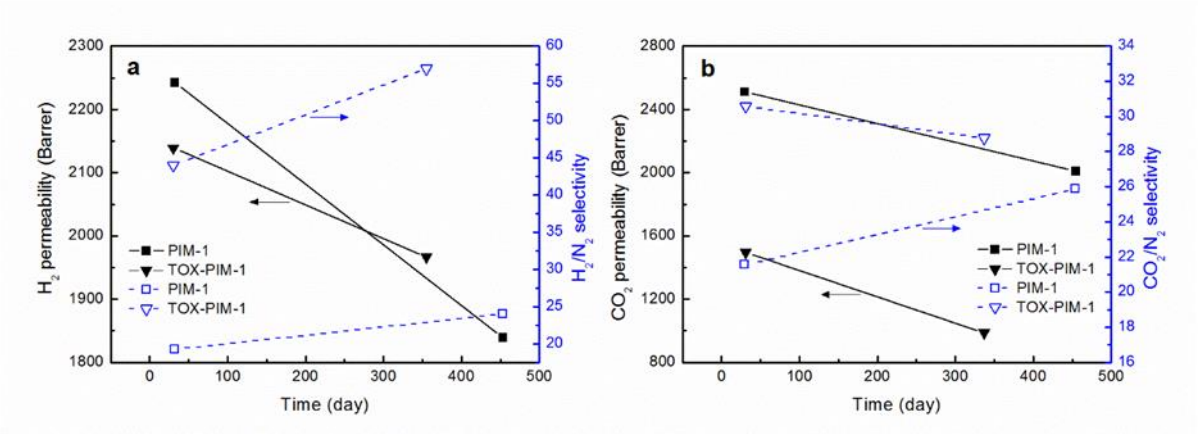

Figure 20. (a) H_2 permeability and H_2/N_2 selectivity; and (b) CO_2 permeability and CO_2/N_2 selectivity of **PIM-1** and representative **TOX-PIM-1** (385 °C, 10 ppm O_2, 24 h).

Guiver and coworkers[196] investigated the decarboxylation-induced crosslinking of **PIM-1** (**DC-PIM**). Pristine **PIM-1** was first carboxylated by controlled hydrolysis of the nitrile group of **PIM-1**, based on a procedure previously reported by the same group.[100,181] Decarboxylation-induced crosslinking was then performed on the carboxylated **PIM-1** by controlled heating of the carboxylated **PIM-1** in a tube furnace in an inert environment. Similar to other thermal crosslinking methods, **DC-PIM** exhibited improvement in gas selectivity at the expense of gas permeability. It also exhibited a decrease of swelling-induced densification for CO_2.[196] No aging studies were performed in this work, but improvement in aging resistance is expected. It should also be noted that recent work has shown that base-catalysed hydrolysis generates a mixture of carboxylated and amide functionality (**Figure 21**). Even the most fully hydrolysed samples retained a substantial proportion of amide, along with carboxylated structures.[197]

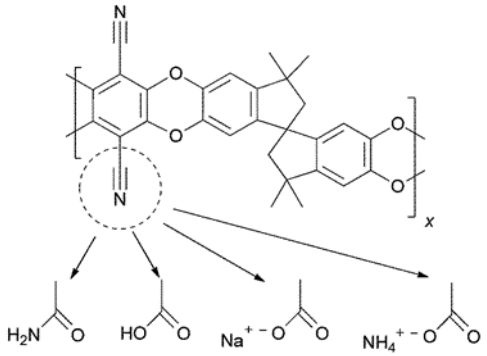

Figure 21. Chemical structures of **PIM-1** and possible hydrolysis products. Reproduced with permission from Ref. [197]. Copyright 2017 The Royal Society of Chemistry.

6.4.2. UV crosslinking

Polymeric membranes (such as polyimide, polyarylate, PEEK etc.) can be crosslinked via a UV-photochemical reaction.[198-201] Patents assigned to UOP claim that PIMs can also be crosslinked by exposure to UV-radiation.[202-204] A few other studies of PIMs exposed to UV irradiation have been performed, although the proposed mechanisms did not necessarily involve crosslinking.[126,130,148,205]

Chung and coworkers[126] investigated a UV irradiation method to tailor the cavity size of a **PIM-1** membrane for H_2/CO_2 separation. The separation of H_2/CO_2 is unusual in PIMs because of the small size of H_2 and the high condensability of CO_2. To achieve such separation, one needs to maximize H_2/CO_2 diffusivity selectivity while minimizing CO_2/H_2 solubility selectivity. The authors proposed that exposing **PIM-1** to UV irradiation will cause the alteration of the spiro-carbon centre in the **PIM-1** backbone. XRD analyses of the films showed that UV-irradiated **PIM-1** tends of have better polymer chain packing and smaller micropores (due to shifting of peak to the right). The results (i.e. densification and decrease in FVEs) were also confirmed by PALS analysis. Gas permeation results revealed that all gas permeabilities decrease,

while gas selectivities increase with increasing UV irradiation time. It was observed that the relative permeability reduction follows the size of gas molecules (higher decrease in permeability for larger gas molecules). This shows that UV irradiation increases the packing of polymer chains, which affects large FVEs. UV irradiation on the other hand has negligible effect on the gas solubility. Overall, the UV-irradiated **PIM-1** favors diffusivity over solubility, whereby the gas permeability increases with decreasing gas kinetic diameter (H_2 > CO_2 > N_2 > CH_4). 4h-UV-treated **PIM-1** achieved H_2 and CO_2 permeability of 452 and 62 Barrer respectively, with H_2/CO_2 selectivity of 7.3, outperforming previously reported polymers. Aging studies over 30 days showed that the aging rate of 4h-UV-treated **PIM-1** is significantly lower than that of an original **PIM-1** film. After 30 days, 4h-UV-treated **PIM-1** showed a hydrogen permeability of ~430 Barrer with H_2/N_2 selectivity of 189, as compared to ~450 Barrer and 167 before aging. However, the improvement by UV treatment gradually decreases with time (**Figure 19**).[126]

Song *et al*. also investigated the effect of UV irradiation on **PIM-1** film.[205] A different mechanism of photo-oxidation was proposed. After UV-irradiation, asymmetric physical changes at the surface of **PIM-1** were observed, where a dense skin layer was formed above a more porous intermediate layer, as observed by SEM. The formation of the intermediate layer was due to the strain induced from densification of the skin layer, of which thickness increases with UV exposure time. Based on the Beer-Lambert expression, the transmitted intensity decreased significantly with depth, which explained the structural changes localized on the surface. The UV-irradiated **PIM-1** also showed ~35–50% increase in Young's modulus, and 11% higher average density of the skin layer than the pristine **PIM-1** film. Song *et al*. also confirmed that crosslinking did not occur, by performing a solubility test. Interestingly, the average

M_w of the UV-irradiated membrane dropped significantly, suggesting chain fragmentation (**Figure 22**). This chain fragmentation was the outcome of the strongly oxidizing singlet oxygen and ozone generation under UV irradiation from local abundance of O_2 in high free volume **PIM-1**. Gas permeation results showed that generally gas permeability decreases and gas pair selectivity increases with irradiation time in air (21 wt% O_2). For example, **PIM-1** sandwiched in quartz and exposed to UV irradiation for 60 min showed a H_2 permeability of ~1500 Barrer and H_2/N_2 selectivity of 48, located considerably above the upper bound (**Figure 19**). However, CO_2 permeability and CO_2/N_2 selectivity were not desirable as it dropped below the upper bound.[205]

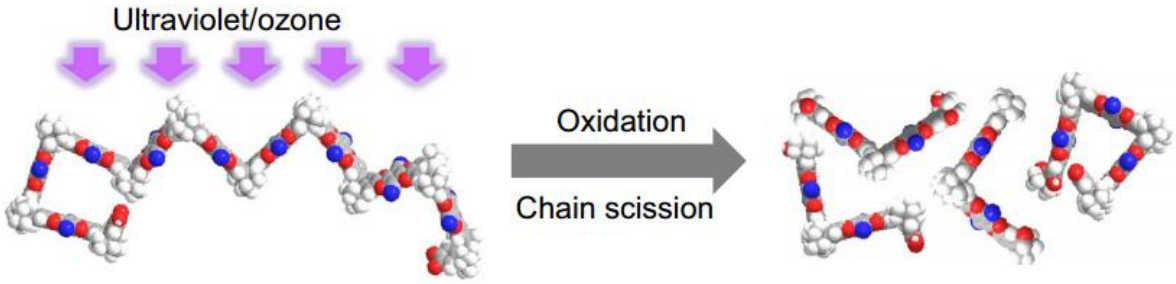

Figure 22. Chain scissoring of **PIM-1** upon UV irradiation. Reproduced with permission from Ref. [205]. Copyright 2017 Nature Publishing Group.

Both thermally crosslinked and UV-treated membranes showed better performance for H_2 separation than CO_2 separation, which could be due to the preference to diffusivity selectivity over solubility selectivity after treatment. Long term studies of UV-treated membranes were not available.

6.4.3. Chemical crosslinking

Chemical crosslinking of high free volume polymers has been previously used to improve gas separation performance.[206-208] In PIMs, several crosslinkers have been used, including 4-azido phenylsulfone,[209] 2,6-bis(4-azidobenzylidene)-4-

methylcyclohexanone,[209] polyethylene glycol biazide (PEG-biazide),[210] and pyrene.[211]

McDonald *et al*. investigated the intermolecular interactions between **PIM-1** and polycyclic aromatic hydrocarbons (PAHs), in order to improve gas sorption and physical properties.[211] Pyrene was shortlisted from different cyclic aromatic hydrocarbons and PAHs, based on their interaction with **PIM-1**, where it causes the aggregation of the **PIM-1** polymer chains at a much lower concentration of > 0.2 mg/ml, compared to other PAHs. Interestingly, blending of pyrene at compositions ≥ 5 wt% resulted in almost zero nitrogen uptake at 77 K, while its effect on the CO_2 uptake at 298 K was much less pronounced.[211] Subsequent study suggested kinetic pore closure assisted by the physical crosslinking of the pyrene, which would only open when there is sufficient solvation pressure.[100] A post-modification approach was used to prepare PIM/PAH composites, by soaking precast **PIM-1** films in methanolic solutions of either pyrene or 1-aminopyrene. Gas sorption experiments suggested that 1-aminopyrene has a stronger effect on reducing the N_2 uptake than pyrene. The composites were also tested for their gas permeability. The modified **PIM-1** films showed a slight decrease in the rate of aging but reduced initial permeability due to filling of FVEs by the pyrene-based additives. Interestingly, **PIM-1**/1-aminopyrene showed a slight increase in CO_2 permeability over time. This was the result of controlled physical aging, where the pore sizes decrease over time to an extent that favours CO_2 sorption, and therefore increased enthalpy of CO_2 adsorption. Strong interactions between **PIM-1** and 1-aminopyrene may be sufficient to rigidify **PIM-1** chains.[211]

6.4.4. Thermally rearranged polymers

Structural features desirable for high selectivity tend to give insoluble materials that are difficult to process. A way to overcome this issue is first to prepare a membrane from a soluble polymer, which is later molecularly rearranged to create the desirable microporosity.[212] Thermal treatment of precursor polymers is one way to create new microcavities which can be tuned for transport and separation of gas molecules.[6] This approach has been used to create so-called thermally rearranged (TR) PIM-based polybenzoxazoles (**spiroTR-PBOs**) with a SBI moiety from newly designed spiroHPIs (H= hydroxyl, PI= polyimide)[213] and with a SBF moiety.[214] The PIM-PIs with different dianhydrides (6FDA, BPDA, PMDA and BPADA) were thermally rearranged to obtain their TR counterparts (conversion of the rotatable imide linkages into a benzoxazole ring; **Figure 23**). **SpiroTR-PBOs** generally showed increased FFV, BET surface areas, remarkable increases in CO_2 permeability and proportional loss in gas selectivity.[213,214]

Budd and coworkers [212] prepared a series of TR-PBOs (**PIM-PBO-1–3**) from PIM-PI-OH precursors (**PIM-PI-OH-1–3**) (**Figure 23**). Since the **PIM-PI-OH-2** film was not mechanically robust, its copolymer with **PIM-PI-OH-1** was prepared instead (**Copol-OH-1–2)**. Furthermore, two preparation methods were used for **PIM-PI-OH-1**: (i) A thermal imidization method (yielding **T-PIM-PI-OH-1**) and (ii) a one-pot polycondensation method (yielding **O-PIM-PI-OH-1**). The two methods produced two different **PIM-PI-OH-1** with different molar masses and BET surface areas. Thermal treatment of **PIM-PI-OH-1** powder increased the BET surface area of **T-PIM-PBO-1** (360 to 440 $m^2\ g^{-1}$) and **O-PIM-PBO-1** (230 to 405 $m^2\ g^{-1}$). In contrast, thermal treatment of **PIM-PI-OH-3** led to a slight decline in BET surface area from 430 to 360 $m^2\ g^{-1}$, suggesting the collapse of the existing free volume. Consistent with other

work, both **PIM-PBO-1s** give higher gas permeabilities coupled with reductions in selectivity. **Copol-PBO-1–2** and **PIM-PBO-3** on the other hand, exhibited similar permeability with either enhanced or similar selectivities. Furthermore, **O-PIM-PBO-1** and **PIM-PBO-3** showed good resistance to physical aging, whereby the "as-cast" permeabilities were achieved after aging for 270 and 197 days, respectively (**Figure 24**).[212]

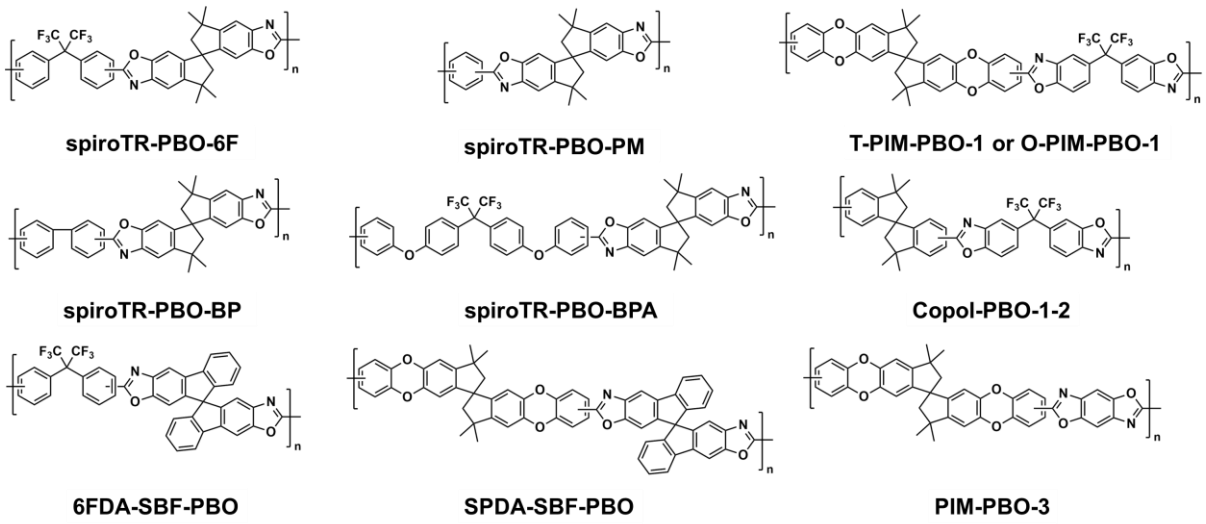

Figure 23. Chemical structures of thermally rearranged (TR) PIMs. (T-PIM-PBO-1 and O-PIM-PBO-1 have the same chemical structures but are produced from thermal imidization method and one-pot polycondensation method, respectively.

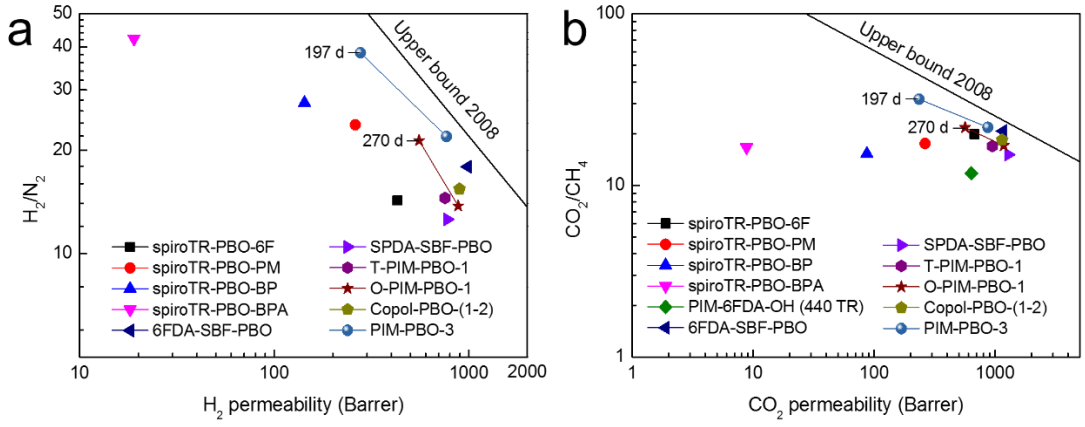

Figure 24. Robeson plots of TR-PIMs for (a) H_2/N_2 and (b) CO_2/CH_4.

6.4.5. Carbon molecular sieves

Micropores can be generated by pyrolysis of a polymeric precursor, producing carbon molecular sieve (CMS) membranes with superior separation performance, well above the trade off line of polymer membrane materials, combined with good thermal and chemical stability.[215] Pinnau and coworkers[216] prepared CMS membranes derived from a PIM (**PIM-6FDA-OH**). The precursor was first heated to 440 °C for thermal rearrangement of **PIM-6FDA-OH**, followed by pyrolysis at different temperatures (530, 600 and 630 °C). A CMS membrane was also prepared by directly heating the pristine polymer from room temperature to 800 °C. Above 600 °C, the presence of ordered, graphitic carbon was observed, and there was a significant decrease in the precursors' d-spacing from ~5.8 Å (of pristine film) to 4.37 Å and 3.8 Å (600 and 800 °C, respectively). CO_2 adsorption capacity and DFT surface area also increased with increasing pyrolysis temperature. In terms of gas transport properties, beyond 530 °C (where the intermediate stage of partial carbonization occurs), very large gains in permeability for all gases were obtained (e.g. 4100 Barrer of membrane treated at 530 °C vs 251 Barrer of **PIM-6FDA-OH**). Further heating to 800 °C caused a rapid drop in permeability and significantly increased gas selectivity due to shrinkage in pore size during the formation of a graphitic molecular sieve structure. The 800 °C treated membrane showed among the best reported gas transport performance (CO_2/CH_4 of 90, H_2/CH_4 of 357, P_{CO_2} of 550 Barrer and P_{H_2} of 2100 Barrer; **Figure 25**).[216] The performance of these CMS membranes in binary gas mode were also investigated.[217] In a mixed gas of CO_2/CH_4, CH_4 permeability increases with feed pressure, potentially due to the small expansion of the amorphous graphitic domains caused by high sorption of CO_2,

which is unique to the CMS membranes derived from PIMs. On the other hand, CO_2 permeability decreases with feed pressure, due to competitive sorption of CH_4, and overall the CO_2/CH_4 selectivity also decreases with increasing feed pressure.[217] The application of PIM-PI-derived CMS membranes in ethylene/ethane separation were also investigated.[152,218]

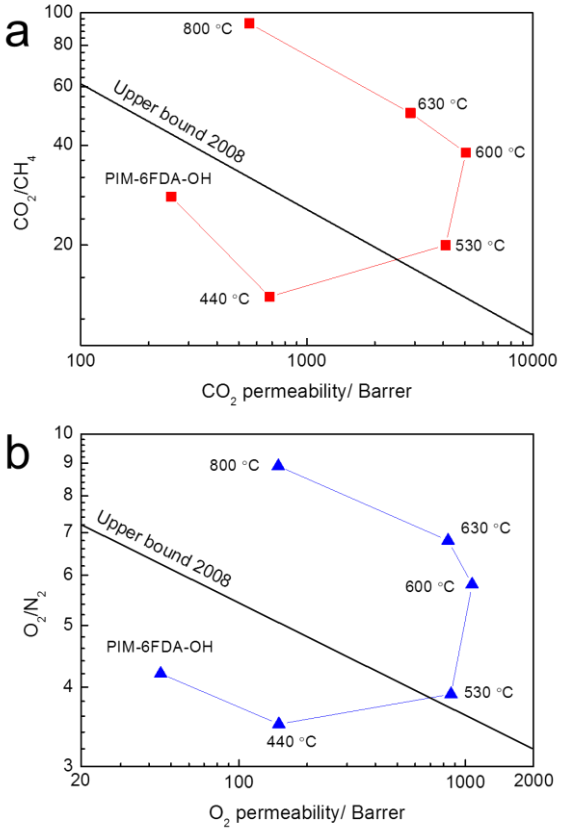

Figure 25. Robeson plots of PIM-derived CMS membranes for (a) CO_2/CH_4 and (b) O_2/N_2.

6.5. Blending with non-porous nanomaterials

There are limited studies on the use of non-porous fillers for PIMs. Budd and coworkers[219] studied the influence of few-layer graphene on the long term permeability of **PIM-1** and compared the improvement to **PIM-1** blended with other fillers of different morphologies, such as f-MWCNT (cylindrical)[220] and fumed silica

(spherical).[221] The results suggested that the morphology of the filler plays an important role in polymer chain packing; going from a spherical, to a cylindrical and a planar nanofiller, increased permeability may be achieved at increasingly lower nanofiller contents. In other words, the enhancement in permeability with low loading of few-layer graphene in **PIM-1** is comparable to higher loadings of cylindrical and spherical shape fillers. At optimum loading of 0.046 vol.%, the initial CO_2 permeability was increased by ~150% to ~13000 Barrer. All **PIM-1**/graphene MMMs showed improvement in aging resistance after eight months' storage under ambient condition, with CO_2 permeability remaining significantly higher than pure **PIM-1**. More work still need to be performed to understand polymer-filler interactions, especially for fillers with different morphologies.[219]

6.6. Blending with microporous nanomaterials

Ending physical aging in superglassy polymer films by blending with microporous fillers was first claimed by Lau *et al*. using **PTMSP**, **PMP** and **PIM-1** as the continuous phase and porous aromatic frameworks (PAFs) as the fillers.[22] PAF-1 (with nanopores of around 1.2 nm and a BET surface area of ~5200 m^2 g^{-1}) is particularly attractive, as the nanopores are capable of intercalation of the polyacetylene or the bulky chemical moieties in PIMs, thus freezing the polymer structure and tuning the aging process. The incorporation of PAF-1 in high free volume polymers increased the CO_2 permeability significantly, owing to the increased pore fraction introduced to the system. Moreover, its addition to these polymers considerably reduced aging (only less than 7% decline in CO_2 permeability in **PIM-1** systems over 240 days; **Figure 26**). For comparison, ZIF-8 was also used as the filler but **PTMSP**/ZIF-8 exhibited almost identical aging performance to pure **PTMSP** films. This suggests that there is polymer chain intercalation within PAF-1

and local interaction of PAF with the chains, that freezes free volume. PAF-1 significantly reduced the mobility of two carbon atoms in the **PIM-1** structure that consequently inhibited flexing, while the dibenzodioxin component of **PIM-1** gains flexibility.[22]

Lau *et al*. further investigated the effect of blending porous aromatic frameworks (PAFs) in **PIM-1** for H_2/N_2 separation.[101] The extraordinary interactions of PAF-1 (which can demonstrate a BET surface area over 3760 $m^2\ g^{-1}$) with **PIM-1** have led to 375% H_2 permeability enhancement, increasing permeabilities of H_2 and N_2 to 5500 Barrer and 1200 Barrer, respectively (**Figure 26**). The group proposed a new aging mechanism, which they coined as selective aging. The incorporation of PAFs induced selective aging of **PIM-1**, that is, an almost negligible drop in hydrogen permeability in **PIM-1**/PAF-1 over 400 days, while N_2 permeability is reduced to just 10% of the original. This causes the H_2/N_2 selectivity to increase from 4.5 to 13 over 400 days of aging. In other words, separation performances improved with age. In comparison, the H_2 and N_2 permeabilities of pure **PIM-1** film decreased by ~90% over 400 days of aging (**Figure 26**). The selective aging mechanism was attributed to the intercalation of bulky moieties of **PIM-1** within the pores of PAF-1, permitting smaller FVEs to remain open, while larger ones collapse with typical physical aging, which explains the drop in N_2 permeability and not H_2 permeability. This was supported by a series of characterization tests including SAXS, WAXS, PALS and solid-state ^{13}C NMR.[101]

In-situ crystallization of porous imine cages (CC3; 0.6 nm, BET surface area of 620 $m^2\ g^{-1}$) from a homogeneous molecular solution of **PIM-1** and CC3 precursor was performed and compared to the blending of preformed CC3 nanocrystals (BET surface area of 770 $m^2\ g^{-1}$).[155] **PIM-1**/CC3 showed some loss of permeability over

time, as **PIM-1** is the dominant phase, but remains significantly higher than pure **PIM-1**. For instance, **PIM-1**/CC3 (with weight ratio 10:3) exhibited a CO_2 permeability of 13000 Barrer and CO_2/N_2 selectivity of 15 after more than a year. **PIM-1**/nanoCC3 MMMs on the other hand lost all of its additional permeability in less than six months, suggesting that the permeability enhancement is dominated by the polymer bulk effects rather than by the porosity of the filler.[155] Even though the *in-situ* crystallization of CC3 improved the CO_2 permeability after aging for ~390 days, the rate of normalized permeability lost was similar to ethanol treated **PIM-1** (**Figure 26**), which suggests that the CC3 may not play a role in supressing aging, but more at providing additional porosity within the crystalline fillers.

Most of the aforementioned fillers are costly or difficult to scale up. This led to sourcing other fillers such as hypercrosslinked polystyrene (HCP), which is cheaper to produce.[222,223] Mitra *et al*. studied the effect of dispersing the HCP particles in a solution of **PIM-1** to reduce aging in **PIM-1**.[222] The HCP was prepared using an emulsion polymerisation process previously reported and have an average spherical particle diameter of ~55 nm and a BET surface area of ~ 1700 $m^2\ g^{-1}$.[224] Ethanol treated **PIM-1**/HCP (21.3 wt%) showed remarkable improvement in CO_2 permeability (20300 Barrer compared to 8200 Barrer of ethanol treated **PIM-1**). Also, the same MMMs showed CO_2 reduction of only 39.9% as compared to 66.3% of ethanol treated **PIM-1** after 150 days, suggesting that some sort of aging reduction mechanism occurred and that its effect was significant (**Figure 26**).[222]

It is clear from the results above that the size and pore size of the porous fillers, as well as the chemistry between additives and polymers, are keys to supressing physical aging or to yield selective-aging membranes.[223]

Loading of poly(ethylene glycol) (PEG)-functionalized multiwall carbon nanotubes (f-MWCNTs) as an inorganic phase in the **PIM-1** polymer matrix has shown some improvement to aging resistance[44,225] and plasticization.[220] To confirm the aging performance, **PIM-1**/f-MWCNT of 2 wt% loading was prepared via a dip-coating method and characterized with PALS.[44] PALS results showed that incorporation of f-MWCNTs did not affect the size of the FVEs, but added additional channels for gas transport, leading to higher CO_2 permeability. The composite membrane also showed only a 17% decline in permeability after 300 days, while the permeability of pure **PIM-1** dropped by 38%. This was confirmed by PALS, where the reduction in size of the FVEs in the composite membrane was slower than for pure **PIM-1** membranes.[44] One feasible reason to explain this is that the additional FVEs introduced by the incorporation of f-MWCNT were not subjected to polymer aging and therefore the resulting composite membrane suffered less aging. Also, it is possible that the interaction of f-MWCNTs with the polymer chains of **PIM-1** could potentially slow down the rearrangement of the polymer chains.

Graphitic carbon nitride (g-C_3N_4) 2D nanosheets were used as a filler in **PIM-1** to improve its gas separation performance.[226] g-C_3N_4 contains triangular ultramicropores at sizes ~3.11 Å, which lies between the kinetic diameters of the lightest gases (such as He and H_2) and some other larger gas molecules (CO_2, N_2 and CH_4) as well as structural defects of 3.1–3.4 Å. Between loadings of 0 to 1 wt%, increasing loading led to increased permeability of all gases tested, but decreased selectivity of CO_2 to other gases. It was believed that the presence of g-C_3N_4 can effectively restrict the conformational freedom of **PIM-1** backbones, which restricts efficient packing, thus explaining the improved permeability. The reduced selectivity on the other hand, was due to the non-selective voids created at the interface

between **PIM-1** and the nanosheets. When loading exceeds 1 wt%, all gas permeabilities decreased, although they remained higher than those of pure **PIM-1**. This trend may be the result of partial agglomeration of restacked g-C_3N_4, which retards gas diffusion. However, the drop in H_2 permeability was less significant, probably owing to the triangular ultramicropores of g-C_3N_4, which permit H_2 diffusion. As a result, H_2/N_2 and H_2/CH_4 selectivities were increased dramatically. Long term permeability results suggest that g-C_3N_4 did not effectively slow down the aging of polymers, as all composite films (0.5 to 1.5 wt%) showed similar trends in aging over 200 days (**Figure 26**). Nevertheless, the CO_2 permeability of MMMs measured after 200 days was still comparable to the initial permeability of pure **PIM-1** film. Since CO_2 sorption and free volume were not measured on these films, the effect of blending g-C_3N_4 on CO_2 sorption and FVEs for fresh and aged membranes is not known.[226]

Chung and coworkers investigated the potential of polysiloxysilsesquioxane (POSS) particles (here disilanolisobutyl, SO1440, 1–3 nm, from Hybrid Plastics, Hattiesburg, MS) in suppressing aging and plasticization while improving gas permeability of **PIM-1**.[227] SO1440 was chosen as it has higher solubility in dichloromethane (DCM) than other POSS particles from Hybrid Plastics Inc. Between loadings of 0.5–2 wt%, all gas permeabilities were higher than pure **PIM-1**, which can be attributed to the additional free volume of the bulky POSS. Beyond 2 wt% and up to 20 wt % (which was the maximum loading used in this work), gas permeability decreased with increased loading as a result of the filling of the FVEs and polymer chain rigidification. On the other hand, the selectivity of CO_2 to other gases generally increased with POSS loadings between 2–10 wt%, which could be due to the interaction of Si–OH group on POSS with CO_2 through hydrogen bonding, as well as **PIM-1** chain mobility

restriction by the bulk POSS cages. Above a loading of 20 wt%, both permeability and selectivity decreased with loading as particles agglomerated within the polymer matrix. An aging study was performed on the **PIM-1**/POSS film with POSS loading of 2 wt%, since it improved both gas selectivity and permeability. The composite film showed better aging resistance than pure **PIM-1** over 120 days of aging. This was because the embedded rigid POSS nanoparticles may increase rigidity and retard segmental motion of polymer chains of the **PIM-1**. As a result, physical aging is retarded.[227]

The same group also investigated the effect of blending of beta-cyclodextrin (β-CD), with a unique 3-dimensional hollow bowl structure, in **PIM-1**.[228] The resulting membrane, **PIM-CD**, was tested periodically over 120 days and compared to pure **PIM-1**. **PIM**-CD-2.0% membrane showed 6% and 21% decrease in H_2 and CH_4 permeability while pure **PIM-1** membrane showed 15% and 52% decrease. The interactions between β-CD and PIM restricted chain movement and thus the **PIM-CD** membrane exhibited much greater resistance to physical aging, especially to smaller free volume pores relevant to transport of H_2 and CO_2.[228]

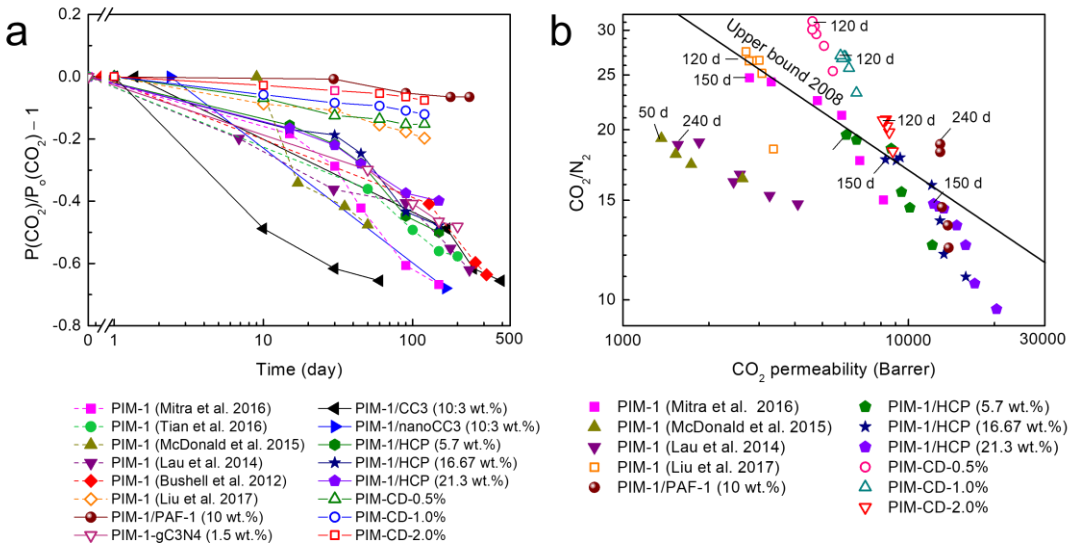

Figure 26. (a) Changes to relative CO_2 permeability against time and (b) double logarithmic CO_2/N_2 Robeson plot of **PIM-1** blended with microporous nanomaterials. PIM-1 permeation data: Mitra et al., [222] Tian et al.,[226] McDonald et al.,[211] Lau et al.,[22] Bushell et al.,[155] Liu et al.[228]

6.7. Synergetic approaches

There are a few reports on the blending of nanofillers followed by crosslinking to improve the performance of high free volume polymer membranes. Chung and coworkers studied the gas separation performance of **PIM-1**/ZIF-71 MMMs with and without UV irradiation.[229] The formation of a dense layer of around 400 nm thickness was also observed for **PIM-1** after UV irradiation, which was in line with the results obtained by Song *et al*.[205] Generally, gas permeabilities of the film increased with increasing loading of ZIF-71 (10–30 wt%). After UV irradiation, CO_2 permeability of **PIM-1**/ZIF-71 (30 wt%) decreased from ~8400 Barrer to 3500 Barrer, while CO_2/N_2 increased from 18.3 to 26.9.[229] No aging study was performed in this work, but similar enhancement to aging resistance after photo oxidation induced by UV irradiation for **PIM-1** is expected.

Song *et al*. investigated the thermal crosslinking of **PIM-1** MMMs blended with nanofillers such as ZIF-8 and SiO_2 (both up to 20 wt%) to further improve the gas permeability of pure **PIM-1** after crosslinking (**TOX-PIM-1**).[230] Without thermal-oxidation, addition of fillers showed similar results to other work, where gas permeability increased with the addition of fillers and selectivity remained relatively unchanged.[221,231,232] Interestingly, after thermal-oxidation, the gas permeability of the film increased, while its ideal selectivity decreased, as a function of increasing loading of both types of fillers, when compared to **TOX-PIM-1**. The increased

permeability was due to the increased gas diffusivity on incorporation of the nanofillers, while the solubility remained relatively unchanged. The overall enhanced diffusion and diminished gas selectivity of **TOX-PIM-1**/nanofillers can be ascribed to a combined effect of molecular sieving in the polymer phase and enhanced diffusion through interfacial defects. An aging study over two years showed that **TOX-PIM-1**/nanofillers also aged similarly to **TOX-PIM-1**, but with different initial permeability/selectivity pairs. After two years of aging, the gas separation performance still remained higher than the Robeson upper bound, indicating that aging in thermally crosslinked **PIM-1** is controlled, with or without addition of nanofillers (**Figure 27**).[230]

Chung and coworkers[123] studied the chemical crosslinking of **PIM-1**/Matrimid membranes using various diamines [ethylenediamine (EDA); trimethylenediamine (TMEDA); *p*-xylenediamine (pXDA); 1,4-diaminobutane (BuDA); and triethylenetetramine (TETA)]. 10 wt% Matrimid was used in the blending, based on their previous work.[188] For such systems, both the chemical structures and pK_a value of the diamines are important in the crosslinking of **PIM-1**/Matrimid, as the distance between the polyimide chains is great due to the low loading (10 wt%), which favors longer and bulkier diamines such as pXDA, BuDA and TETA. Among those, TETA demonstrated the greatest degree of crosslinking, giving a H_2 permeability and H_2/N_2 selectivity of 395 Barrer and 91.9, respectively, after 2 h modification in TETA solution. It was also shown that the degree of crosslinking increases with the duration of modification from 10 min to 2 h, as indicated by the drop in permeability and gain in selectivity. All gas transport properties of TETA-modified **PIM-1**/Matrimid lay above the Robeson upper bound, but aging studies were not performed.

Chung and coworkers[228] also investigated the thermal treatment of 3D PIM-CD (PIM incorporated with beta-cyclodextrin, β-CD). After thermal treatment, PIM-CD exhibited a superior molecular sieve ability for propylene/propane separation, about three times higher than the original untreated membranes. Even though aging studies were not performed, the approach could potentially be effective in producing a more aging resistant CMS membrane.[228]

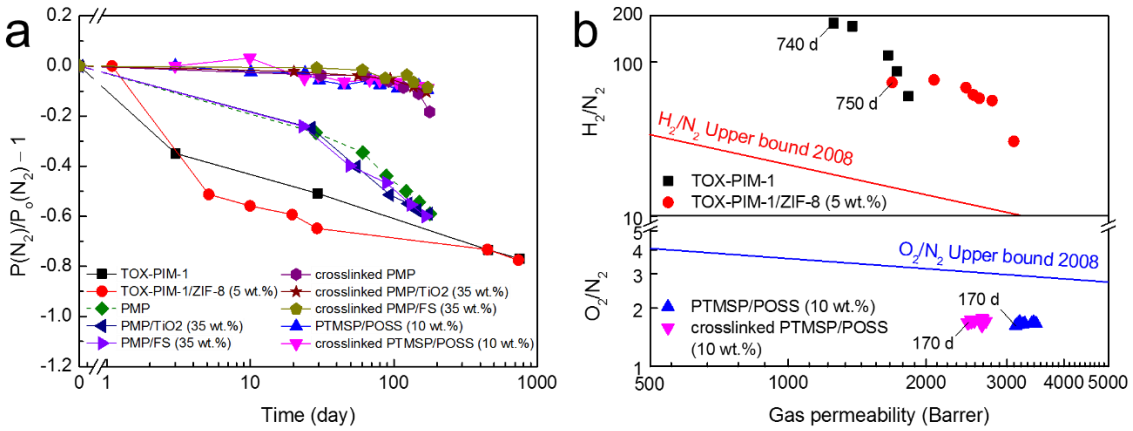

Figure 27. (a) Changes to relative N_2 permeability against time and (b) H_2/N_2 and O_2/N_2 Robeson plot of high free volume polymers (**PIM-1**, **PMP**, and **PTMSP**) modified with more than one approach (i.e. synergetic approach). N_2 permeability was chosen for comparison purposes. A higher drop in N_2 permeability with time indicates better gas separation performance.

6.8. Summary

Enhanced aging resistance of PIM membranes has been achieved based on new polymer design (PIMs and PIM-PIs) and post treatment of the films. A structural redesign of the polymer backbone led to aging-resistant membranes as well as the discovery of high performance PIMs (**TPIM-1**,[96] **PIM-Trip-TB**,[60] **PIM-BTrip-TB**[67], **PIM-EA-TB**,[61] and **PIM-TMN-Trip**;[149] **Figure 11**) and PIM-PIs (**KAUST-PI-1**,[98]

KAUST-PI-2[98] and **PIM-PI-EA**;[167] **Figure 13**), all of which have a more rigid polymer backbone. Several design approaches can be used to improve the long-term performance of new PIM membranes. Improved aging resistance of a membrane can be achieved by (i) improving the aging rate, i.e., modified membranes with similar initial gas permeabilities of that of the unmodified membranes but with slower aging rate, (ii) improving initial gas permeabilities, i.e., modified membranes with enhanced initial gas permeabilities with similar aging rate (aging from a higher permeability and reaching stability at a higher permeability value), (iii) modified membrane with graceful aging profile, i.e. selective aging that improves gas performance (faster aging rate for large pore and slower aging rate for smaller pore) and (iv) the use of strongly interacting substituents (e.g. hydroxyl) to lock in free volume via hydrogen bonding.

Copolymerization and polymer blending, as well as modification of polymer side groups, are less effective in surpassing the upper bound (except for **TZPIM-1** and **TZPIM-2**), but a wide range of gas separation performances (a range of permeability-selectivity pairs) can be tailored.

Post-modification methods have produced membranes with outstanding gas separation performances. Thermally crosslinked and UV-treated PIMs such as **TOX-PIM-1**,[153] **4h-UV-treated PIM-1**[126] and **1h-UV-treated PIM-1**[205] showed remarkable gas transport property and aging profiles. On the other hand, thermal rearrangement is comparatively less effective, with PIM-based polyimides which have initial high BET surface areas and free volume delivering performance consistently below the 2008 upper bound.[213,214,217] In contrast, PIM-derived CMS membranes were stable and exhibited remarkable performance when heated beyond 600 °C.[216,217]

The blending approach has the potential to completely stop aging, or induce selective aging which increases the gas selectivity, as exemplified by **PIM-1**/PAF-1.[101] The loading, interactions between the continuous phase and fillers, compatibility of the fillers to the polymers in terms of structure, surface area and size, as well as quality of dispersion, all have strong effects on the resulting film. This approach, however, needs to be optimized in order to harvest the greatest potential of the fillers, or otherwise the improvement in aging may be decreased by poor mixing (agglomeration) and/or inefficient filling of the polymer free spaces. The stability and cost of the fillers, as well as the ability to form thin film composite membranes, need to be considered.

Several blending methods to improve aging resistance have been identified: (i) Blending of non-porous nanofillers which lead to inefficient packing, (ii) blending of porous nanofillers which increase the initial permeability of the composite, for which after aging the permeability remains higher than that of the pure polymer, (iii) blending of porous frameworks which retard aging over time, retaining much of the initial permeability of the polymer, and (iv) blending of porous frameworks which selectively age the polymer (e.g. reduction in size of the large FVEs, which improve gas selectivity over time).

Figure 28 shows the double logarithmic Robeson plots of all high free volume polymer membranes in this review. Strictly speaking, polymers modified with fillers and CMS membranes should not be included in Robeson plots, but are included here for comparison purposes only. It was observed that blending consistently produced gas separation performance in the high CO_2 permeability region (10^4 to 10^5 Barrer; CO_2/N_2 selectivity of 5 to 20).

Table 5 brings together key data for the most important polymers discussed in this review. Values of BET surface area and FFV are included, where available, but very few aging studies have involved such measurements. Physical aging is associated with changes in the amount and distribution of free volume, and aging studies would ideally include detailed microstructural characterization of aged membrane samples. Unfortunately, the experimental tools available for investigating free volume are much less sensitive than the permeability measurements themselves. For example, for SBFDA-DMN after aging for 200 days, the apparent BET surface area drops from 686 to 608 m^2 g^{-1}, a decrease of just 11%, while the H_2 permeability drops from 2966 to 878 barrer, a decrease of 70%. There is a need for higher resolution techniques for evaluating changes in free volume distribution.

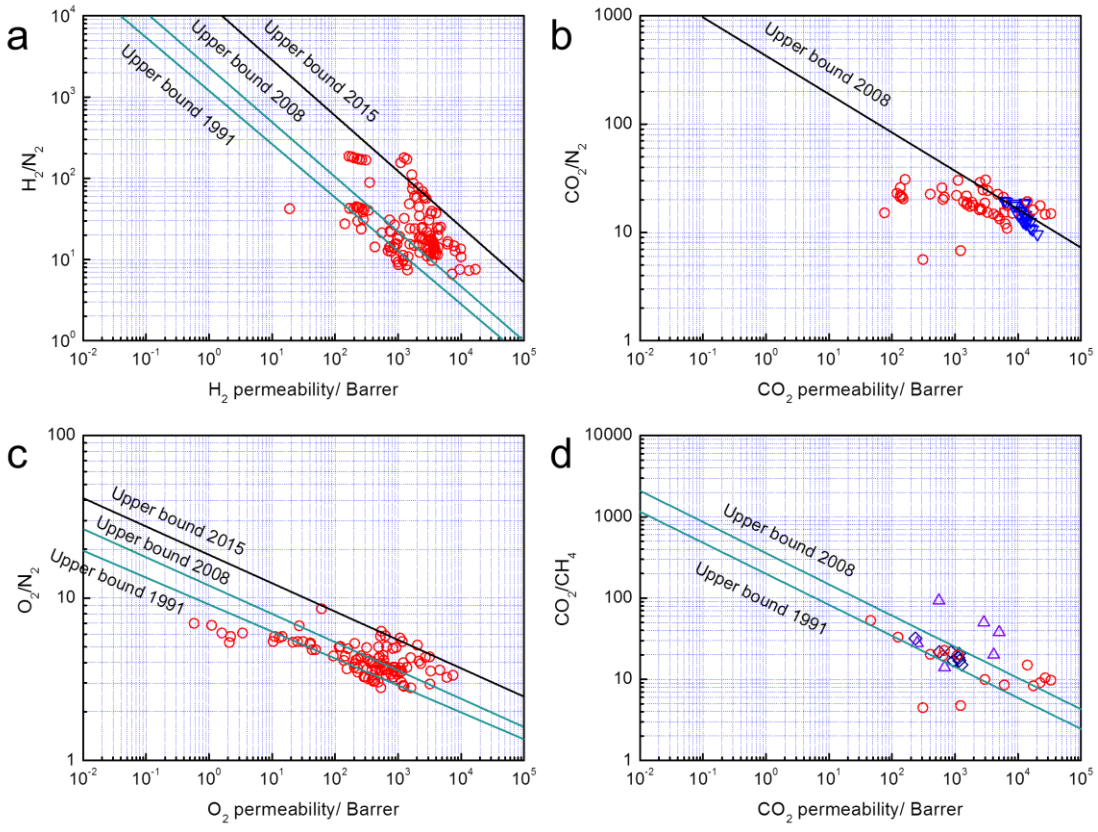

Figure 28. Double logarithmic (a) H_2/N_2, (b) CO_2/N_2, (c) O_2/N_2 and (d) CO_2/CH_4 Robeson plots of high free volume polymer membranes reviewed in this work. PIMs modified by fillers are denoted as blue inverted triangles. CMS membranes derived from high free volume polymers are denoted as violet triangles. Thermally-rearranged PIM polymers are denoted as navy blue diamonds.

Table 5. Gas transport properties of fresh and aged PIMs and PIM-PIs.[a]

Polymer	Age (day)	S_{BET} ($m^2 g^{-1}$)	FFV (%)	Permeability (Barrer)					Selectivity					Ref
				H_2	CO_2	O_2	N_2	CH_4	H_2/N_2	CO_2/N_2	O_2/N_2	H_2/CH_4	CO_2/CH_4	
PIMs														
PIM-1	1	720–820	24–26	5010.0	13600.0	2270.0	823.0	1360.0	6.1	16.5	2.8	3.7	10.0	[158]
	1380	-	-	1544.0	-	317.0	64.0	-	24.1	-	5.0	-	-	[59]
PIM-EA-TB	1	1030	-	7760.0	7140.0	2150.0	525.0	699.0	14.8	13.6	4.1	11.1	10.2	[61]
	2	-	-	6155.0	4780.0	1590.0	370.0	502.0	16.6	12.9	4.3	12.3	9.5	[61]
	470	-	-	4442.0	2644.0	933.0	188.0	219.0	23.6	14.1	5.0	20.3	12.1	[60]
PIM-Trip-TB	1	900	-	8039.0	9709.0	2718.0	629.0	905.0	12.8	15.4	4.3	8.9	10.7	[60]
	100	-	-	4740.0	3951.0	1073.0	189.0	218.0	25.1	20.9	5.7	21.7	18.1	[60]
PIM-Btrip-TB	1	870	-	9976.0	13205.0	3292.0	926.0	1440.0	10.8	14.3	3.6	6.9	9.2	[67]
	166	-	-	4280.0	4147.0	1166.0	216.0	283.0	19.8	19.2	5.4	15.1	14.7	[67]
TPIM-1	1	860	-	4300.0	-	1213.0	303.0	-	14.2	-	4.0	-	-	[59]
	15	-	-	2666.0	1549.0	368.0	54.0	50.0	49.4	28.7	6.8	53.3	31.0	[96]
	780	-	-	1105.0	-	61.0	7.1	-	155.6	-	8.6	-	-	[59]
TPIM-2	1	610	-	1010.0	-	511.0	117.0	-	8.6	-	4.4	-	-	[59]
	15	-	-	655.0	434.0	101.0	18.0	18.0	36.4	24.1	5.6	36.4	24.1	[96]
	720	-	-	354.0	-	27.0	4.0	-	88.5	-	6.8	-	-	[59]
PIM-TMN-Trip	1	1050	31.4	16900.0	33300.0	7470.0	2230.0	3420.0	7.6	14.9	3.3	4.9	9.7	[149]
	14	-	-	13400.0	27000.0	5950.0	1830.0	2590.0	7.3	14.8	3.3	5.2	10.4	[149]
	39	-	-	9590.0	22500.0	4600.0	1270.0	2470.0	7.6	17.7	3.6	3.9	9.1	[149]
	365	-	-	9840.0	14100.0	3160.0	727.0	943.0	13.5	19.4	4.3	10.4	15.0	[149]
PIM-TMN-SBI	1	1015	27.6	7190.0	17500.0	3200.0	1080.0	2100.0	6.7	16.2	3.0	3.4	8.3	[149]

	14	-	-	1370.0	2980.0	485.0	160.0	300.0	8.6	18.6	3.0	4.6	9.9	[149]
TB-Ad-Me	1	615	-	1800.0	1820.0	437.0	121.0	162.0	14.9	15.0	3.6	11.1	11.2	[65]
	180	-	-	745.0	635.0	145.0	33.0	41.0	22.6	19.2	4.4	18.2	15.5	[65]
PIM-HPB-2	1	537	-	1413.0	3800.0	534.0	190.0	361.0	7.4	20.0	2.8	3.9	10.5	[164]
	145	-	-	1000.0	2390.0	340.0	107.0	192.0	9.3	22.3	3.2	5.2	12.4	[164]
PIM-CH_3-HPB	1	560	-	1220.0	2620.0	408.0	122.0	230.0	10.0	21.5	3.3	5.3	11.4	[164]
	147	-	-	856.0	1630.0	256.0	60.0	132.0	14.3	27.2	4.3	6.5	12.3	[164]
PIM-Br-HPB	1	410	-	930.0	2130.0	301.0	92.0	177.0	10.1	23.2	3.3	5.3	12.0	[164]
	146	-	-	694.0	1430.0	203.0	54.0	102.0	12.9	26.5	3.8	6.8	14.0	[164]
PIM-CN-HPB	1	440	-	1200.0	2390.0	386.0	123.0	212.0	9.8	19.4	3.1	5.7	11.3	[164]
	147	-	-	734.0	1300.0	205.0	52.0	93.0	14.1	25.0	3.9	7.9	14.0	[164]
Amine-PIM-1	1	-	-	2210.0	1230.0	662.0	181.0	259.0	12.2	6.8	3.7	8.5	4.7	[70]
	540	-	-	1060.0	309.0	232.0	55.0	69.0	19.3	5.6	4.2	15.4	4.5	[70]
Crosslinked PIMs														
TOX-PIM-1 (385 °C, 24 h, 1 mbar)	1	-	-	1820.0	1100.0	245.0	30.1	15.9	60.5	36.5	8.1	114.5	69.2	[153]
	30	-	-	1649.0	514.0	128.0	14.8	6.6	111.4	34.7	8.6	249.8	77.9	[153]
	455	-	-	1380.0	310.0	70.0	8.1	4.1	170.4	38.3	8.6	339.9	76.4	[153]
TOX-PIM-1 (385 °C, 24 h,10 ppm O_2)	1	-	-	2768.0	3945.0	853.0	196.0	145.0	14.1	20.1	4.4	19.1	27.2	[153]
	30	-	-	2139.0	1488.0	348.0	48.0	27.0	44.6	31.0	7.3	79.2	55.1	[153]
	335	-	-	1967.0	995.0	262.0	34.4	18.9	57.2	28.9	7.6	104.1	52.6	[153]
Thermally rearranged PIMs														
O-PIM-PBO-1	1	405	-	881.0	1176.0	226.0	64.0	69.0	13.8	18.4	3.5	12.8	17.0	[212]
	270	-	-	555.0	564.0	111.0	26.0	26.0	21.3	21.7	4.3	21.3	21.7	[212]
PIM-PBO-3	1	360	-	768.0	870.0	134.0	35.0	40.0	21.9	24.9	3.8	19.2	21.8	[212]
	197	-	-	277.0	235.0	39.0	7.2	7.4	38.5	32.6	5.4	37.4	31.8	[212]
Blending with nanomaterials														

PIM-1/graphene KA1-7(6)	1	-	-	4660.0	12700.0	2260.0	870.0	1450.0	5.4	14.6	2.6	3.2	8.8	[219]
	226	-	-	3970.0	9240.0	1800.0	980.0	620.0	4.1	9.4	1.8	6.4	14.9	[219]
PIM-1/graphene KA1-7(3)	1	-	-	4730.0	9840.0	1850.0	570.0	800.0	8.3	17.3	3.2	5.9	12.3	[219]
	236	-	-	3450.0	6660.0	1250.0	340.0	460.0	10.1	19.6	3.7	7.5	14.5	[219]
PIM-1/graphene KA1-7(2)	1	-	-	4470.0	7830.0	1560.0	410.0	550.0	10.9	19.1	3.8	8.1	14.2	[219]
	236	-	-	3210.0	5680.0	1070.0	260.0	330.0	12.3	21.8	4.1	9.7	17.2	[219]
PIM-1/PAF-1	1	-	-	5533.1	-	-	1191.4	2233.3	4.6	-	-	2.5	-	[101]
	30	-	-	5504.0	-	-	1044.9	1744.4	5.3	-	-	3.2	-	[101]
	90	-	-	5436.0	-	-	911.3	1405.6	6.0	-	-	3.9	-	[101]
	180	-	-	5438.2	-	-	704.5	1155.6	7.7	-	-	4.7	-	[101]
	240	-	-	5400.0	-	-	719.6	1061.1	7.5	-	-	5.1	-	[101]
	400	-	-	5165.5	-	-	400.7	466.7	12.9	-	-	11.1	-	[101]
PIM-1/HCP (5.7 wt%)	1	-	-	-	12081.0	-	961.0	-	-	12.6	-	-	-	[222]
	15	-	-	-	10174.0	-	703.0	-	-	14.5	-	-	-	[222]
	30	-	-	-	9446.0	-	609.0	-	-	15.5	-	-	-	[222]
	45	-	-	-	8737.0	-	473.0	-	-	18.5	-	-	-	[222]
	90	-	-	-	6647.0	-	347.0	-	-	19.2	-	-	-	[222]
	150	-	-	-	6050.0	-	314.0	-	-	19.3	-	-	-	[222]
PIM-1/HCP (16.67 wt%)	1	-	-	-	15913.0	-	1443.0	-	-	11.0	-	-	-	[222]
	15	-	-	-	13254.0	-	1104.0	-	-	12.0	-	-	-	[222]
	30	-	-	-	12963.0	-	938.0	-	-	13.8	-	-	-	[222]
	45	-	-	-	12010.0	-	751.0	-	-	16.0	-	-	-	[222]
	90	-	-	-	9072.0	-	518.0	-	-	17.5	-	-	-	[222]
	150	-	-	-	8369.0	-	477.0	-	-	17.5	-	-	-	[222]
PIM-1/HCP (21.3 wt%)	1	-	-	-	20394.0	-	2109.0	-	-	9.7	-	-	-	[222]
	15	-	-	-	17002.0	-	1600.0	-	-	10.6	-	-	-	[222]

	30	-	-	-	15852.0	-	1267.0	-	-	12.5	-	-	-	[222]
	45	-	-	-	14707.0	-	1084.0	-	-	13.6	-	-	-	[222]
	90	-	-	-	12799.0	-	882.0	-	-	14.5	-	-	-	[222]
	150	-	-	-	12256.0	-	831.0	-	-	14.7	-	-	-	[222]
PIM-1/pyrene (10 wt%)	9	-	-	-	153.9	-	7.5	-	-	20.4	-	-	-	[211]
	17	-	-	-	141.9	-	6.7	-	-	21.3	-	-	-	[211]
	35	-	-	-	138.2	-	6.5	-	-	21.2	-	-	-	[211]
	50	-	-	-	138.2	-	6.2	-	-	22.2	-	-	-	[211]
PIM-1/aminopyrene (10 wt%)	9	-	-	-	77.4	-	5.1	-	-	15.2	-	-	-	[211]
	17	-	-	-	122.4	-	5.3	-	-	23.0	-	-	-	[211]
	35	-	-	-	136.3	-	5.3	-	-	26.0	-	-	-	[211]
	50	-	-	-	160.2	-	5.2	-	-	30.9	-	-	-	[211]
PIM-1/POSS (98:2)	1	-	9.1	-	6730.0	1249.8	415.5	644.1	-	16.2	3.0	-	10.4	[227]
	10	-	-	-	-	1064.4	330.8	471.5	-	-	3.2	-	-	[227]
	20	-	-	-	-	1029.2	310.0	436.3	-	-	3.3	-	-	[227]
	30	-	-	-	-	994.1	294.1	413.9	-	-	3.4	-	-	[227]
	60	-	-	-	-	896.6	247.7	332.4	-	-	3.6	-	-	[227]
	120	-	-	-	-	784.7	217.4	260.5	-	-	3.6	-	-	[227]
PIM-CD-0.5%	1	-	7.9	2994.0	5435.0	994.0	214.0	315.0	14.0	25.4	4.6	9.5	17.3	[228]
	10	-	-	2849.1	5061.1	888.7	179.8	247.7	15.8	28.1	4.9	11.5	20.4	[228]
	30	-	-	2765.0	4757.1	814.7	161.1	214.3	17.2	29.5	5.1	12.9	22.2	[228]
	60	-	-	2747.3	4694.5	810.6	153.9	208.9	17.9	30.5	5.3	13.1	22.5	[228]
	90	-	-	2723.9	4601.7	804.7	153.0	200.1	17.8	30.1	5.3	13.6	23.0	[228]
	120	-	-	2672.8	4609.8	787.7	148.1	198.2	18.0	31.1	5.3	13.5	23.3	[228]
PIM-CD-1.0%	1	-	8.3	3365.0	6574.0	1123.0	283.0	447.0	11.9	23.2	4.0	7.5	14.7	[228]
	10	-	-	3239.4	6194.0	1016.3	240.8	359.6	13.5	25.7	4.2	9.0	17.2	[228]

	30	-	-	3138.4	6021.2	991.0	223.9	335.4	14.0	26.9	4.4	9.4	18.0	[228]
	60	-	-	3112.1	5957.6	984.3	221.2	322.8	14.1	26.9	4.4	9.6	18.5	[228]
	90	-	-	3085.8	5857.3	967.1	219.0	320.1	14.1	26.7	4.4	9.6	18.3	[228]
	120	-	-	3059.5	5781.5	958.4	213.6	317.4	14.3	27.1	4.5	9.6	18.2	[228]
PIM-CD-2.0%	1	-	8.8	3889.0	8812.0	1671.0	481.0	716.0	8.1	18.3	3.5	5.4	12.3	[228]
	10	-	-	3823.9	8566.1	1580.8	432.7	612.1	8.8	19.8	3.7	6.2	14.0	[228]
	30	-	-	3758.8	8418.5	1559.1	414.8	590.8	9.1	20.3	3.8	6.4	14.2	[228]
	60	-	-	3737.1	8336.6	1546.6	399.6	582.8	9.4	20.9	3.9	6.4	14.3	[228]
	90	-	-	3686.4	8238.2	1524.9	396.9	562.8	9.3	20.8	3.8	6.6	14.6	[228]
	120	-	-	3664.7	8139.8	1521.8	391.5	552.2	9.4	20.8	3.9	6.6	14.7	[228]
Synergy approach														
TOX-PIM-1/ZIF-8 (5 wt%)	1	-	-	3086.0	2745.0	608.0	100.0	73.0	30.9	27.5	6.1	42.3	37.6	[230]
	10	-	-	2609.6	1363.7	337.6	44.8	28.1	58.2	30.4	7.5	92.7	48.5	[230]
	20	-	-	2541.9	1228.3	320.6	41.2	25.9	61.7	29.8	7.8	98.3	47.5	[230]
	30	-	-	2429.1	1138.0	286.7	35.5	23.8	68.5	32.1	8.1	102.1	47.8	[230]
	450	-	-	2075.0	840.4	214.6	27.0	18.0	76.7	31.1	7.9	115.5	46.8	[230]
	740	-	-	1671.7	645.6	172.1	22.7	14.2	73.7	28.5	7.6	117.9	45.5	[230]
PIM-PIs														
Spirobisindane (SBI)														
PIM-PI-EA (PIM-PI-12)	1	620	-	4230.0	7340.0	1380.0	369.0	457.0	11.5	19.9	3.7	9.3	16.1	[167]
	273	-	-	2860.0	-	659.0	131.0	-	21.8	-	5.0	-	-	[167]
Spirobifluorene (SBF)														
SBFDA-DMN	1	686	-	2966.0	-	850.0	226.0	-	13.1	-	3.8	-	-	[168]
	10	-	-	2146.0	-	593.0	143.0	-	15.0	-	4.1	-	-	[168]
	200	608	-	878.0	-	161.0	33.0	-	26.6	-	4.9	-	-	[168]
Tröger's base (TB)														

TBDA-SBIDA	1	733	-	3200.0	5140.0	1132.0	373.0	591.0	8.6	13.8	3.0	5.4	8.7	[166]
	509	-	-	-	2476.0	575.0	152.0	-	-	16.3	3.8	-	-	[166]
TBDA-SBFDA	1	739	-	2901.0	4476.0	941.0	264.0	371.0	11.0	17.0	3.6	7.8	12.1	[166]
	405	-	-	1200.0	1621.0	386.0	106.0	125.0	11.3	15.3	3.6	9.6	13.0	[166]
4MTBDA-PMDA	1	650	-	3300.0	4460.0	1080.0	290.0	360.0	11.4	15.4	3.7	9.2	12.4	[166]
	333	-	-	1531.0	1689.0	394.0	99.0	114.0	15.5	17.1	4.0	13.4	14.8	[166]
4MTBDA-6FDA	1	584	-	1446.0	1672.0	408.0	133.0	116.0	10.9	12.6	3.1	12.5	14.4	[166]
	524	-	-	964.0	1008.0	229.0	62.0	60.0	15.5	16.3	3.7	16.1	16.8	[166]
Triptycene														
6FDA-DAT1	1	320	-	198.0	120.0	25.4	4.7	3.2	42.1	25.5	5.4	61.9	37.5	[171]
	150	-	-	170.0	102.0	21.4	4.0	2.7	42.5	25.5	5.4	63.0	37.8	[171]
6FDA-DAT2	1	450	-	281.0	210.0	43.3	9.0	7.1	31.2	23.3	4.8	39.6	29.6	[171]
	150	-	-	229.0	160.0	40.7	7.7	5.3	29.7	20.8	5.3	43.2	30.2	[171]
KAUST-PI-1	1	752	-	4183.0	-	827.0	169.0	-	24.8	-	4.9	-	-	[59]
	15	-	-	3983.0	2389.0	627.0	107.0	105.0	37.2	22.3	5.9	37.9	22.8	[98]
	150	-	-	3431.0	-	542.0	87.0	-	39.4	-	6.2	-	-	[59]
KAUST-PI-2	1	740	-	2436.0	-	582.0	131.0	-	18.6	-	4.4	-	-	[59]
	15	-	-	2368.0	2071.0	490.0	98.0	101.0	24.2	21.1	5.0	23.4	20.5	[98]
	870	-	-	1255.0	-	205.0	39.0	-	32.2	-	5.3	-	-	[59]
KAUST-PI-7	1	840	-	-	-	865.0	240.0	-	-	-	3.6	-	-	[59]
	15	-	-	3198.0	4391.0	842.0	225.0	354.0	14.2	19.5	3.7	9.0	12.4	[162]
	660	-	-	2164.0	-	490.0	115.0	-	18.8	-	4.3	-	-	[59]

[a] Note: Day 1 is generally defined as the first day of measurement after drying of methanol-treated film (which is usually after drying for 24 h). The gas permeability data varies with the measurement technique, film thickness, film preparation technique and film history. The actual measurement and report of the initial permeability of the film (i.e. day 1) should be referred to the references provided

7. Concluding remarks

7.1. Importance of Robeson plots for membrane aging studies

We have considered most, if not all, PIM and PIM-based polymers that are promising for gas separation applications, and all the studies related to the physical aging of high free volume polymers up to 2017. Effective approaches for mitigating aging are assessed based on the initial gas transport properties, as well as on the changes to the gas selectivity and permeability of the polymer film over time, for industrially important gas pairs. The permeability data collected from the literature were presented in Robeson plots when possible, to better evaluate the effectiveness of the approaches in mitigating aging. The Robeson plot allows the comparison of different polymers which are aged differently (with different aging conditions and aging duration), provided the same gas pairs are measured. By representing the aging results in a Robeson plot, the gas separation performance of a new polymer membrane can be evaluated against the upper bound, and the shift of the gas permeability-selectivity data over time from the upper bound can be observed. This provides a more complete picture of the aging profile than just a report of change in gas permeability over time. For example, a rapid drop in large FVEs and slower drop in small FVEs in a polymer film could shift a point that is above the Robeson upper bound to a more favorable position, as shown by **PIM-1/PAF-1**[101] and **TOX-PIM-1.**[153] Similarly, a relatively modest drop in larger FVEs compared to the smaller FVEs would cause an undesirable shift of points that are above the upper bound to be closer to the upper bound (or data points that are below the upper bound to shift further below the upper bound).[70,212,233] However, complete gas permeability data are not always available for all Robeson plots for different gas pairs. Also,

improvement in aging resistance is less useful if the initial gas transport properties of the polymer are not industrially competitive for gas separation. The Robeson plot allows one to compare the performance of the membrane with ease, should the data be available. However, the Robeson plot needs to be used with caution, as it does not account for the format of the membrane tested (flat sheet vs hollow fiber), the thickness of the main layer (single polymer vs thin film composite) or the transmembrane pressure at which the permeability is measured. Nevertheless, representing the aging profile of polymer films in the Robeson plot still allows membranologists to identify approaches with high potential to solve aging problems. A plot of gas selectivity against gas permeance for thin film composites, that takes account of the thickness of the membrane, may be more relevant to practical gas separation applications.

7.2. Elimination of thermal history

As high free volume polymers (such as PTMSP and PIMs) age rapidly, aging occurs as soon as the film is formed. The removal of thermal history of the film via annealing above the glass transition temperature (T_g) is not possible for such polymers, due to the very high or immeasurable T_g. Instead, these high free volume polymers are soaked in non-solvents such as methanol or ethanol. When soaked, the film is swollen and the trapped solvents used in the film preparation, as well as adsorbed contaminants, are removed from the micropores, therefore generating more free volume, leading to an increase in the gas permeability of the films. Furthermore, gas selectivity may also increase after conditioning when a larger amount of small FVEs relevant for transport of small gas molecules are generated. To ease comparison, conditioning protocols should be as consistent as possible for each type of polymer so that the polymer measured has a comparable initial aging state. For PIMs,

common practice involves soaking the film in methanol for 24 h at room temperature. The film can then be heated *in vacuo* to remove the methanol before measurement of its permeability. When the time-lag method is used, the film is directly degassed in the permeation test apparatus under vacuum.

Here we suggest a preferred procedure to eliminate the thermal history of a high free volume polymer such as a PIM: The film is first soaked in methanol (slowly by introducing the edge of the film to the methanol until the film is fully immersed; methanol being the preferred non-solvent) and kept in the methanol bath for at least 12 h at room temperature. The film is subsequently removed from the methanol bath and kept at RT under N_2 flow for at least 12 h, before being heated to 50 °C under vacuum for another 24 h. Precaution may need to be taken (for instance, by having a glass Petri dish sitting on the film) to ensure that the film does not curl up during the treatment. Vacuum is applied to facilitate removal of the methanol in the film as well as to ensure all films undergo a vacuum stage regardless of the gas measurement technique. Note that the methanol soaking technique widely applied for membrane films may be less suitable for thin film composites as it may delaminate the thin film from the substrate.

7.3. Measurement and reporting of gas permeability and aging rate

We observed that polymers with different structures age differently. Depending on the structure of the polymer backbone, and on interactions with any fillers that may be present, aging affects various sizes of FVEs within the polymer film. Understanding of the aging of a polymer film is incomplete when the permeability of just a single gas is tracked over the aging time of the film, as the experiment is unable to differentiate the changes to FVEs of different sizes. It has been shown that

the rate of aging, as tracked by gas permeability, is dependent on the size of the gas molecule probe.[34] Here we suggest measuring the gas permeabilities of at least one important gas pair when studying aging of polymer films.

Pinnau and co-workers suggest that the gas permeability of a high free volume polymer be reported about 10–15 days after film conditioning, as there exists a quasi-steady-state after a rapid initial drop in the gas permeability and increase in the gas selectivity.[162] It is suggested that reporting the gas permeability within the first two weeks does not truly represent the performance of the polymer film, since the permeation data are highly dependent on the time at which the permeation is measured and the conditions of both the environment and the film. We agree with the suggestion by Pinnau *et al.* that the permeability should be reported after the quasi-steady-state has been reached, and two weeks after film conditioning may be suitable for most PIMs and PIM-PIs. This would represent a more realistic permeability of the film. Subsequent measurement of the long-term performance can be performed periodically up to several years.

7.4. Aging and storing conditions

Aging of a high free volume polymer occurs rapidly in the first few days/weeks, followed by slower aging over several years. Most typical aging protocols involve storing the film at room temperature in a sealed bag or Petri dish. To improve comparison of aging results across the literature, we propose that films should be aged at RT in a sealed container (can be a desiccator), with desiccant, to isolate the film from any contaminants or humid air.

7.5. Promising approaches for mitigating aging

In this review, we have assessed the aging performance of membranes produced from polymers with different backbones and functional groups, and considered the effects of post-modification and of blending with other materials. Looking forward, we recommend the three most promising approaches for mitigating aging, and indicate their advantages and limitations.

I. Design of polymer backbone

Design of polymer backbone architecture remains one of the most popular approaches in the search for new properties and performance. Indeed, this is the same approach that enabled the discovery of PIMs. Due to the wide range of possibilities within this domain, this approach gives one of the greatest degrees of freedom in tailoring the polymer for a targeted application. However, such an approach may also involve complex synthesis procedures and produce low yields.

II. Blending of microporous fillers

Blending of microporous fillers into the polymer allows one to produce polymer-based membranes with enhanced gas separation performance. In PIMs, such blending can be targeted towards stopping the FVEs of the PIM film from collapsing. Blending with microporous fillers has shown some promising aging resistant performances, but the high cost and scalability issues of some of the best fillers (e.g. PAFs) remain a hindrance to practical application. In addition, blending of microporous fillers is less suitable for thin film composite membranes, especially for fillers with size similar to, or larger than, the thickness of the membrane active layer.

III. Post-modification of the polymer structure

Since physical aging involves the collapse of the FVEs, the post-modification approach to induce crosslinking appears to be an effective method. So far, both

thermal crosslinking and UV irradiation-induced photo-oxidation of PIMs have produced aging resistant PIM membranes. PIM-based CMS membranes show remarkable gas separation performance, exceeding conventional CMS membranes derived from other polymers. PIM CMS membranes, like other CMS membranes, are not susceptible to plasticization or swelling, but scalability, pore blocking, and brittleness remain challenges.

Overall, these approaches indicate the way forward in identifying an effective solution to the problem of physical aging, enabling stable gas separation performance that exceeds all conventionally used gas separation membranes, and that can be maintained over a commercially useful period. In future research, these approaches will need increasingly to be applied to thin (<1 μm) films that represent the active separation layers in commercially viable asymmetric or thin film composite membranes.

Author Information

Corresponding Authors

*E-mail: peter.budd@manchester.ac.uk

*E-mail: neil.mckeown@ed.ac.uk

Notes

The authors declare no competing financial interest

Biographies

Ze-Xian (Nicholas) Low received his Ph.D. in Chemical Engineering at Monash University under the direction of Prof. Huanting Wang in 2015. He then joined Dr. Darrell Patterson's, and later Prof. Davide Mattia's, group as a postdoctoral research associate in the Centre of Advanced Separations Engineering, University of Bath. His current research focuses on the advanced characterization of polymer membranes, 3D printing of polymer membranes, and hybrid membranes for water purification.

Peter Budd is a Chartered Chemist and is Professor of Polymer Chemistry at the University of Manchester. He obtained his BSc (1978) and PhD (1981) from Manchester. He spent eight years as a research chemist with BP before taking up an academic position at Manchester in 1989. He has extensive experience in materials development relevant to membrane processes and other applications. He is co-inventor (with McKeown) of "Polymers of Intrinsic Microporosity" (PIMs).

Neil McKeown is the Crawford Tercentenary Chair of Chemistry at the University of Edinburgh. His expertise is in the synthesis of organic materials with a focus on the preparation of membrane-forming Polymers of Intrinsic Microporosity (PIMs), of which he is co-inventor (with Budd) and for which he was awarded the 2008 Beilby Medal and the 2017 Tilden Medal by the Royal Society of Chemistry.

Darrell Patterson completed his PhD in Chemical and Biochemical Engineering at Imperial College London, in 2001. He worked as a Technology Development Consultant for Atkins Water between 2001 until 2003. He then went on to Imperial College as a postdoctoral research associate, developing novel methods of enhancing solvent based pharmaceutical reactions through integration with solvent resistant membranes. He returned to the University of Auckland in 2005 where he

worked as a Lecturer and then Senior Lecturer in the Department of Chemical and Materials Engineering, before joining the University of Bath in 2011. His research was recognised with a University of Auckland Early Career Research Excellence Award in 2009 and a Highly Commended awarding in the IChemE Sir Frederick Warner Prize in 2011. He passed away on 19th February 2017, while this manuscript was in preparation.

Acknowledgements

The work is supported by Programme Grant EP/M01486X/1 (SynFabFun) funded by the Engineering and Physical Sciences Research Council (EPSRC). The authors are grateful to Dr. Mariolino Carta, Dr. Richard Malpass-Evans, Dr. Andrew Foster, Dr. Wayne Harrison, Dr. Rupesh Bhavsar, Dr. Sara Sorribas, Dr. Qilei Song, Dr. Bo Wang, Dr. Maria-Chiara Ferrari, Dr. Patricia Gorgojo, Dr. John Chew, Prof. Davide Mattia and Marzieh Tamaddondar for their valuable discussions. The authors also gratefully acknowledge the permissions to reproduce the copyright material in this review. Darrell Patterson sadly passed away on 19th February 2017. This contribution is dedicated to his memory.

References

(1) Baker, R. W.; Low, B. T. Gas Separation Membrane Materials: a Perspective. *Macromolecules* **2014,** *47*, 6999-7013.

(2) Park, H. B.; Kamcev, J.; Robeson, L. M.; Elimelech, M.; Freeman, B. D. Maximizing the Right Stuff: the Trade-Off Between Membrane Permeability and Selectivity. *Science* **2017,** *356*.

(3) Masuda, T.; Isobe, E.; Higashimura, T.; Takada, K. Poly [1-(Trimethylsilyl)-1-Propyne]: a New High Polymer Synthesized with Transition-Metal Catalysts and Characterized by Extremely High Gas Permeability. *J. Am. Chem. Soc.* **1983,** *105*, 7473-7474.

(4) Nemser, S. M.; Roman, I. C.; U.S. Patent 5,051,114, 1991.

(5) Budd, P. M.; Ghanem, B. S.; Makhseed, S.; McKeown, N. B.; Msayib, K. J.; Tattershall, C. E. Polymers of Intrinsic Microporosity (PIMs): Robust, Solution-processable, Organic Nanoporous Materials. *Chem. Commun.* **2004**, 230-231.

(6) Park, H. B.; Jung, C. H.; Lee, Y. M.; Hill, A. J.; Pas, S. J.; Mudie, S. T.; Van Wagner, E.; Freeman, B. D.; Cookson, D. J. Polymers with Cavities Tuned for Fast Selective Transport of Small Molecules and Ions. *Science* **2007,** *318*, 254-258.

(7) Drioli, E.; Barbieri, G.; Brunetti, A. *Membrane Engineering for the Treatment of Gases Volume 2: Gas-separation Issues Combined with Membrane Reactors: Edition 2*; Royal Society of Chemistry: Croydon, U. K., 2017.
(8) Bernardo, P.; Clarizia, G. 30 Years of Membrane Technology for Gas Separation. *Chem. Eng. Trans.* **2013,** *32*, 1999-2004.
(9) Baker, R. W. Future Directions of Membrane Gas Separation Technology. *Ind. Eng. Chem. Res.* **2002,** *41*, 1393-1411.
(10) Wessling, M.; Schoeman, S.; Van der Boomgaard, T.; Smolders, C. Plasticization of Gas Separation Membranes. *Gas. Sep. Purif.* **1991,** *5*, 222-228.
(11) Chiou, J.; Barlow, J. W.; Paul, D. R. Plasticization of Glassy Polymers by CO2. *J. Appl. Polym. Sci.* **1985,** *30*, 2633-2642.
(12) Hutchinson, J. M. Physical Aging of Polymers. *Prog. Polym. Sci.* **1995,** *20*, 703-760.
(13) Nagai, K.; Nakagawa, T. Effects of Aging on the Gas Permeability and Solubility in Poly (1-Trimethylsilyl-1-Propyne) Membranes Synthesized with Various Catalysts. *J. Membr. Sci.* **1995,** *105*, 261-272.
(14) Hu, Y.; Shiotsuki, M.; Sanda, F.; Freeman, B. D.; Masuda, T. Synthesis and Properties of Indan-Based Polyacetylenes That Feature the Highest Gas Permeability Among All the Existing Polymers. *Macromolecules* **2008,** *41*, 8525-8532.
(15) Chapala, P. P.; Bermeshev, M. V.; Starannikova, L. E.; Belov, N. A.; Ryzhikh, V. E.; Shantarovich, V. P.; Lakhtin, V. G.; Gavrilova, N. N.; Yampolskii, Y. P.; Finkelshtein, E. S. A Novel, Highly Gas-Permeable Polymer Representing a New Class of Silicon-Containing Polynorbornens As Efficient Membrane Materials. *Macromolecules* **2015,** *48*, 8055-8061.
(16) Budd, P. M.; McKeown, N. B.; Fritsch, D. Free Volume and Intrinsic Microporosity in Polymers. *J. Mater. Chem.* **2005,** *15*, 1977-1986.
(17) McKeown, N. B.; Budd, P. M. Polymers of Intrinsic Microporosity (PIMs): Organic Materials for Membrane Separations, Heterogeneous Catalysis and Hydrogen Storage. *Chem. Soc. Rev.* **2006,** *35*, 675-683.
(18) McKeown, N. B.; Budd, P. M. Exploitation of Intrinsic Microporosity in Polymer-Based Materials. *Macromolecules* **2010,** *43*, 5163-5176.
(19) Robeson, L. M. Correlation of Separation Factor Versus Permeability for Polymeric Membranes. *J. Membr. Sci.* **1991,** *62*, 165-185.
(20) Robeson, L. M. The Upper Bound Revisited. *J. Membr. Sci.* **2008,** *320*, 390-400.
(21) Swaidan, R.; Ghanem, B.; Pinnau, I. Fine-Tuned Intrinsically Ultramicroporous Polymers Redefine the Permeability/Selectivity Upper Bounds of Membrane-Based Air and Hydrogen Separations. *ACS Macro Lett.* **2015,** *4*, 947-951.
(22) Lau, C. H.; Nguyen, P. T.; Hill, M. R.; Thornton, A. W.; Konstas, K.; Doherty, C. M.; Mulder, R. J.; Bourgeois, L.; Liu, A. C.; Sprouster, D. J. Ending Aging in Super Glassy Polymer Membranes. *Angew. Chem.* **2014,** *126*, 5426-5430.
(23) Cangialosi, D.; Boucher, V. M.; Alegría, A.; Colmenero, J. Physical Aging in Polymers and Polymer Nanocomposites: Recent Results and Open Questions. *Soft Matter* **2013,** *9*, 8619-8630.
(24) Rowe, B.; Freeman, B.; Paul, D. In *Membrane Engineering for the Treatment of Gases*; Royal Society of Chemistry: Croydon, U. K., 2011.
(25) Struik, L. C. E. *Physical Aging in Amorphous Polymers and Other Materials*; Elsevier Amsterdam, 1978.
(26) Kim, J.; Koros, W. J.; Paul, D. R. Physical Aging of Thin 6FDA-Based Polyimide Membranes Containing Carboxyl Acid Groups. Part I. Transport Properties. *Polymer* **2006,** *47*, 3094-3103.
(27) Tiwari, R. R.; Smith, Z. P.; Lin, H.; Freeman, B.; Paul, D. Gas Permeation in Thin Films of “High Free-Volume” Glassy Perfluoropolymers: Part I. Physical Aging. *Polymer* **2014,** *55*, 5788-5800.
(28) Yavari, M.; Maruf, S.; Ding, Y.; Lin, H. Physical Aging of Glassy Perfluoropolymers in Thin Film Composite Membranes. Part II. Glass Transition Temperature and the Free Volume Model. *J. Membr. Sci.* **2017,** *525*, 399-408.

(29) Drozdov, A. D. The Effect of Temperature on Physical Aging of Glassy Polymers. *J. Appl. Polym. Sci.* **2001,** *81*, 3309-3320.
(30) Davis, W. J.; Pethrick, R. A. Investigation of Physical Ageing in Polymethylmethacrylate Using Positron Annihilation, Dielectric Relaxation and Dynamic Mechanical Thermal Analysis. *Polymer* **1998,** *39*, 255-266.
(31) Cowie, J.; Harris, S.; McEwen, I. Physical Aging in Poly (vinyl acetate). 2. Relative Rates of Volume and Enthalpy Relaxation. *Macromolecules* **1998,** *31*, 2611-2615.
(32) Huang, Y.; Paul, D. R. Effect of Temperature on Physical Aging of Thin Glassy Polymer Films. *Macromolecules* **2005,** *38*, 10148-10154.
(33) Huang, Y.; Paul, D. Physical Aging of Thin Glassy Polymer Films Monitored by Gas Permeability. *Polymer* **2004,** *45*, 8377-8393.
(34) Bernardo, P.; Bazzarelli, F.; Tasselli, F.; Clarizia, G.; Mason, C.; Maynard-Atem, L.; Budd, P.; Lanč, M.; Pilnáček, K.; Vopička, O. Effect of Physical Aging on The Gas Transport and Sorption in PIM-1 Membranes. *Polymer* **2017,** *113*, 283-294.
(35) Pilnáček, K.; Vopička, O.; Lanč, M.; Dendisová, M.; Zgažar, M.; Budd, P. M.; Carta, M.; Malpass-Evans, R.; McKeown, N. B.; Friess, K. Aging of Polymers of Intrinsic Microporosity Tracked by Methanol Vapour Permeation. *J. Membr. Sci.* **2016,** *520*, 895-906.
(36) Huang, Y.; Paul, D. Physical Aging of Thin Glassy Polymer Films Monitored by Optical Properties. *Macromolecules* **2006,** *39*, 1554-1559.
(37) Pfromm, P.; Koros, W. Accelerated Physical Ageing of Thin Glassy Polymer Films: Evidence from Gas Transport Measurements. *Polymer* **1995,** *36*, 2379-2387.
(38) Huang, Y.; Wang, X.; Paul, D. R. Physical Aging of Thin Glassy Polymer Films: Free Volume Interpretation. *J. Membr. Sci.* **2006,** *277*, 219-229.
(39) Huang, Y.; Paul, D. R. Experimental Methods for Tracking Physical Aging of Thin Glassy Polymer Films by Gas Permeation. *J. Membr. Sci.* **2004,** *244*, 167-178.
(40) Rowe, B. W.; Pas, S. J.; Hill, A. J.; Suzuki, R.; Freeman, B. D.; Paul, D. A variable energy positron annihilation lifetime spectroscopy study of physical aging in thin glassy polymer films. *Polymer* **2009,** *50*, 6149-6156.
(41) Dorkenoo, K. D.; Pfromm, P. H. Accelerated Physical Aging of Thin Poly [1-(trimethylsilyl)-1-propyne] Films. *Macromolecules* **2000,** *33*, 3747-3751.
(42) Tiwari, R. R.; Smith, Z. P.; Lin, H.; Freeman, B.; Paul, D. Gas Permeation in Thin Films of “High Free-Volume” Glassy Perfluoropolymers: Part II. CO2 Plasticization and Sorption. *Polymer* **2015,** *61*, 1-14.
(43) Yavari, M.; Le, T.; Lin, H. Physical Aging of Glassy Perfluoropolymers in Thin Film Composite Membranes. Part I. Gas Transport Properties. *J. Membr. Sci.* **2017,** *525*, 387-398.
(44) Koschine, T.; Rätzke, K.; Faupel, F.; Khan, M. M.; Emmler, T.; Filiz, V.; Abetz, V.; Ravelli, L.; Egger, W. Correlation of Gas Permeation and Free Volume in New and Used High Free Volume Thin Film Composite Membranes. *J. Polym. Sci., Part B: Polym. Phys.* **2015,** *53*, 213-217.
(45) Tiwari, R. R.; Jin, J.; Freeman, B.; Paul, D. Physical Aging, CO2 Sorption and Plasticization in Thin Films of Polymer with Intrinsic Microporosity (PIM-1). *J. Membr. Sci.* **2017,** *537*, 362-371.
(46) McKeown, N. The Synthesis of Polymers of Intrinsic Microporosity. *Sci. China Chem.* **2017,** *60*, 1023-1032.
(47) Eastmond, G. C.; Paprotny, J.; Steiner, A.; Swanson, L. Synthesis of Cyanodibenzo [1, 4] Dioxines and Their Derivatives by Cyano-activated Fluoro Displacement Reactions. *New. J. Chem.* **2001,** *25*, 379-384.
(48) Budd, P. M.; Elabas, E. S.; Ghanem, B. S.; Makhseed, S.; McKeown, N. B.; Msayib, K. J.; Tattershall, C. E.; Wang, D. Solution‐Processed, Organophilic Membrane Derived from A Polymer of Intrinsic Microporosity. *Adv. Mater.* **2004,** *16*, 456-459.
(49) Du, N.; Song, J.; Robertson, G. P.; Pinnau, I.; Guiver, M. D. Linear High Molecular Weight Ladder Polymer via Fast Polycondensation of 5, 5′, 6, 6′‐Tetrahydroxy‐

3, 3, 3′, 3′-tetramethylspirobisindane with 1, 4-Dicyanotetrafluorobenzene. *Macromol. Rapid Comm.* **2008,** *29*, 783-788.
(50) Satilmis, B.; Budd, P. M. Selective Dye Adsorption by Chemically-Modified and Thermally-Treated Polymers of Intrinsic Microporosity. *J. Colloid Interface Sci.* **2017,** *492*, 81-91.
(51) Ponomarev, I. I.; Blagodatskikh, I. V.; Muranov, A. V.; Volkova, Y. A.; Razorenov, D. Y.; Ponomarev, I. I.; Skupov, K. M. Dimethyl Sulfoxide as a Green Solvent for Successful Precipitative Polyheterocyclization Based on Nucleophilic Aromatic Substitution, Resulting in High Molecular Weight PIM-1. *Mendeleev Commun.* **2016,** *26*, 362-364.
(52) Zhang, P.; Jiang, X.; Wan, S.; Dai, S. Advancing Polymers of Intrinsic Microporosity by Mechanochemistry. *J. Mater. Chem. A* **2015,** *3*, 6739-6741.
(53) Kricheldorf, H. R.; Fritsch, D.; Vakhtangishvili, L.; Schwarz, G. Cyclic Ladder Polymers by Polycondensation of Silylated Tetrahydroxy-Tetramethylspirobisindane with 1, 4-Dicyanotetrafluorobenzene. *Macromol. Chem. Phys.* **2005,** *206*, 2239-2247.
(54) Kricheldorf, H. R.; Fritsch, D.; Vakhtangishvili, L.; Lomadze, N.; Schwarz, G. Cyclic Ladder Polymers Based on 5, 5 ‘, 6, 6 ‘-Tetrahydroxy-3, 3, 3 ‘, 3 ‘-Tetramethylspirobisindane and 2, 3, 5, 6-Tetrafluoropyridines. *Macromolecules* **2006,** *39*, 4990-4998.
(55) Zhang, J.; Jin, J.; Cooney, R.; Zhang, S. Fluoride-Mediated Polycondensation for the Synthesis of Polymers of Intrinsic Microporosity. *Polymer* **2015,** *76*, 168-172.
(56) Kricheldorf, H. (Ed.) *Silicon in Polymer Synthesis*; Springer -Verlag: Berlin, Germany, 1996.
(57) Song, J.; Du, N.; Dai, Y.; Robertson, G. P.; Guiver, M. D.; Thomas, S.; Pinnau, I. Linear High Molecular Weight Ladder Polymers by Optimized Polycondensation of Tetrahydroxytetramethylspirobisindane and 1, 4-Dicyanotetrafluorobenzene. *Macromolecules* **2008,** *41*, 7411-7417.
(58) Kricheldorf, H. R.; Lomadze, N.; Fritsch, D.; Schwarz, G. Cyclic and Telechelic Ladder Polymers Derived from Tetrahydroxytetramethylspirobisindane and 1, 4-Dicyanotetrafluorobenzene. *J. Polym. Sci. A Polym. Chem.* **2006,** *44*, 5344-5352.
(59) Swaidan, R.; Ghanem, B.; Litwiller, E.; Pinnau, I. Physical Aging, Plasticization and Their Effects on Gas Permeation in “Rigid” Polymers of Intrinsic Microporosity. *Macromolecules* **2015,** *48*, 6553-6561.
(60) Carta, M.; Croad, M.; Malpass-Evans, R.; Jansen, J. C.; Bernardo, P.; Clarizia, G.; Friess, K.; Lanč, M.; McKeown, N. B. Triptycene Induced Enhancement of Membrane Gas Selectivity for Microporous Tröger's Base Polymers. *Adv. Mater.* **2014,** *26*, 3526-3531.
(61) Carta, M.; Malpass-Evans, R.; Croad, M.; Rogan, Y.; Jansen, J. C.; Bernardo, P.; Bazzarelli, F.; McKeown, N. B. An Efficient Polymer Molecular Sieve for Membrane Gas Separations. *Science* **2013,** *339*, 303-307.
(62) McKeown, N. B. Polymers of Intrinsic Microporosity. *ISRN Materials Science* **2012,** *2012*, Article ID 513986.
(63) Tröger, J. Ueber Einige Mittelst Nascirenden Formaldehydes Entstehende Basen. *Adv. Synth. Catal.* **1887,** *36*, 225-245.
(64) Spielman, M. The Structure of Troeger's Base. *J. Am. Chem. Soc.* **1935,** *57*, 583-585.
(65) Carta, M.; Croad, M.; Jansen, J. C.; Bernardo, P.; Clarizia, G.; McKeown, N. B. Synthesis of Cardo-polymers Using Tröger's Base Formation. *Polym. Chem.* **2014,** *5*, 5255-5261.
(66) Carta, M.; Malpass-Evans, R.; Croad, M.; Rogan, Y.; Lee, M.; Rose, I.; McKeown, N. B. The Synthesis of Microporous Polymers Using Tröger's Base Formation. *Polym. Chem.* **2014,** *5*, 5267-5272.

(67) Rose, I.; Carta, M.; Malpass-Evans, R.; Ferrari, M.-C.; Bernardo, P.; Clarizia, G.; Jansen, J. C.; McKeown, N. B. Highly Permeable Benzotriptycene-Based Polymer of Intrinsic Microporosity. *ACS Macro Lett.* **2015,** *4*, 912-915.
(68) Khdhayyer, M. R.; Esposito, E.; Fuoco, A.; Monteleone, M.; Giorno, L.; Jansen, J. C.; Attfield, M. P.; Budd, P. M. Mixed Matrix Membranes Based on UIO-66 MOFs in the Polymer of Intrinsic Microporosity PIM-1. *Sep. Purif. Technol.* **2017,** *173*, 304-313.
(69) Du, N.; Park, H. B.; Robertson, G. P.; Dal-Cin, M. M.; Visser, T.; Scoles, L.; Guiver, M. D. Polymer Nanosieve Membranes for CO2-capture Applications. *Nature Mater.* **2011,** *10*, 372-375.
(70) Mason, C. R.; Maynard-Atem, L.; Heard, K. W.; Satilmis, B.; Budd, P. M.; Friess, K.; Lanč, M.; Bernardo, P.; Clarizia, G.; Jansen, J. C. Enhancement of CO2 Affinity in a Polymer of Intrinsic Microporosity by Amine Modification. *Macromolecules* **2014,** *47*, 1021-1029.
(71) Jue, M. L.; Breedveld, V.; Lively, R. P. Defect-Free PIM-1 Hollow Fiber Membranes. *J. Membr. Sci.* **2017,** *530*, 33-41.
(72) Li, P.; Chung, T.; Paul, D. Temperature Dependence of Gas Sorption and Permeation in PIM-1. *J. Membr. Sci.* **2014,** *450*, 380-388.
(73) Thomas, S.; Pinnau, I.; Du, N.; Guiver, M. D. Pure-And Mixed-Gas Permeation Properties of a Microporous Spirobisindane-Based Ladder Polymer (PIM-1). *J. Membr. Sci.* **2009,** *333*, 125-131.
(74) Budd, P. M.; McKeown, N. B.; Ghanem, B. S.; Msayib, K. J.; Fritsch, D.; Starannikova, L.; Belov, N.; Sanfirova, O.; Yampolskii, Y.; Shantarovich, V. Gas Permeation Parameters and Other Physicochemical Properties of a Polymer of Intrinsic Microporosity: Polybenzodioxane PIM-1. *J. Membr. Sci.* **2008,** *325*, 851-860.
(75) Chung, T.-S.; Lin, W.-H.; Vora, R. H. The Effect of Shear Rates on Gas Separation Performance of 6FDA-durene Polyimide Hollow Fibers. *J. Membr. Sci.* **2000,** *167*, 55-66.
(76) Lively, R. P.; Dose, M. E.; Xu, L.; Vaughn, J. T.; Johnson, J.; Thompson, J. A.; Zhang, K.; Lydon, M. E.; Lee, J.-S.; Liu, L. A High-Flux Polyimide Hollow Fiber Membrane to Minimize Footprint and Energy Penalty for CO2 Recovery from Flue Gas. *J. Membr. Sci.* **2012,** *423*, 302-313.
(77) Budd, P. M.; McKeown, N. B. Highly Permeable Polymers for Gas Separation Membranes. *Polym. Chem.* **2010,** *1*, 63-68.
(78) Bondi, A. A. *Physical Properties of Molecular Crystals Liquids, and Glasses*; Wiley: New York, 1968.
(79) Freeman, B.; Yampolskii, Y.; Pinnau, I. *Materials Science of Membranes for Gas and Vapor Separation*; John Wiley & Sons: Chichester, UK, 2006.
(80) Tao, S. Positronium Annihilation in Molecular Substances. *J. Chem. Phys.* **1972,** *56*, 5499-5510.
(81) Eldrup, M.; Lightbody, D.; Sherwood, J. N. The Temperature Dependence of Positron Lifetimes in Solid Pivalic Acid. *Chem. Phys.* **1981,** *63*, 51-58.
(82) Shantarovich, V.; Kevdina, I.; Yampolskii, Y. P.; Alentiev, A. Y. Positron Annihilation Lifetime Study of High and Low Free Volume Glassy Polymers: Effects of Free Volume Sizes on the Permeability and Permselectivity. *Macromolecules* **2000,** *33*, 7453-7466.
(83) Budd, P. M.; Msayib, K. J.; Tattershall, C. E.; Ghanem, B. S.; Reynolds, K. J.; McKeown, N. B.; Fritsch, D. Gas Separation Membranes from Polymers of Intrinsic Microporosity. *J. Membr. Sci.* **2005,** *251*, 263-269.
(84) Hofmann, D.; Entrialgo-Castano, M.; Lerbret, A.; Heuchel, M.; Yampolskii, Y. Molecular Modeling Investigation of Free Volume Distributions in Stiff Chain Polymers with Conventional and Ultrahigh Free Volume: Comparison Between Molecular Modeling and Positron Lifetime Studies. *Macromolecules* **2003,** *36*, 8528-8538.

(85) Golemme, G.; Nagy, J.; Fonseca, A.; Algieri, C.; Yampolskii, Y. 129 Xe-NMR Study of Free Volume in Amorphous Perfluorinated Polymers: Comparsion with Other Methods. *Polymer* **2003,** *44*, 5039-5045.
(86) Alentiev, A. Y.; Shantarovich, V.; Merkel, T.; Bondar, V.; Freeman, B.; Yampolskii, Y. P. Gas and Vapor Sorption, Permeation, and Diffusion in Glassy Amorphous Teflon AF1600. *Macromolecules* **2002,** *35*, 9513-9522.
(87) Alentiev, A. Y.; Yampolskii, Y. P.; Shantarovich, V.; Nemser, S.; Plate, N. High Transport Parameters and Free Volume of Perfluorodioxole Copolymers. *J. Membr. Sci.* **1997,** *126*, 123-132.
(88) Jansen, J. C.; Macchione, M.; Tocci, E.; De Lorenzo, L.; Yampolskii, Y. P.; Sanfirova, O.; Shantarovich, V. P.; Heuchel, M.; Hofmann, D.; Drioli, E. Comparative Study of Different Probing Techniques for the Analysis of the Free Volume Distribution in Amorphous Glassy Perfluoropolymers. *Macromolecules* **2009,** *42*, 7589-7604.
(89) Heuchel, M.; Fritsch, D.; Budd, P. M.; McKeown, N. B.; Hofmann, D. Atomistic Packing Model and Free Volume Distribution of a Polymer with Intrinsic Microporosity (PIM-1). *J. Membr. Sci.* **2008,** *318*, 84-99.
(90) Emmler, T.; Heinrich, K.; Fritsch, D.; Budd, P. M.; Chaukura, N.; Ehlers, D.; Rätzke, K.; Faupel, F. Free Volume Investigation of Polymers of Intrinsic Microporosity (PIMs): PIM-1 and PIM1 Copolymers Incorporating Ethanoanthracene Units. *Macromolecules* **2010,** *43*, 6075-6084.
(91) Yampolskii, Y.; Belov, N. Investigation of Polymers by Inverse Gas Chromatography. *Macromolecules* **2015,** *48*, 6751-6767.
(92) Yampolskii, Y. P. Methods for Investigation of the Free Volume in Polymers. *Russ. Chem. Rev.* **2007,** *76*, 59-78.
(93) Stull, D. R.; Westrum, E. F.; Sinke, G. C. *The Chemical Thermodynamics of Organic Compounds*; J. Wiley: New York, 1969.
(94) Yampolskii, Y. P.; Kaliuzhnyi, N.; Durgar'yan, S. Thermodynamics of Sorption in Glassy Poly (Vinyltrimethylsilane). *Macromolecules* **1986,** *19*, 846-850.
(95) Gregg, S.; Sing, K. S. *Adsorption, Surface Science and Porosity*; Academic Press: New York, 1982.
(96) Ghanem, B. S.; Swaidan, R.; Ma, X.; Litwiller, E.; Pinnau, I. Energy‐Efficient Hydrogen Separation by AB‐Type Ladder‐Polymer Molecular Sieves. *Adv. Mater.* **2014,** *26*, 6696-6700.
(97) Swaidan, R.; Ghanem, B. S.; Litwiller, E.; Pinnau, I. Pure- and Mixed-Gas CO2/CH4 Separation Properties of Pim-1 and an Amidoxime-Functionalized PIM-1. *J. Membr. Sci.* **2014,** *457*, 95-102.
(98) Ghanem, B. S.; Swaidan, R.; Litwiller, E.; Pinnau, I. Ultra‐Microporous Triptycene‐based Polyimide Membranes for High‐Performance Gas Separation. *Adv. Mater.* **2014,** *26*, 3688-3692.
(99) Kupgan, G.; Liyana-Arachchi, T. P.; Colina, C. M. NLDFT Pore Size Distribution in Amorphous Microporous Materials. *Langmuir* **2017,** *33*, 11138-11145.
(100) Weber, J.; Du, N.; Guiver, M. D. Influence of Intermolecular Interactions on the Observable Porosity in Intrinsically Microporous Polymers. *Macromolecules* **2011,** *44*, 1763-1767.
(101) Lau, C. H.; Konstas, K.; Thornton, A. W.; Liu, A. C.; Mudie, S.; Kennedy, D. F.; Howard, S. C.; Hill, A. J.; Hill, M. R. Gas‐Separation Membranes Loaded with Porous Aromatic Frameworks that Improve with Age. *Angew. Chem. Int. Ed.* **2015,** *54*, 2669-2673.
(102) Thommes, M. Physical Adsorption Characterization of Nanoporous Materials. *Chem. Ing. Tech.* **2010,** *82*, 1059-1073.
(103) Ritter, N.; Antonietti, M.; Thomas, A.; Senkovska, I.; Kaskel, S.; Weber, J. Binaphthalene-Based, Soluble Polyimides: the Limits of Intrinsic Microporosity. *Macromolecules* **2009,** *42*, 8017-8020.

(104) Farha, O. K.; Spokoyny, A. M.; Hauser, B. G.; Bae, Y.-S.; Brown, S. E.; Snurr, R. Q.; Mirkin, C. A.; Hupp, J. T. Synthesis, Properties, and Gas Separation Studies of a Robust Diimide-based Microporous Organic Polymer. *Chem. Mater.* **2009,** *21*, 3033-3035.
(105) Weber, J.; Schmidt, J.; Thomas, A.; Böhlmann, W. Micropore Analysis of Polymer Networks by Gas Sorption and 129Xe NMR Spectroscopy: Toward a Better Understanding of Intrinsic Microporosity. *Langmuir* **2010,** *26*, 15650-15656.
(106) Rodriguezreinoso, F.; Linaressolano, A. In *Chemistry and Physics of Carbon*; CRC Press: Boca Raton, 1989; Vol. 21.
(107) Linares-Solano, A.; de Lecea, C. S.-M.; Alcaniz-Monge, J.; Cazorla-Amorós, D. Further Advances in the Characterization of Microporous Carbons by Physical Adsorption of Gases. *Tanso* **1998,** *1998*, 316-325.
(108) Ravikovitch, P. I.; Vishnyakov, A.; Russo, R.; Neimark, A. V. Unified Approach to Pore Size Characterization of Microporous Carbonaceous Materials from N2, Ar, and CO2 Adsorption Isotherms. *Langmuir* **2000,** *16*, 2311-2320.
(109) Siriwardane, R. V.; Shen, M.-S.; Fisher, E. P.; Poston, J. A. Adsorption of CO2 on Molecular Sieves and Activated Carbon. *Energy Fuels* **2001,** *15*, 279-284.
(110) Lozano-Castelló, D.; Cazorla-Amorós, D.; Linares-Solano, A. Usefulness of CO2 Adsorption at 273 K for the Characterization of Porous Carbons. *Carbon* **2004,** *42*, 1233-1242.
(111) Cazorla-Amorós, D.; Alcaniz-Monge, J.; Linares-Solano, A. Characterization of Activated Carbon Fibers by CO2 Adsorption. *Langmuir* **1996,** *12*, 2820-2824.
(112) Cazorla-Amorós, D.; Alcaniz-Monge, J.; De la Casa-Lillo, M.; Linares-Solano, A. CO2 as an Adsorptive to Characterize Carbon Molecular Sieves and Activated Carbons. *Langmuir* **1998,** *14*, 4589-4596.
(113) Vishnyakov, A.; Ravikovitch, P. I.; Neimark, A. V. Molecular Level Models for CO2 Sorption in Nanopores. *Langmuir* **1999,** *15*, 8736-8742.
(114) Fraissard, J.; Ito, T. 129 Xe NMR Study of Adsorbed Xenon: a New Method for Studying Zeolites and Metal-zeolites. *Zeolites* **1988,** *8*, 350-361.
(115) Breck, D. W. In *Chemistry and Use*; Wiley: New York, 1974; Vol. 636.
(116) Nagasaka, B.; Eguchi, T.; Nakayama, H.; Nakamura, N.; Ito, Y. Positron Annihilation and 129 Xe NMR Studies of Free Volume in Polymers. *Radiat. Phys. Chem.* **2000,** *58*, 581-585.
(117) Suzuki, T.; Miyauchi, M.; Yoshimizu, H.; Tsujita, Y. Characterization of Microvoids in Glassy Polymers by Means of 129xe Nmr Spectroscopy. *Polym. J.* **2001,** *33*, 934-938.
(118) Hofmann, D.; Fritz, L.; Ulbrich, J.; Schepers, C.; Böhning, M. Detailed‐Atomistic Molecular Modeling of Small Molecule Diffusion and Solution Processes in Polymeric Membrane Materials. *Macromol. Theory Simul.* **2000,** *9*, 293-327.
(119) Theodorou, D. N. *Principles of Molecular Simulation of Gas Transport in Polymers*; John Wiley & Sons: Chichester, England, 2006.
(120) Theodorou, D. N.; Suter, U. W. Detailed Molecular Structure of a Vinyl Polymer Glass. *Macromolecules* **1985,** *18*, 1467-1478.
(121) Theodorou, D. N.; Suter, U. W. Atomistic Modeling of Mechanical Properties of Polymeric Glasses. *Macromolecules* **1986,** *19*, 139-154.
(122) Xu, Q. *Nanoporous Materials: Synthesis and Applications*; CRC Press: Boca Raton, 2013.
(123) Yong, W. F.; Li, F. Y.; Chung, T.-S.; Tong, Y. W. Highly Permeable Chemically Modified PIM-1/Matrimid Membranes for Green Hydrogen Purification. *J. Mater. Chem. A* **2013,** *1*, 13914-13925.
(124) Weber, J.; Su, Q.; Antonietti, M.; Thomas, A. Exploring Polymers of Intrinsic Microporosity–Microporous, Soluble Polyamide and Polyimide. *Macromol. Rapid Comm.* **2007,** *28*, 1871-1876.

(125) Du, N.; Robertson, G. P.; Song, J.; Pinnau, I.; Thomas, S.; Guiver, M. D. Polymers of Intrinsic Microporosity Containing Trifluoromethyl and Phenylsulfone Groups as Materials for Membrane Gas Separation†. *Macromolecules* **2008,** *41*, 9656-9662.
(126) Li, F. Y.; Xiao, Y.; Ong, Y. K.; Chung, T. S. UV‐Rearranged PIM‐1 Polymeric Membranes for Advanced Hydrogen Purification and Production. *Adv. Energy Mater.* **2012,** *2*, 1456-1466.
(127) McDermott, A. G.; Budd, P. M.; McKeown, N. B.; Colina, C. M.; Runt, J. Physical Aging of Polymers of Intrinsic Microporosity: a SAXS/WAXS Study. *J. Mater. Chem. A* **2014,** *2*, 11742-11752.
(128) Ritter, N.; Senkovska, I.; Kaskel, S.; Weber, J. Intrinsically Microporous Poly (Imide)s: Structure− Porosity Relationship Studied by Gas Sorption and X-Ray Scattering. *Macromolecules* **2011,** *44*, 2025-2033.
(129) McDermott, A. G.; Larsen, G. S.; Budd, P. M.; Colina, C. M.; Runt, J. Structural Characterization of a Polymer of Intrinsic Microporosity: X-Ray Scattering with Interpretation Enhanced by Molecular Dynamics Simulations. *Macromolecules* **2010,** *44*, 14-16.
(130) Li, F.; Xiao, Y.; Chung, T.-S. N.; U.S. Patent 20130247756, 2013.
(131) Czichos, H.; Saito, T.; Smith, L. E. (Eds.) *Springer Handbook of Metrology and Testing*; Springer: Berlin, Germany, 2011.
(132) Dorkenoo, K. D.; Pfromm, P. H. Accelerated Physical Aging of Thin Poly[1-(trimethylsilyl)-1-propyne] Films. *Macromolecules* **2000,** *33*, 3747-3751.
(133) McCaig, M.; Paul, D. R. Effect of Film Thickness on the Changes in Gas Permeability of a Glassy Polyarylate Due to Physical Aging part I. Experimental Observations. *Polymer* **2000,** *41*, 629-637.
(134) McCaig, M.; Paul, D. R.; Barlow, J. Effect of Film Thickness on the Changes in Gas Permeability of a Glassy Polyarylate Due to Physical Aging part II. Mathematical Model. *Polymer* **2000,** *41*, 639-648.
(135) Huang, Y.; Paul, D. R. Physical Aging of Thin Glassy Polymer Films Monitored by Gas Permeability. *Polymer* **2004,** *45*, 8377-8393.
(136) Harms, S.; Rätzke, K.; Faupel, F.; Chaukura, N.; Budd, P.; Egger, W.; Ravelli, L. Aging and Free Volume in a Polymer of Intrinsic Microporosity (PIM-1). *J. Adhes.* **2012,** *88*, 608-619.
(137) Wijmans, J.; Baker, R. The Solution-Diffusion Model: a Review. *J. Membr. Sci.* **1995,** *107*, 1-21.
(138) Vieth, W.; Howell, J.; Hsieh, J. Dual Sorption Theory. *J. Membr. Sci.* **1976,** *1*, 177-220.
(139) Horn, N. R.; Paul, D. R. Carbon Dioxide Plasticization of Thin Glassy Polymer Films. *Polymer* **2011,** *52*, 5587-5594.
(140) Wind, J. D.; Staudt-Bickel, C.; Paul, D. R.; Koros, W. J. Solid-State Covalent Cross-Linking of Polyimide Membranes for Carbon Dioxide Plasticization Reduction. *Macromolecules* **2003,** *36*, 1882-1888.
(141) Ismail, A. F.; Lorna, W. Penetrant-Induced Plasticization Phenomenon in Glassy Polymers for Gas Separation Membrane. *Sep. Purif. Technol.* **2002,** *27*, 173-194.
(142) Scholes, C. A.; Chen, G. Q.; Stevens, G. W.; Kentish, S. E. Plasticization of Ultra-Thin Polysulfone Membranes by Carbon Dioxide. *J. Membr. Sci.* **2010,** *346*, 208-214.
(143) Wonders, A.; Paul, D. R. Effect of CO2 Exposure History on Sorption and Transport in Polycarbonate. *J. Membr. Sci.* **1979,** *5*, 63-75.
(144) Rowe, B. W.; Freeman, B. D.; Paul, D. R. Physical Aging of Ultrathin Glassy Polymer Films Tracked by Gas Permeability. *Polymer* **2009,** *50*, 5565-5575.
(145) Cui, L.; Qiu, W.; Paul, D.; Koros, W. J. Responses of 6FDA-based Polyimide Thin Membranes to CO2 Exposure and Physical Aging as Monitored by Gas Permeability. *Polymer* **2011,** *52*, 5528-5537.
(146) Žák, M.; Klepic, M.; Šťastná, L. Č.; Sedláková, Z.; Vychodilová, H.; Hovorka, Š.; Friess, K.; Randová, A.; Brožová, L.; Jansen, J. C. Selective Removal of Butanol

from Aqueous Solution by Pervaporation with a PIM-1 Membrane and Membrane Aging. *Sep. Purif. Technol.* **2015,** *151*, 108-114.
(147) Lau, C. H.; Konstas, K.; Doherty, C. M.; Kanehashi, S.; Ozcelik, B.; Kentish, S. E.; Hill, A. J.; Hill, M. R. Tailoring Physical Aging in Super Glassy Polymers with Functionalized Porous Aromatic Frameworks for CO2 Capture. *Chem. Mater.* **2015,** *27*, 4756-4762.
(148) Li, F. Y.; Chung, T.-S. Physical Aging, High Temperature and Water Vapor Permeation Studies of UV-Rearranged PIM-1 Membranes for Advanced Hydrogen Purification and Production. *Int. J. Hydrogen Energ.* **2013,** *38*, 9786-9793.
(149) Rose, I.; Bezzu, C. G.; Carta, M.; Comesaña-Gándara, B.; Lasseuguette, E.; Ferrari, M. C.; Bernardo, P.; Clarizia, G.; Fuoco, A.; Jansen, J. C. Polymer Ultrapermeability from the Inefficient Packing of 2D Chains. *Nature Mater.* **2017,** *15*, 932-938.
(150) Merkel, T. C.; Bondar, V.; Nagai, K.; Freeman, B. D. Sorption and Transport of Hydrocarbon and Perfluorocarbon Gases in Poly(1-Trimethylsilyl-1-Propyne). *J. Polym. Sci., Part B: Polym. Phys.* **2000,** *38*, 273-296.
(151) Tocci, E.; De Lorenzo, L.; Bernardo, P.; Clarizia, G.; Bazzarelli, F.; Mckeown, N. B.; Carta, M.; Malpass-Evans, R.; Friess, K.; Pilnáček, K. t. Molecular Modeling and Gas Permeation Properties of a Polymer of Intrinsic Microporosity Composed of Ethanoanthracene and Tröger's Base Units. *Macromolecules* **2014,** *47*, 7900-7916.
(152) Salinas, O.; Ma, X.; Litwiller, E.; Pinnau, I. High-Performance Carbon Molecular Sieve Membranes for Ethylene/Ethane Separation Derived from an Intrinsically Microporous Polyimide. *J. Membr. Sci.* **2016,** *500*, 115-123.
(153) Song, Q.; Cao, S.; Pritchard, R. H.; Ghalei, B.; Al-Muhtaseb, S. A.; Terentjev, E. M.; Cheetham, A. K.; Sivaniah, E. Controlled Thermal Oxidative Crosslinking of Polymers of Intrinsic Microporosity Towards Tunable Molecular Sieve Membranes. *Nat. Commun.* **2014,** *5*.
(154) Li, F. Y.; Xiao, Y.; Chung, T.-S.; Kawi, S. High-Performance Thermally Self-Cross-Linked Polymer of Intrinsic Microporosity (PIM-1) Membranes for Energy Development. *Macromolecules* **2012,** *45*, 1427-1437.
(155) Bushell, A. F.; Budd, P. M.; Attfield, M. P.; Jones, J. T.; Hasell, T.; Cooper, A. I.; Bernardo, P.; Bazzarelli, F.; Clarizia, G.; Jansen, J. C. Nanoporous Organic Polymer/Cage Composite Membranes. *Angew. Chem. Int. Ed.* **2013,** *52*, 1253-1256.
(156) Ghanem, B. S.; McKeown, N. B.; Budd, P. M.; Fritsch, D. Polymers of Intrinsic Microporosity Derived from Bis (Phenazyl) Monomers. *Macromolecules* **2008,** *41*, 1640-1646.
(157) Freeman, B. D. Basis of Permeability/Selectivity Tradeoff Relations in Polymeric Gas Separation Membranes. *Macromolecules* **1999,** *32*, 375-380.
(158) Bezzu, C. G.; Carta, M.; Tonkins, A.; Jansen, J. C.; Bernardo, P.; Bazzarelli, F.; McKeown, N. B. A Spirobifluorene‐Based Polymer of Intrinsic Microporosity with Improved Performance for Gas Separation. *Adv. Mater.* **2012,** *24*, 5930-5933.
(159) Swaidan, R.; Ghanem, B.; Al-Saeedi, M.; Litwiller, E.; Pinnau, I. Role of Intrachain Rigidity in the Plasticization of Intrinsically Microporous Triptycene-Based Polyimide Membranes in Mixed-Gas CO2/CH4 Separations. *Macromolecules* **2014,** *47*, 7453-7462.
(160) Rabbani, M. G.; Reich, T. E.; Kassab, R. M.; Jackson, K. T.; El-Kaderi, H. M. High CO2 Uptake and Selectivity by Triptycene-Derived Benzimidazole-Linked Polymers. *Chem. Commun.* **2012,** *48*, 1141-1143.
(161) Ghanem, B. S.; Hashem, M.; Harris, K. D.; Msayib, K. J.; Xu, M.; Budd, P. M.; Chaukura, N.; Book, D.; Tedds, S.; Walton, A. Triptycene-Based Polymers of Intrinsic Microporosity: Organic Materials That Can Be Tailored for Gas Adsorption. *Macromolecules* **2010,** *43*, 5287-5294.
(162) Swaidan, R.; Al-Saeedi, M.; Ghanem, B.; Litwiller, E.; Pinnau, I. Rational Design of Intrinsically Ultramicroporous Polyimides Containing Bridgehead-Substituted Triptycene for Highly Selective and Permeable Gas Separation Membranes. *Macromolecules* **2014,** *47*, 5104-5114.

(163) Short, R.; Carta, M.; Bezzu, C. G.; Fritsch, D.; Kariuki, B. M.; McKeown, N. B. Hexaphenylbenzene-Based Polymers of Intrinsic Microporosity. *Chem. Commun.* **2011,** *47*, 6822-6824.
(164) Carta, M.; Bernardo, P.; Clarizia, G.; Jansen, J. C.; McKeown, N. B. Gas Permeability of Hexaphenylbenzene Based Polymers of Intrinsic Microporosity. *Macromolecules* **2014,** *47*, 8320-8327.
(165) Ghanem, B. S.; McKeown, N. B.; Budd, P. M.; Selbie, J. D.; Fritsch, D. High‐Performance Membranes from Polyimides with Intrinsic Microporosity. *Adv. Mater.* **2008,** *20*, 2766-2771.
(166) Lee, M.; Bezzu, C. G.; Carta, M.; Bernardo, P.; Clarizia, G.; Jansen, J. C.; McKeown, N. B. Enhancing the Gas Permeability of Tröger's Base Derived Polyimides of Intrinsic Microporosity. *Macromolecules* **2016,** *49*, 4147-4154.
(167) Rogan, Y.; Malpass-Evans, R.; Carta, M.; Lee, M.; Jansen, J. C.; Bernardo, P.; Clarizia, G.; Tocci, E.; Friess, K.; Lanč, M. A Highly Permeable Polyimide with Enhanced Selectivity for Membrane Gas Separations. *J. Mater. Chem. A* **2014,** *2*, 4874-4877.
(168) Ma, X.; Ghanem, B.; Salines, O.; Litwiller, E.; Pinnau, I. Synthesis and Effect of Physical Aging on Gas Transport Properties of a Microporous Polyimide Derived from a Novel Spirobifluorene-Based Dianhydride. *ACS Macro Lett.* **2015,** *4*, 231-235.
(169) Ghanem, B. S.; McKeown, N. B.; Budd, P. M.; Al-Harbi, N. M.; Fritsch, D.; Heinrich, K.; Starannikova, L.; Tokarev, A.; Yampolskii, Y. Synthesis, Characterization, and Gas Permeation Properties of a Novel Group of Polymers with Intrinsic Microporosity: PIM-Polyimides. *Macromolecules* **2009,** *42*, 7881-7888.
(170) Rogan, Y.; Starannikova, L.; Ryzhikh, V.; Yampolskii, Y.; Bernardo, P.; Bazzarelli, F.; Jansen, J. C.; McKeown, N. B. Synthesis and Gas Permeation Properties of Novel Spirobisindane-Based Polyimides of Intrinsic Microporosity. *Polym. Chem.* **2013,** *4*, 3813-3820.
(171) Alghunaimi, F.; Ghanem, B.; Alaslai, N.; Swaidan, R.; Litwiller, E.; Pinnau, I. Gas Permeation and Physical Aging Properties of Iptycene Diamine-based Microporous Polyimides. *J. Membr. Sci.* **2015,** *490*, 321-327.
(172) Ma, X.; Swaidan, R.; Belmabkhout, Y.; Zhu, Y.; Litwiller, E.; Jouiad, M.; Pinnau, I.; Han, Y. Synthesis and Gas Transport Properties of Hydroxyl-Functionalized Polyimides with Intrinsic Microporosity. *Macromolecules* **2012,** *45*, 3841-3849.
(173) Ma, X.; Salinas, O.; Litwiller, E.; Pinnau, I. Novel Spirobifluorene-And Dibromospirobifluorene-Based Polyimides of Intrinsic Microporosity for Gas Separation Applications. *Macromolecules* **2013,** *46*, 9618-9624.
(174) Guiver, M. D.; Robertson, G. P.; Dai, Y.; Bilodeau, F.; Kang, Y. S.; Lee, K. J.; Jho, J. Y.; Won, J. Structural Characterization and Gas‐Transport Properties of Brominated Matrimid Polyimide. *J. Polym. Sci. A Polym. Chem.* **2002,** *40*, 4193-4204.
(175) Zhuang, Y.; Seong, J. G.; Do, Y. S.; Jo, H. J.; Cui, Z.; Lee, J.; Lee, Y. M.; Guiver, M. D. Intrinsically Microporous Soluble Polyimides Incorporating Tröger's Base for Membrane Gas Separation. *Macromolecules* **2014,** *47*, 3254-3262.
(176) Zhuang, Y.; Seong, J. G.; Do, Y. S.; Lee, W. H.; Lee, M. J.; Guiver, M. D.; Lee, Y. M. High-Strength, Soluble Polyimide Membranes Incorporating Tröger's Base for Gas Separation. *J. Membr. Sci.* **2016,** *504*, 55-65.
(177) Wang, Z.; Wang, D.; Zhang, F.; Jin, J. Tröger's Base-Based Microporous Polyimide Membranes for High-Performance Gas Separation. *ACS Macro Lett.* **2014,** *3*, 597-601.
(178) Wang, Z.; Wang, D.; Jin, J. Microporous Polyimides with Rationally Designed Chain Structure Achieving High Performance for Gas Separation. *Macromolecules* **2014,** *47*, 7477-7483.
(179) Sydlik, S. A.; Chen, Z.; Swager, T. M. Triptycene Polyimides: Soluble Polymers with High Thermal Stability and Low Refractive Indices. *Macromolecules* **2011,** *44*, 976-980.

(180) Cho, Y. J.; Park, H. B. High Performance Polyimide with High Internal Free Volume Elements. *Macromol. Rapid Comm.* **2011,** *32*, 579-586.
(181) Du, N.; Robertson, G. P.; Song, J.; Pinnau, I.; Guiver, M. D. High-performance Carboxylated Polymers of Intrinsic Microporosity (PIMs) with Tunable Gas Transport Properties†. *Macromolecules* **2009,** *42*, 6038-6043.
(182) Mason, C. R.; Maynard-Atem, L.; Al-Harbi, N. M.; Budd, P. M.; Bernardo, P.; Bazzarelli, F.; Clarizia, G.; Jansen, J. C. Polymer of Intrinsic Microporosity Incorporating Thioamide Functionality: Preparation and Gas Transport Properties. *Macromolecules* **2011,** *44*, 6471-6479.
(183) Patel, H. A.; Yavuz, C. T. Noninvasive Functionalization of Polymers of Intrinsic Microporosity for Enhanced CO2 Capture. *Chem. Commun.* **2012,** *48*, 9989-9991.
(184) Maier, G. Gas Separation by Polymer Membranes: Beyond the Border. *Angew. Chem. Int. Ed.* **2013,** *52*, 4982-4984.
(185) Swaidan, R.; Ghanem, B.; Litwiller, E.; Pinnau, I. Effects of Hydroxyl-Functionalization and Sub-Tg Thermal Annealing on High Pressure Pure-And Mixed-Gas CO2/CH4 Separation by Polyimide Membranes Based on 6FDA and Triptycene-Containing Dianhydrides. *J. Membr. Sci.* **2015,** *475*, 571-581.
(186) Du, N.; Robertson, G. P.; Pinnau, I.; Guiver, M. D. Polymers of Intrinsic Microporosity with Dinaphthyl and Thianthrene Segments. *Macromolecules* **2010,** *43*, 8580-8587.
(187) Ma, X.; Pinnau, I. A Novel Intrinsically Microporous Ladder Polymer and Copolymers Derived from 1, 1′, 2, 2′-Tetrahydroxy-Tetraphenylethylene for Membrane-Based Gas Separation. *Polym. Chem.* **2016,** *7*, 1244-1248.
(188) Yong, W.; Li, F.; Xiao, Y.; Li, P.; Pramoda, K.; Tong, Y.; Chung, T. Molecular Engineering of PIM-1/Matrimid Blend Membranes for Gas Separation. *J. Membr. Sci.* **2012,** *407*, 47-57.
(189) Hao, L.; Li, P.; Chung, T.-S. PIM-1 as an Organic Filler to Enhance the Gas Separation Performance of Ultem Polyetherimide. *J. Membr. Sci.* **2014,** *453*, 614-623.
(190) Du, N.; Robertson, G. P.; Pinnau, I.; Thomas, S.; Guiver, M. D. Copolymers of Intrinsic Microporosity Based on 2, 2′, 3, 3′-Tetrahydroxy-1, 1′-dinaphthyl. *Macromol. Rapid Comm.* **2009,** *30*, 584-588.
(191) Du, N.; Robertson, G. P.; Pinnau, I.; Guiver, M. D. Polymers of Intrinsic Microporosity Derived from Novel Disulfone-Based Monomers†. *Macromolecules* **2009,** *42*, 6023-6030.
(192) Wang, Z. G.; Liu, X.; Wang, D.; Jin, J. Tröger's Base-Based Copolymers with Intrinsic Microporosity for CO2 Separation and Effect of Tröger's Base on Separation Performance. *Polym. Chem.* **2014,** *5*, 2793-2800.
(193) Ma, X.; Mukaddam, M.; Pinnau, I. Bifunctionalized Intrinsically Microporous Polyimides with Simultaneously Enhanced Gas Permeability and Selectivity. *Macromol. Rapid Comm.* **2016,** *37*, 900-904.
(194) Yong, W. F.; Li, F. Y.; Xiao, Y. C.; Chung, T. S.; Tong, Y. W. High Performance Pim-1/Matrimid Hollow Fiber Membranes for CO2/CH4, O2/N2 and CO2/N2 Separation. *J. Membr. Sci.* **2013,** *443*, 156-169.
(195) Yong, W. F.; Lee, Z. K.; Chung, T. S.; Weber, M.; Staudt, C.; Maletzko, C. Blends of a Polymer of Intrinsic Microporosity and Partially Sulfonated Polyphenylenesulfone for Gas Separation. *Chemsuschem* **2016,** *9*, 1953-1962.
(196) Du, N.; Dal-Cin, M. M.; Robertson, G. P.; Guiver, M. D. Decarboxylation-induced Cross-linking of Polymers of Intrinsic Microporosity (PIMs) for Membrane Gas Separation†. *Macromolecules* **2012,** *45*, 5134-5139.
(197) Satilmis, B.; Budd, P. M. Base-Catalysed Hydrolysis of Pim-1: Amide Versus Carboxylate Formation. *RSC Adv.* **2014,** *4*, 52189-52198.
(198) Yates, S. F.; McGuirl, M. C.; Tonev, T. G.; Liu, C.; Chiou, J.; Arzadon, A.; U.S. Patent 8,337,598, 2012.
(199) McCaig, M.; Paul, D. Effect of UV Crosslinking and Physical Aging on the Gas Permeability of Thin Glassy Polyarylate Films. *Polymer* **1999,** *40*, 7209-7225.

(200) Zhong, S.; Liu, C.; Na, H. Preparation and Properties of UV Irradiation-Induced Crosslinked Sulfonated Poly (Ether Ether Ketone) Proton Exchange Membranes. *J. Membr. Sci.* **2009,** *326*, 400-407.
(201) Kita, H.; Inada, T.; Tanaka, K.; Okamoto, K.-i. Effect of Photocrosslinking on Permeability and Permselectivity of Gases Through Benzophenone-Containing Polyimide. *J. Membr. Sci.* **1994,** *87*, 139-147.
(202) Liu, C.; Schott, M. E.; Bowen, T. C.; U.S. Patent 8,814,982, 2014.
(203) Liu, C.; Wilson, S. T.; Lesch, D. A.; U.S. Patent 7,758,751, 2010.
(204) Liskey, C. W.; Hamoy, M. B.; Liu, C.; U.S. Patent 9,238,202, 2013.
(205) Song, Q.; Cao, S.; Zavala-Rivera, P.; Lu, L. P.; Li, W.; Ji, Y.; Al-Muhtaseb, S. A.; Cheetham, A. K.; Sivaniah, E. Photo-Oxidative Enhancement of Polymeric Molecular Sieve Membranes. *Nat. Commun.* **2013,** *4*, 1918.
(206) Kelman, S. D.; Matteucci, S.; Bielawski, C. W.; Freeman, B. Crosslinking Poly (1-Trimethylsilyl-1-Propyne) and Its Effect on Solvent Resistance and Transport Properties. *Polymer* **2007,** *48*, 6881-6892.
(207) Shao, L.; Samseth, J.; Hägg, M.-B. Crosslinking and Stabilization of Nanoparticle Filled PMP Nanocomposite Membranes for Gas Separations. *J. Membr. Sci.* **2009,** *326*, 285-292.
(208) Jia, J.; Baker, G. L. Cross‐Linking of Poly [1‐(Trimethylsilyl)‐1‐Propyne] Membranes Using Bis (Aryl Azides). *J. Polym. Sci., Part B: Polym. Phys.* **1998,** *36*, 959-968.
(209) Du, N.; Cin, M. M. D.; Pinnau, I.; Nicalek, A.; Robertson, G. P.; Guiver, M. D. Azide‐based Cross‐Linking of Polymers of Intrinsic Microporosity (PIMs) for Condensable Gas Separation. *Macromol. Rapid Comm.* **2011,** *32*, 631-636.
(210) Khan, M. M.; Bengtson, G.; Shishatskiy, S.; Gacal, B. N.; Rahman, M. M.; Neumann, S.; Filiz, V.; Abetz, V. Cross-Linking of Polymer of Intrinsic Microporosity (PIM-1) via Nitrene Reaction and Its Effect on Gas Transport Property. *Eur. Polym. J.* **2013,** *49*, 4157-4166.
(211) McDonald, T. O.; Akhtar, R.; Lau, C. H.; Ratvijitvech, T.; Cheng, G.; Clowes, R.; Adams, D. J.; Hasell, T.; Cooper, A. I. Using Intermolecular Interactions to Crosslink PIM-1 and Modify Its Gas Sorption Properties. *J. Mater. Chem. A* **2015,** *3*, 4855-4864.
(212) Shamsipur, H.; Dawood, B. A.; Budd, P. M.; Bernardo, P.; Clarizia, G.; Jansen, J. C. Thermally Rearrangeable Pim-Polyimides for Gas Separation Membranes. *Macromolecules* **2014,** *47*, 5595-5606.
(213) Li, S.; Jo, H. J.; Han, S. H.; Park, C. H.; Kim, S.; Budd, P. M.; Lee, Y. M. Mechanically Robust Thermally Rearranged (TR) Polymer Membranes with Spirobisindane for Gas Separation. *J. Membr. Sci.* **2013,** *434*, 137-147.
(214) Ma, X.; Salinas, O.; Litwiller, E.; Pinnau, I. Pristine and Thermally-Rearranged Gas Separation Membranes from Novel O-Hydroxyl-Functionalized Spirobifluorene-Based Polyimides. *Polym. Chem.* **2014,** *5*, 6914-6922.
(215) Ismail, A. F.; David, L. A Review on the Latest Development of Carbon Membranes for Gas Separation. *J. Membr. Sci.* **2001,** *193*, 1-18.
(216) Ma, X.; Swaidan, R.; Teng, B.; Tan, H.; Salinas, O.; Litwiller, E.; Han, Y.; Pinnau, I. Carbon Molecular Sieve Gas Separation Membranes Based on an Intrinsically Microporous Polyimide Precursor. *Carbon* **2013,** *62*, 88-96.
(217) Swaidan, R.; Ma, X.; Litwiller, E.; Pinnau, I. High Pressure Pure-And Mixed-Gas Separation of CO2/CH4 by Thermally-Rearranged and Carbon Molecular Sieve Membranes Derived from a Polyimide of Intrinsic Microporosity. *J. Membr. Sci.* **2013,** *447*, 387-394.
(218) Salinas, O.; Ma, X.; Litwiller, E.; Pinnau, I. Ethylene/Ethane Permeation, Diffusion and Gas Sorption Properties of Carbon Molecular Sieve Membranes Derived from the Prototype Ladder Polymer of Intrinsic Microporosity (PIM-1). *J. Membr. Sci.* **2016,** *504*, 133-140.

(219) Althumayri, K.; Harrison, W. J.; Shin, Y.; Gardiner, J. M.; Casiraghi, C.; Budd, P. M.; Bernardo, P.; Clarizia, G.; Jansen, J. C. The Influence of Few-layer Graphene on The Gas Permeability of The High-free-volume Polymer PIM-1. *Phil. Trans. R. Soc. A* **2016,** *374*, 20150031.
(220) Khan, M. M.; Filiz, V.; Bengtson, G.; Shishatskiy, S.; Rahman, M. M.; Lillepaerg, J.; Abetz, V. Enhanced Gas Permeability by Fabricating Mixed Matrix Membranes of Functionalized Multiwalled Carbon Nanotubes and Polymers of Intrinsic Microporosity (PIM). *J. Membr. Sci.* **2013,** *436*, 109-120.
(221) Ahn, J.; Chung, W.-J.; Pinnau, I.; Song, J.; Du, N.; Robertson, G. P.; Guiver, M. D. Gas Transport Behavior of Mixed-matrix Membranes Composed of Silica Nanoparticles in a Polymer of Intrinsic Microporosity (PIM-1). *J. Membr. Sci.* **2010,** *346*, 280-287.
(222) Mitra, T.; Bhavsar, R. S.; Adams, D. J.; Budd, P. M.; Cooper, A. I. Pim-1 Mixed Matrix Membranes for Gas Separations Using Cost-Effective Hypercrosslinked Nanoparticle Fillers. *Chem. Commun.* **2016,** *52*, 5581-5584.
(223) Lau, C. H.; Mulet, X.; Konstas, K.; Doherty, C. M.; Sani, M. A.; Separovic, F.; Hill, M. R.; Wood, C. D. Hypercrosslinked Additives for Ageless Gas‐Separation Membranes. *Angew. Chem. Int. Ed.* **2016,** *55*, 1998-2001.
(224) Li, B.; Huang, X.; Liang, L.; Tan, B. Synthesis of Uniform Microporous Polymer Nanoparticles and Their Applications for Hydrogen Storage. *J. Mater. Chem.* **2010,** *20*, 7444-7450.
(225) Khan, M. M.; Filiz, V.; Bengtson, G.; Shishatskiy, S.; Rahman, M.; Abetz, V. Functionalized Carbon Nanotubes Mixed Matrix Membranes of Polymers of Intrinsic Microporosity for Gas Separation. *Nanoscale Res. Lett.* **2012,** *7*, 1-12.
(226) Tian, Z.; Wang, S.; Wang, Y.; Ma, X.; Cao, K.; Peng, D.; Wu, X.; Wu, H.; Jiang, Z. Enhanced Gas Separation Performance of Mixed Matrix Membranes from Graphitic Carbon Nitride Nanosheets and Polymers of Intrinsic Microporosity. *J. Membr. Sci.* **2016,** *514*, 15-24.
(227) Yong, W. F.; Kwek, K. H. A.; Liao, K.-S.; Chung, T.-S. Suppression of Aging and Plasticization in Highly Permeable Polymers. *Polymer* **2015,** *77*, 377-386.
(228) Liu, J.; Xiao, Y.; Liao, K.-S.; Chung, T.-S. Highly Permeable and Aging Resistant 3d Architecture from Polymers of Intrinsic Microporosity Incorporated with Beta-Cyclodextrin. *J. Membr. Sci.* **2017,** *523*, 92-102.
(229) Hao, L.; Liao, K.-S.; Chung, T.-S. Photo-Oxidative PIM-1 Based Mixed Matrix Membranes with Superior Gas Separation Performance. *J. Mater. Chem. A* **2015,** *3*, 17273-17281.
(230) Song, Q.; Cao, S.; Pritchard, R. H.; Qiblawey, H.; Terentjev, E. M.; Cheetham, A. K.; Sivaniah, E. Nanofiller-Tuned Microporous Polymer Molecular Sieves for Energy and Environmental Processes. *J. Mater. Chem. A* **2016,** *4*, 270-279.
(231) Bushell, A. F.; Attfield, M. P.; Mason, C. R.; Budd, P. M.; Yampolskii, Y.; Starannikova, L.; Rebrov, A.; Bazzarelli, F.; Bernardo, P.; Jansen, J. C. Gas Permeation Parameters of Mixed Matrix Membranes Based on The Polymer of Intrinsic Microporosity PIM-1 and The Zeolitic Imidazolate Framework ZIF-8. *J. Membr. Sci.* **2013,** *427*, 48-62.
(232) Smith, S. J.; Ladewig, B. P.; Hill, A. J.; Lau, C. H.; Hill, M. R. Post-Synthetic Ti Exchanged UIO-66 Metal-Organic Frameworks That Deliver Exceptional Gas Permeability in Mixed Matrix Membranes. *Sci. Rep.* **2015,** *5*.
(233) Olivieri, L.; Ligi, S.; De Angelis, M. G.; Cucca, G.; Pettinau, A. Effect of Graphene and Graphene Oxide Nanoplatelets on the Gas Permselectivity and Aging Behavior of Poly (trimethylsilyl propyne)(PTMSP). *Ind. Eng. Chem. Res.* **2015,** *54*, 11199-11211.

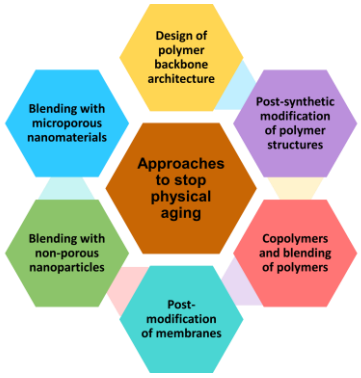
Design of polymer backbone architecture
Post-synthetic modification of polymer structures
Blending with microporous nanomaterials
Approaches to stop physical aging
Blending with non-porous nanoparticles
Copolymers and blending of polymers
Post-modification of membranes